GEOLOGY OF THE PRECAMBRIAN ROCKS OF THE SOUTHERN MANZANO MOUNTAINS, NEW MEXICO

BY

PAUL WINSTON BAUER

B.S., University of Massachusetts, Amherst, 1978

THESIS

Submitted in Partial Fulfillment of the
Requirements for the Degree of

Master of Science in Geology

The University of New Mexico
Albuquerque, New Mexico

May, 1983

TABLE OF CONTENTS

TABLE OF CONTENTS (cont'd.)

TABLE OF CONTENTS (cont'd.) Page

ABSTRACT

The southern Manzano Mountains, New Mexico, located 60 km south of Albuquerque, are a Precambrian-cored, fault-bounded uplift which forms the eastern topographic high of the Rio Grande rift. Proterozoic metasedimentary rocks of the Sais, Blue Springs, and White Ridge formations consist of thin to thick-bedded schists and quartzites which vary greatly in composition and texture. The Sevilleta formation is a structurally and stratigraphically complex association of quartzites, schists, and amphibolites which may have been basaltic sills and flows, and felsic metaigneous rocks which may represent metamorphosed rhyolitic tuffs or flows. The post-tectonic Priest quartz monzonite intrudes the metasedimentary rocks.

Three generations of folding are recognized. An early episode of penetrative deformation (F_1) is characterized by intrafolial isoclinal folds and transposition of compositional layering parallel to the F_1 axial plane foliation (S_1). Microscopically, S_1 is a primary schistosity, but locally appears to be a spaced cleavage. The question of whether S_1 is the earliest penetrative fabric is unresolved.

F_2 deformation, which overprints S_1, is the major map-scale event and is characterized by open to tight folds, local transposition, and disharmonic folding. S_2 is a strong crenulation cleavage, commonly seen as a metamorphic segregation of quartz and mica-rich layers. Locally it is difficult to distinguish S_1 from S_2, as axial plane foliation development varies throughout the map area.

F_3 is a weak, regionally non-penetrative event defined by chevron kink folds in schists and broad folds in more competent strata. F_3 has little effect on the map-scale deformational pattern.

The northeast-striking, northwest-dipping Paloma fault is a poorly understood fault with unknown displacement which parallels or sub-parallels Precambrian lithologies in the map area. The Laramide age, west-dipping Montosa reverse fault to the east separates Precambrian from Paleozoic rocks. These two faults are similar in style and join to the north, suggesting that they may be coeval.

The Manzano Mountains are dominated by a N35°E-trending F_1 and F_2 fabric. F_2 folds plunge about 35° to the S40°W. The map area is divided into western and eastern structural domains, separated by the Paloma fault. The western region contains structurally complex Sevilleta rocks, whereas the eastern area is dominated by southwest-plunging, map-scale F_2 folds in the Sais and Blue Springs formations. This apparent difference in deformation may be due in part to the mechanical behavior of Sevilleta formation versus more competent beds, and in part to different deformational environments on either side of the fault. Other major, as yet unrecognized structures such as bedding-plane thrust faults may be present. The Sevilleta may be separated from adjacent rocks by such a structure.

Equilibrium mineral assemblages and garnet-biotite geothermometry yield peak regional metamorphic conditions of about 500°C and 4 kb. A change along strike from chloritoid-garnet schist to staurolite-garnet schist may indicate higher temperatures in the southern map area. These higher temperatures may be related to intrusion of the Priest pluton. Contact metamorphism around the Priest quartz monzonite pluton intrusion

results in overprinted mineral assemblages, most noticeably with abundant sillimanite in pelitic schists. Cataclastic textures indicative of post-thermal tectonism commonly are seen.

F_1 regional transposition and isoclinal folding may have formed either in a crustal regime of stacked thrust sheets or in a regime of recumbent thrust or fold nappes. F_2 folds probably formed in a compressional stress field with horizontal shortening in a N60°W - S60°E direction with yielding to the southeast. A speculative tectonic model is proposed in which a mechanism of crust-mantle delamination followed by compressional ensialic orogeny forms successive fold generations in rocks as the orogenic belt migrates southward.

LIST OF FIGURES

LIST OF FIGURES (cont'd.) Page

LIST OF FIGURES (cont'd.) Page

LIST OF FIGURES (cont'd.) Page

LIST OF TABLES

INTRODUCTION

Setting

The Manzano Mountains of central New Mexico consist of a northerly-trending, elongate, eastward-tilted fault block on the eastern flank of the Rio Grande rift. The Manzanos extend northward to the Manzanita and Sandia mountains and southward to the Los Pinos Mountains (fig. 1). This Precambrian-cored mountain chain forms a topographic high between the rift and the Estancia basin to the east. Precambrian rocks are mid-Proterozoic (Bolton, 1976) metasediments and metavolcanics intruded by Precambrian granitic plutons. Structural relief between Precambrian basement rocks flooring the rift graben and the highest Precambrian outcrops in the adjacent Manzano Mountains is at least 8000 m (Birch, 1980). Buried range-marginal normal faults can be approximately located by the gravity data (Birch 1980). The exact geometry of these faults is unknown. The Manzanos are bounded to the east by unconformable Paleozoic strata and the Montosa fault, a high-angle reverse fault, up on the west, which has overturned Paleozoic beds along the eastern fault surface.

Previous Work

Previous maps by Stark (1956) and Myers and McKay (1974) in the southern Manzanos were published at scales of 1:48,000 and 1:24,000,

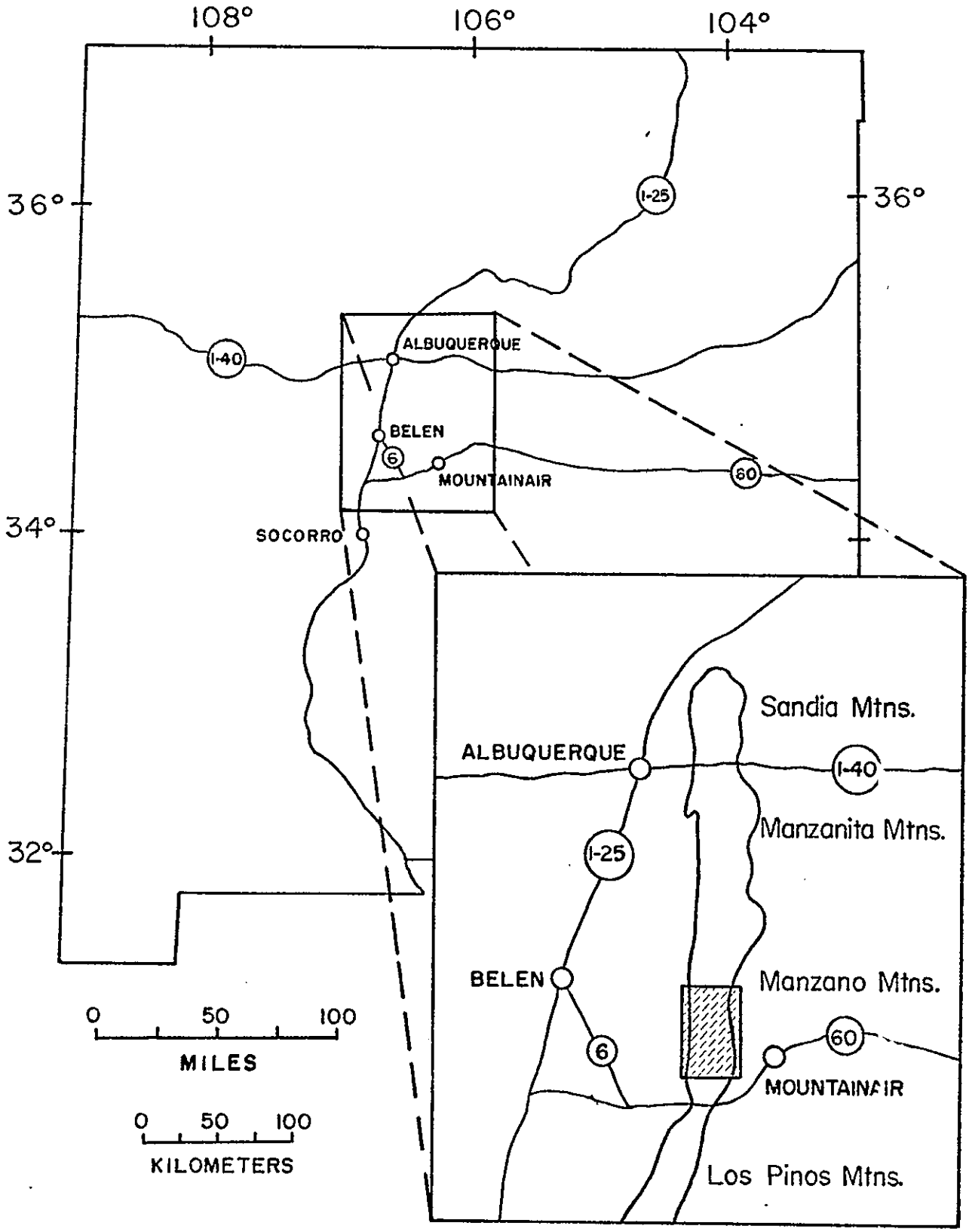

Figure 1. Index map with location of southern Manzano Mountain study area (shaded region).

respectively. Stark (1956) described an older sequence of quartzites, mica schists, metasiltstones, and phyllites composing the Sais, Blue Springs, and White Ridge units, and a younger succession of metarhyolite, amphibolite, and basic schist of the Sevilleta and basic schist units. Many interbedded lithologies are present within each of these units, although Stark's map does not show them. Stark recognized two periods of Precambrian folding: an early set of tight folds with an axial plane schistosity, and a late schistosity-forming, cross-folding event. Myers and McKay (1974) generalized Precambrian lithology and structure.

Map Area and Physiography

The present study area of approximately 40 km^2 encompasses most of the Precambrian rocks exposed within the southwest quarter of the U.S.G.S. 15-minute Torreon quadrangle, Torrance and Valencia counties, New Mexico. The area is bounded on the north by a line between Monte Largo Canyon and Manzano Peak, and on the south by latitude 34°13' (fig. 1). This area is the southern half of Stark's 1956 map of the southern Manzanos. The southwestern map area lies within the Casa Colorado land grant; the remainder of the area is within the Cibola National Forest and the Manzano Wilderness area.

Erosion in the map area has removed all Phanerozoic cover from the Proterozoic metaigneous, metasedimentary, and granitic basement rocks. The backbone of the mountain range is a northeast-trending, topographically high, linear crest formed of resistant quartzites. Elevations along this spine range from the highest point in the Manzanos

at 3078 m (10,098 ft) on Manzano Peak in the northern map area, to about 2300 m (7500 ft) in the southern area. The average elevation of the western mountain-flanking pediment gravels is about 1800 m (6000 ft), whereas the eastern Paleozoics sit at about 2300 - 2400 m (7500 - 8000 ft). Radiating from the central crest are steep-sided, east-west trending ridges. Deeply eroded canyons generally provide continuous rock exposure. In the southern area, fairly moderate relief and arid conditions result in excellent rock exposure. Farther north, a combination of steep, scree-covered slopes and abundant, dense vegetation provides outcrop exposure which ranges from poor to good.

Field Work

Field work was done between August, 1980 and May, 1982. Mapping was done on a greatly enlarged (from 1:62,500 to 1:6,000) U.S.G.S. 15-minute quadrangle map. Aerial photographs (scale 1:24,000) were used on occasion. Access to the eastern mountain flank was along Forest Service road 422 off of New Mexico route 60. Western access was provided by the multitude of primitive roads which crisscross the plains between Belen and the Manzanos.

Acknowledgments

My thesis committee of J. F. Callender, J. A. Grambling, and A. M. Kudo of the University of New Mexico, and R. C. Holcombe of the

University of Queensland, Australia provided enlightening discussion and invaluable guidance both in and out of the classroom. In particular, special thanks to J. F. Callender for his continual enthusiastic support, inspiration, and extraordinary assistance above and beyond the call of duty. D. B. Codding provided microprobe data, darkroom facilities, photographs, and an occasional bird identification. To Judy Salas thanks for brandishing such a trustworthy and virtuous drafting quill, and for all your cheerfully donated advice. J. Gomez prepared thin sections of the highest order, which were a great relief. I would also like to thank V. Grady for her flying fingers, and J. R. R. and J. D. J. for nothing in particular. I would like to congratulate my mom "Peg" for bringing me up right, and finally, I must thank the flora and fauna of the Manzano Mountains for teaching me so much.

This thesis represents partial fulfillment of the requirements of a M.S. degree at the University of New Mexico. Field work and research expenses were supported in part by grants from the New Mexico Geological Society, the Geological Society of America, Sigma Xi, and the Student Research Allocations Committee of the University of New Mexico. Field vehicles and research facilities were furnished by the Geology Department at the University of New Mexico.

PRECAMBRIAN LITHOLOGY

Previous Work

The first mapping of Precambrian rocks in this mountain chain was done by Stark and Dapples (1946) in the Los Pinos Mountains. They described five mappable units which were, from oldest to youngest: (1) the Sais quartzite; (2) the Blue Springs schist; (3) the White Ridge quartzite; (4) the Sevilleta metarhyolite; and (5) the Priest granite. Stark and Dapples mapped these units according to the dominant rock type, although they noted that the first four units contained many interlayered lithologies.

In 1949 Reiche published a report and map of the North Manzano Mountains in which he defined a series of lower metaclastic rocks (gray slates, phyllites, schistose grits) and an overlying thick series of upper metaclastics which were similar to the Sais-Blue Springs-White Ridge sequence described by Stark and Dapples. Above the metaclastics Reiche mapped a thick pile of pinkish, somewhat schistose and gneissic metaigneous rocks with minor interlayered slates, basic dikes, and sills correlative with a sequence Stark and Dapples called the Sevilleta metarhyolite. Based on the orientations of compositional layering, the contact between the lower and upper metaclastics was mapped as an angular unconformity by Reiche. Recent work by Blount (1982) based on detailed structural analysis argues that this contact cannot represent

an unconformity, but instead is either a rotational fault or a transposed boundary.

Stark (1956) completed the reconnaissance mapping of the Manzanita-Manzano-Los Pinos chain when he published a report and map of the South Manzano Mountains. He traced the five lithologic units northward into the southern Manzanos. Stark's map was based on planimetric sheets (scale 1:31,680) using aerial photographs and an altimeter for location. Due to the small scale (1:48,000) and the lack of topographic contours on Stark's geologic map, it is difficult to precisely match locations to the more recent U.S.G.S. topographic sheets. Whereas Stark generalized and grouped lithologies, the present study has detailed all lithologies possible at a scale of 1:12,000. This enhancement has resulted in the delineation of previously unrecognized major structural and stratigraphic features within the rocks. The limit of resolution on the map is about 10 m; that is, individual beds with an apparent thickness of less than 10 m were not drawn on the final map. As a matter of convenience and simplicity Stark's five formational names will be employed, but within each formation (except for the Priest granite) lithologic sub-units will be described. No stratigraphic order is implied with the use of these names.

To allay confusion related to the description of sub-units, Stark's units will be referred to as the Sais, Blue Springs, White Ridge, and Sevilleta formations so that, as much as possible, Stark's original generalized formational boundaries will apply.

Table 1 shows the structural notation used in this report.

Table 1. Structural notation used in this report (after Turner and Weiss, 1963; R. J. Holcombe, personal commun., 1982)

Metamorphic events M_1, M_2, . . .

Deformation events D_1, D_2, . . .

Fold generations F_1, F_2, . . .

S-surfaces (foliations) S_0, S_1, . . .

(S_0 = compositional layering)

Observed fold hinges B_1^0, B_2^0, . . .

(B_2^0 = a fold in S_0 with S_2 as axial plane)

Statistically defined fold axes β_1, β_2, . . .

Intersection lineations L_{10}, L_{20}, L_{21}, . . .

(L_{21} = an intersection of S_2 and S_1 as measured on S_1)

Sais Formation

The Sais formation crops out along the eastern map boundary where it is in fault contact with Paleozoic rocks to the east and is intruded by the Priest quartz monzonite to the south. The Sais can be divided stratigraphically into four major sub-units. From oldest to youngest these are: (1) Blue-gray to pinkish blue-gray, vitreous, well-recrystallized, massive to thin-bedded, medium-grained orthoquartzite. This unit is generally poorly exposed, commonly strongly fractured, lacks crossbeds, and contains color variations ranging from white to red quartzite. Local, thin, quartz-muscovite schists are exposed within the quartzite. Brecciated white-pink quartzite is seen in several areas adjacent to the Montosa fault. (2) Orange-weathering quartz-muscovite schist which grades to a distinctive red schist north of Pine Shadow Spring. (3) Red, maroon to purple, generally thin-bedded orthoquartzite containing abundant crossbeds and interbeds of spotted quartzite, thin purple and white quartzites, orange-weathering, purple quartzites, pink micaceous quartzite with very thin schistose interlayers, and dark gray quartzites. A very prominent resistant red quartzite is common in the southern area of Sais exposure. The thin-bedded purplish quartzites commonly exhibit striking fold mullions. (4) A group of generally light-colored, resistant, massive to thin-bedded, medium-grained orthoquartzites consisting of a sequence of pink-white to red, resistant, vitreous quartzite; dark, chlorite-muscovite schist; a thin-bedded, mixed sequence of quartzite and schist; and a pink-white, resistant quartzite which is locally intensely fractured.

A typical Sais quartzite is 99 percent strained, lobate quartz grains from 0.2 to 0.4 mm long, plus minor amounts of muscovite, biotite, chlorite, and opaque oxides. Coarse-grained Sais schists may consist of 70 percent muscovite, 20 percent chlorite, 10 percent quartz, and minor amounts of biotite, feldspar, and opaques. Fine-grained Sais schists may be 50 percent quartz, 30 percent chlorite, 20 percent muscovite, with minor amounts of biotite and opaque.

The Sais formation represents metamorphosed sandstones and pelites, probably deposited in either a shallow water deltaic, continental shelf, or floodplain environment. Each of these settings could form crossbedded, thin, continuous sandstone and shale beds.

Blue Springs Formation

The Blue Springs formation is a complex unit composed of various thin-bedded, fine-grained metasedimentary rocks. The bulk of this formation consists of dark chlorite-muscovite schist and finely laminated, extremely fine-grained quartzite, although other interlayered lithologies are present.

The dark chlorite-muscovite schists range from greenish-gray to dark gray and include beds of quartz-muscovite schist, fine-grained muscovite schist, medium-grained quartz-muscovite phyllite, fine-grained gray meta-argillite, and drab, medium-grained quartzite. This unit is generally conspicuous due to common lenticular and fish-hook shaped quartz veins, lenses, and pods. Elongation of these quartz features parallel to the dominant schistosity (S_2), to fold noses, and to enveloping surfaces strongly suggests that they are stretched and transposed quartz veins (fig. 2). Vein quartz may make up more than 40

Figure 2. Chlorite schist unit of the Blue Springs formation showing folded and transposed vein quartz. Trace of F_2 axial plane is vertical.

percent of some outcrops. Well developed schistosities generally are preserved, commonly with an overprinted crenulation cleavage. The large percentage of vein quartz was probably added after lithification. In thin section the rock is composed of an average of quartz, 50 percent; chlorite, 30 percent; muscovite, 20 percent; and a minor amount of opaques. Both chlorite and muscovite crystals are aligned in alternating layers of coarse-grained quartz-rich and fine-grained muscovite-rich rock. Adjacent to the Priest intrusion the schist is altered to a very dark quartz-rich silicified schist.

The thinly laminated, fine-grained, siliceous facies of the Blue Springs is brightly colored in pink, green, and gray and nearly without exception exhibits small folds. Folds are generally tight, and characteristically disharmonic (fig. 3). In thin section this rock is approximately 90 percent quartz with minor amounts of muscovite, chlorite, microcline, and opaques. The thin laminae are defined by layers of fine versus less fine quartz grains, and by differing amounts of the coloring agents chlorite, muscovite, and opaques. Quartz grains average 0.4 mm in diameter, show intense strain textures, and lack triple boundary equilibrium textures. Muscovite crystals are sub- to anhedral and are well aligned in the foliation. Adjacent to the Priest pluton this unit looses its distinctive colorful laminae, appearing as dark, massive, fine-grained siliceous rock. Thin sections show this contact facies to be biotite-rich, with an average mode of 50 percent quartz, 40 percent biotite, plus small amounts of muscovite, opaques, and sericite. Quartz grains are less than 0.05 mm in diameter, whereas scattered muscovite grains are up to 0.2 mm long, and biotite grains

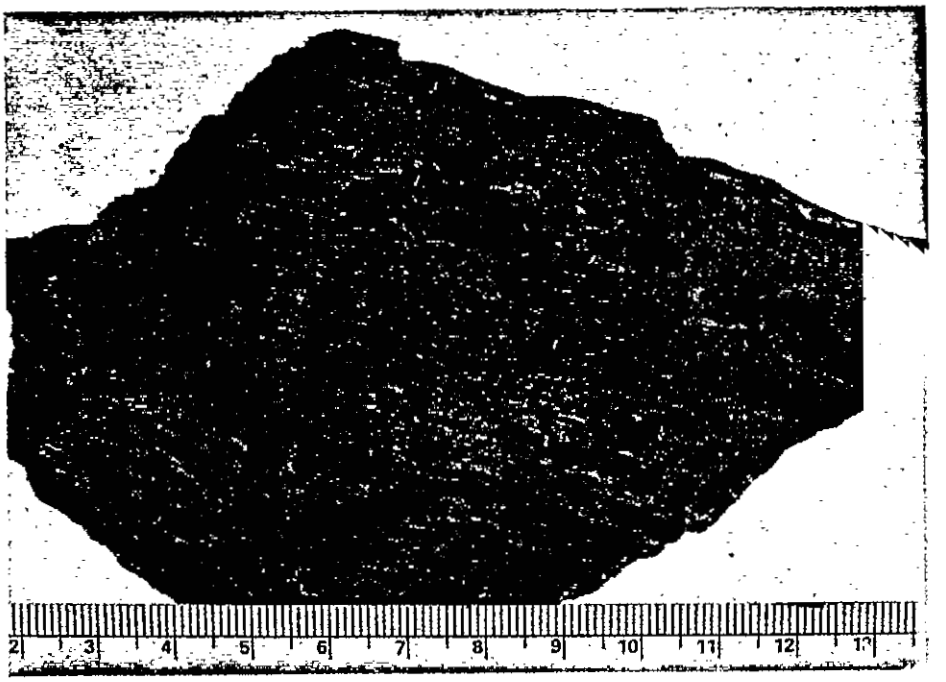

Figure 3. Fine-grained, finely-laminated quartzite facies of the Blue Springs formation. Note disharmonic folds. Scale is in cm.

generally less than 0.1 mm long. Biotite commonly is altered to a dirty yellowish green sericitic material along rock fractures.

Stark (1956, p. 8) calls this unit a siltstone and states that these rocks ". . . are only slightly metamorphosed and probably represent the original rock from which most of the highly metamorphosed sericitic, chloritic, and porphyroblastic schists were derived." Grambling (1982) refers to the rock as a metachert.

The Blue Springs formation within the map area contains none of the large, massive "quartz reefs" described by Reiche (1949), Stark (1956), and Grambling (1982) in the Blue Springs farther north.

The protolith of the laminated siliceous facies is uncertain. The thin laminations are probably either original layers or tectonic layers. The rock is siliceous enough to have been a chert, and cherts may be finely layered, but the nearly mylonitic quartz grain texture suggests caution in choosing a protolith. Grambling (personal commun., 1982) suspects the mylonite texture is post-metamorphic. The chlorite schist was probably an Fe-rich impure shale before metamorphism. These rocks may have accumulated in a fairly deep-water, low-energy basin.

White Ridge Formation

The White Ridge formation of Stark (1956) appears in outcrop on both limbs of a large synform. It is not clear that the rocks Stark called White Ridge on either side of the synform are actually stratigraphically correlative. It is more likely that they are separate

lithologies that may or may not lie on opposite limbs of a synform (for discussion see structure section).

The eastern limb consists of a sequence of generally thin-bedded resistant quartzites with interbedded schists and schistose quartzites. From east to west the White Ridge formation consists of a distinctive, red, well-recrystallized, very resistant quartzite; a schistose quartzite with thin interbeds of light-colored schist and quartzite; a pink-gray-white thin-bedded resistant quartzite; a thin, very resistant, gray quartzite; another schistose quartzite with thin interbeds of light-colored schist and quartzite; a pink to white, resistant, massive, hematitic quartzite; a gray micaceous quartzite to quartzose schist; a massive, gray, extremely resistant quartzite with thin interbeds of pink, vitreous, hematitic quartzite with local crossbeds, which underlies the highest peaks in the Manzano Mountains, and finally a thick sequence of brightly orange weathering, pinkish, micaceous quartzite. Compositional layering (S_0/S_1) and cleavage (S_2) surfaces of quartzites are commonly plated by a thin, reflective mica layer.

In places, gray to brown quartz schists with small knobs of slightly bluish quartz crop out. Grains appear extremely strained, elongated, and granulated within the dominant foliation. This rock is probably penetratively transposed rather than sedimentary in origin, as fish-hook fold noses are present and nearby crossbeds have no unique stratigraphic top direction.

In the northwestern map area the White Ridge formation supposedly reappears to define the western limb of a large synform. The eastern sequence has an apparent thickness at least five times that of the

western. The western limb consists of reddish quartzite, muscovite chlorite schist, resistant light-colored quartzite, and micaceous quartzite, and appears more similar to the eastern Sais rocks than to the White Ridge.

Typical resistant White Ridge quartzites from the eastern map area are 99 percent quartz with minor amounts of muscovite, biotite, chlorite, and opaque. The less pure quartzites contain 5 to 10 percent muscovite, biotite, chlorite, and opaque.

Based on crossbeds and lithology the White Ridge is a metamorphosed sequence of fairly well-sorted, oxidized sandstones and impure sandstones that were deposited in a shallow-water environment.

Sevilleta Formation

The Sevilleta formation is a stratigraphically and structurally complex association of metaigneous and metasedimentary rocks. More than half of the entire mapped area is composed of Sevilleta rocks. This formation contains the widest range of lithologies, and outwardly exhibits the most complex deformational patterns. Exposures of Sevilleta rocks are excellent in the southern half of the map area, becoming fair to poor in the north where vegetation and steep, scree-covered slopes reduce outcrop.

The Sevilleta formation is divided here into a western felsic metaigneous terrain and an eastern amphibolitic terrain. The boundary is drawn where one or the other becomes the more dominant rock type. The western terrain consists mainly of felsic metaigneous rock with

relatively minor amounts of amphibolite, quartzite, and schist. Felsic metaigneous rocks are generally pink or gray, blocky-fracturing, commonly somewhat schistose, with light-colored quartz and feldspar megacrysts which may be relict phenocrysts (fig. 4). Textural and compositional variations occur widely; some rocks show well-developed thin compositional bands, whereas others are massive. Generally, compositional layering is vague to absent, although parallel planar features which may be flow bands are common and range considerably in thickness. In places it is difficult distinguishing felsic metaigneous rocks from red orthoquartzite. It is not clear that all the felsic rocks described as metarhyolite in the field are actually rhyolites. One pink metarhyolite specimen (SMZ-6) turned out to have a matrix composed of as much as 70 percent fine-grained (0.05-0.1 mm) quartz crystals with plagioclase, microcline, and minor amounts of muscovite, biotite, and opaques. Megacrysts of 2.0 mm-long quartz and plagioclase crystals form elongate pods. In the matrix, quartz grains are angular, have fairly straight boundaries, and exhibit moderately well developed triple-junction equilibrium textures, whereas the quartz grains in the pods are strained, embayed, and form mosaics of sutured grain boundaries (fig. 5). Although the pods look remarkably like phenocrysts, two alternative possibilities are that they are either the product of metasomatism within an orthoquartzite, or a silicified rhyolite that has been diagenetically enriched in silica.

A more typical gray metarhyolite (SMZ-4) contains a matrix of quartz, plagioclase, microperthite, alkali feldspar, biotite, and opaques with megacrysts of the feldspars. Alternating layers of quartz-rich and feldspar-biotite-rich layers with a strong alignment of

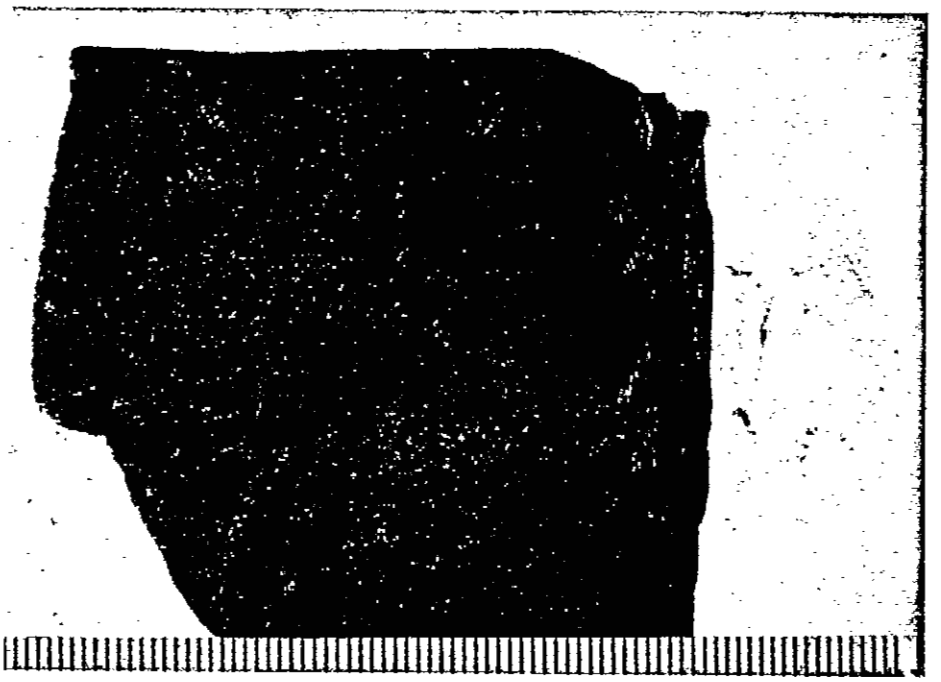

Figure 4. Typical Sevilleta metarhyolite, with white megacrysts of quartz and feldspar. Each division on scale = 1 mm.

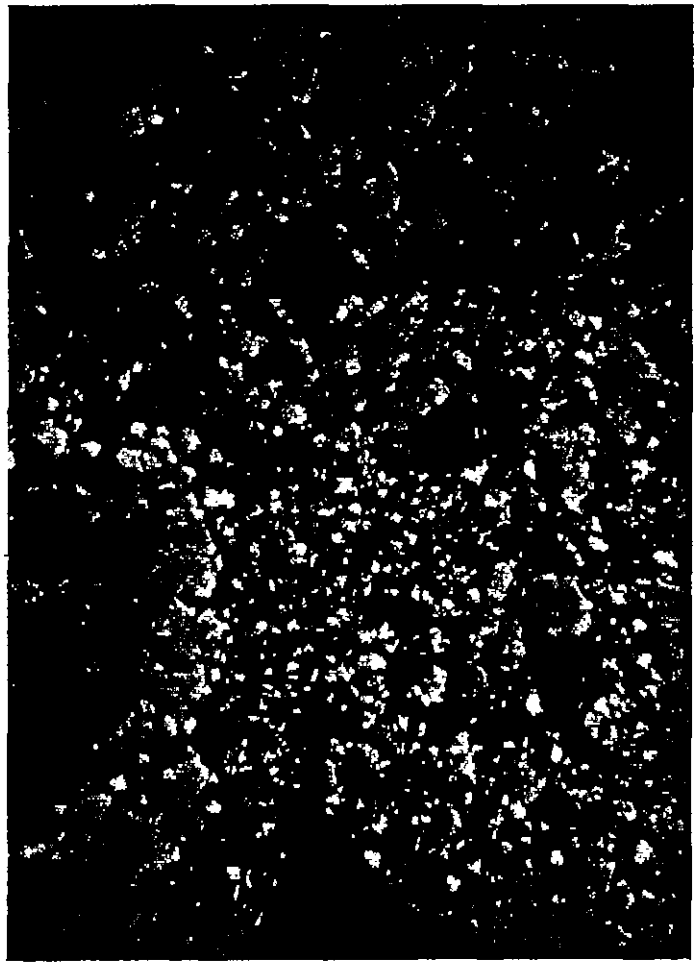

Figure 5. Photomicrograph of Sevilleta metarhyolite with plagioclase and quartz megacrysts (lower left) and fine-grained matrix of quartz-feldspar-biotite-opaques. Field is 2.9 mm across.

biotite give the rock a thinly banded gneissic look. Quartz crystals are strained, show rough equilibrium textures, and have sutured grain boundaries.

A third slightly greenish metarhyolite specimen (SMZ-17) contains a matrix of quartz, with minor biotite, muscovite, apatite, and opaques, plus 50 percent epidote. The epidote is probably a pre-metamorphic diagenetic alteration product, since crystals are aligned within the foliation. Strained megacrysts of white plagioclase 1.5 to 2.0 mm long are embayed and included by smaller quartz and biotite crystals. Quartz grains have planar boundaries and show excellent 120° equilibrium textures.

Interlayered with metarhyolites are mafic sill-like units ranging from dark green chlorite-hornblende schist to black hornblende amphibolite. These units are sparse and tend to be discontinuous. Several micaceous quartzites and schists also crop out within the large metarhyolite sequence. These mafic and metasedimentary beds indicate the large amount of internal deformation within the metarhyolitic terrain. Units pinch out along strike, tight to isoclinal folds are common, and minor copper and gold mineralization and intense brecciation and alteration occur locally.

The amphibolitic eastern terrain of the Sevilleta formation contains approximately equal volumes of mafic metaigneous and metasedimentary rock. Mafic rocks compose a wide range of textures and compositions. Some of the common facies are: (1) feldspar-hornblende schist with small lenticular feldspar megacrysts; (2) coarse-grained metadiorite; (3) chlorite-hornblende amphibolite with large coarse-grained metadioritic pods and stringers; and (4) fine- to

coarse-grained black amphibolite. In places fine- and coarse-grained plagioclase-hornblende rocks form composite units. Mafic units have apparent thicknesses from a few centimeters to more than 500 m, and may thicken, thin, fork, and pinch out along strike. Although many can be followed uninterrupted for several kilometers, a thick unit may be expressed farther along strike by two or more thinner units. In places, mafic rocks interfinger with adjacent metasedimentary rocks. Amphibolites commonly show a gradation in grain size and degree of alteration along contacts with metaclastic rocks. It is not clear whether these are chilled zones or effects caused by metamorphic recrystallizations.

Stark (1956) stated that primary igneous textures such as vesicles, amygdules, and ellipsoidal flow tops are seen in the Los Pinos Mountains within the mafic rocks. None of the rocks in the southern Manzanos show these features. Fine-grained borders and stringers of mafic schist in adjacent rocks suggest that mafic bodies in the southern Manzanos may be sills. The evidence is suggestive, but not conclusive, for hypabyssal basaltic protoliths for the amphibolites. Border zones could reflect local chemical metamorphic diffusion effects rather than chilled zones. Local minor infingering may be an original sedimentary feature, although this seems unlikely. Lateral pinching out of amphibolites may well be a deformation feature rather than an intrusive igneous morphology.

A wide variety of metasedimentary rock occurs within the amphibolitic terrain. Quartzites are generally thin-bedded, micaceous, and white to gray, although some more massive, vitreous facies are present. Well-preserved crossbeds are seen locally. Quartz-muscovite schist and quartzose schists are common. A very coarse-grained

garnet-staurolite-muscovite-biotite schist crops out in several unconnected places in the northern half of the area. This lithology provides a good marker bed and may be one infolded stratigraphic horizon. Garnet-staurolite units appear to grade northward to a prominent garnet-chloritoid schist. Chloritoid porphyroblasts are euhedral, up to 3.0 cm long, twinned, and extremely poikioblastic with quartz inclusions (fig. 6). The matrix consists of small crystals of quartz, muscovite, chlorite, garnet, and ilmenite.

A single outcrop of a very conspicuous lithology about 5 m thick occurs in section 7 near the head of Monte Largo Canyon. Smoothly rounded inclusions of granite, quartzite, and aplite, which look remarkably like rounded clasts, are set within a banded quartz schist matrix. Clasts range in diameter from less than 1 cm to more than 20 cm (fig. 7). Cross-sectional shapes range from circular to oval, with elongate clasts oriented parallel to the matrix foliation. The matrix shows alternating bands of white quartz and black schist generally less than 0.5 cm wide. Minor folds cut across the foliation; a reflective mica layering appears on compositional layer surfaces. Stark (1956) believed that this unit had an igneous matrix since he noted that it graded above and below into metarhyolite. The rounded clasts would then have been older cobbles incorporated into a rising or flowing rhyolitic magma. It is not clear that this unit grades into metarhyolite. The matrix enclosing the clasts and adjacent units look like metasedimentary rocks, and the clasts could simply be cobbles in a metaconglomerate.

Felsic metaigneous rocks may have been either rhyolitic ash-flow tuffs or rhyolitic flows. No direct evidence exists for either interpretation. The interbedded metasediments and mafic rocks may be

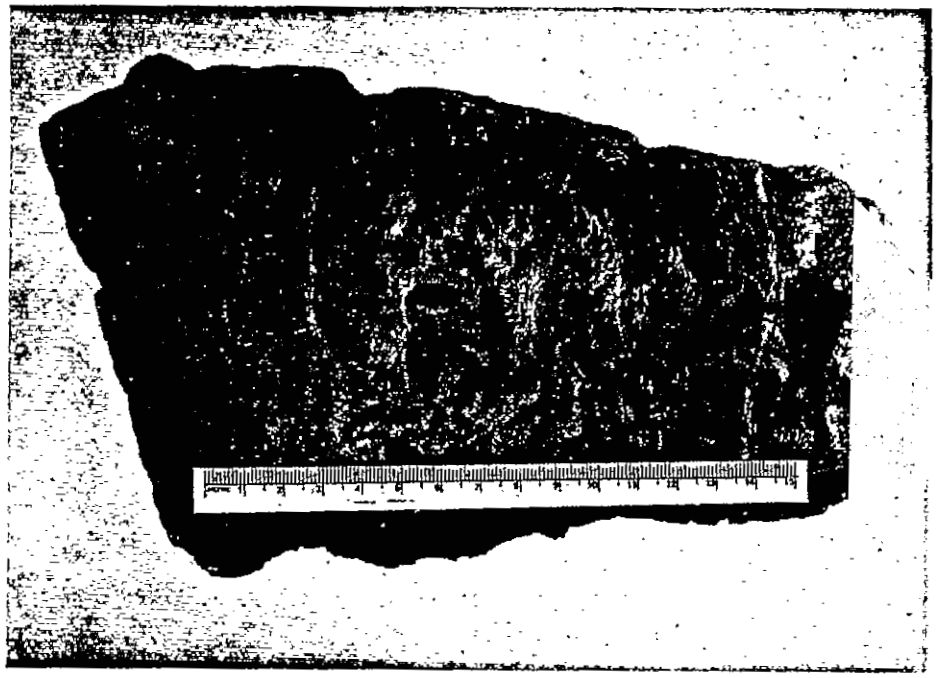

Figure 6. Chloritoid-muscovite schist of the Sevilleta formation. Chloritoid porphyroblasts are up to 3.0 cm long. Scale is in cm.

Figure 7. Rounded clasts of aplite in a schistose matrix from the Sevilleta formation in Monte Largo Canyon. Pencil is 15 cm long.

either structurally infolded or stratigraphic layers within the felsic metaigneous stack.

Amphibolites and mafic schists are discontinuous along strike and interfinger with adjacent metasediments. Based on this and their mineralogy these rocks were probably either basaltic sills or flows.

Priest Quartz Monzonite

The Priest pluton is largely " . . . a coarse grained biotite-quartz-feldspar phanerite with large phenocrysts or porphyroblasts of light-pink microcline" (Stark, 1952, p. 19). The Priest is more precisely a quartz monzonite. Fresh surfaces are pink, whereas weathered rock is gray and crumbly. Dikes of pegmatite, aplite, quartz, and epidote intrude the nearby country rock. Inclusions of metasedimentary rock are common around the intrusive contact. Penetrative fabric is not seen in the Priest quartz monzonite. For an expanded discussion on the petrology and structure of the Priest pluton, see Stark (1956, p. 19).

STRUCTURE

Previous Work

"Careful search was made for any structures that might indicate overturning, but, . . . no evidence was found of close folding or repetition of beds."

Stark and Dapples, 1946, p. 1140

"Precambrian folds in the area are, with one very minor exception, possibilities, not demonstrated facts."

Reiche, 1949, p. 1197

Early workers in the Precambrian rocks of the Manzano-Los Pinos chain concluded that the structural history of these rocks was straightforward. Stark (1956), however, described two episodes of Precambrian folding in the South Manzanos; an early folding of metaclastics into a large, northeast-trending syncline, and a later, mild cross-folding with development of small crenulations. Mallon (1966) recognized three periods of folding; the two Stark described plus an earlier period of isoclinal folding. Recent workers within these rocks have recognized these three deformations (Bauer, 1982; Cavin and others, 1982; Grambling, 1982; Blount, 1982).

Primary Structures

Unambiguous crossbeds within the purple quartzite unit of the Sais formation consistently indicate that these westward-dipping beds are

right-side up. Crossbeds are well preserved and delineated by either thin hematitic layers or purple and white laminae. Numerous minor folds have bent this unit, and consistently west facing crossbeds attest to fold asymmetry.

Additional local crossbeds, usually defined by thin, dark, hematitic layers in quartzites of the Sevilleta and White Ridge formations (fig. 8), do not consistently indicate tops. Closely spaced crossbeds in these rocks commonly show opposing tops.

Unambiguous graded beds are rare. Thin, interlayered, coarse-grained and fine-grained pelitic beds are seen, but the certainty of stratigraphic tops is low. Graded beds were recognized microscopically in one quartzite sample.

Geometry

Foliations

S_1 Axial plane foliation. Compositional layering (S_0) and the S_1 cleavage are generally parallel at the outcrop. S_1 is seen microscopically only in quartz-rich layers of alternating quartz and mica-rich domains of some micaceous schists. Within these compositional layers small muscovite, and in some samples chlorite plates show a penetrative fabric of preferred orientation oblique to compositional bands. In the center of the quartz-rich layers, micas may be perpendicular to the compositional boundaries, but swing around into the compositional band orientation adjacent to the mica-rich layers. Locally S_1 appears as an apparent spaced cleavage (fig. 9). In one

Figure 8. Well-preserved, overturned cross-bed in a White Ridge quartzite. Lens cap is 5 cm in diameter.

Figure 9. Photomicrograph of apparent spaced S_1 cleavage formed by differentiated layers of mica and quartz in pelitic chlorite schist of the Sevilleta formation. Field is 2.0 mm across. S_1 is vertical in picture.

thin section muscovite/quartz compositional layering is cut by a strong schistosity which may be S_1 (fig. 10). No cleavage is parallel to the compositional layering. This was the only section in which S_0 and S_1 were strongly discordant.

Several transposition textures thought to represent F_1 deformation have been identified. Pods and stringers of light-colored plagioclase and quartz, elongate parallel to compositional layers, float in a matrix of black, hornblende-rich rock in some Sevilleta amphibolites. In nearby beds these light minerals have formed somewhat discontinuous compositional layers within the mafic rock (fig. 11). Scattered, small, fishhook shaped fold noses sit isolated from other silicic layers. A second mesoscopic transposition texture in what may be a metachert is similar to the amphibolite texture. Small, elongate, en echelon pods composed of quartz grains sit in a microcrystalline quartz matrix. Microscopically, these pods are a mosaic of strained quartz grains with lobate boundaries. In quartzites, isolated isoclinal fold noses and blobs of quartz elongate parallel to S_0/S_1 are suggestive of transposition (fig. 12).

All contoured stereograms are lower hemisphere equal-area stereographic projections contoured using the Kalsbeck counting grid. Figure 13 is a contoured equal-area stereographic plot of poles to S_0/S_1. The statistical pole maximum at S65°E, 29° corresponds to S_0/S_1 planes oriented at N25°E, 61NW.

S_2 Axial plane foliation. S_2 is the dominant mesoscopic and microscopic penetrative fabric element in nearly all rocks. It is a well-spaced crenulation cleavage, with a metamorphic differentiation in

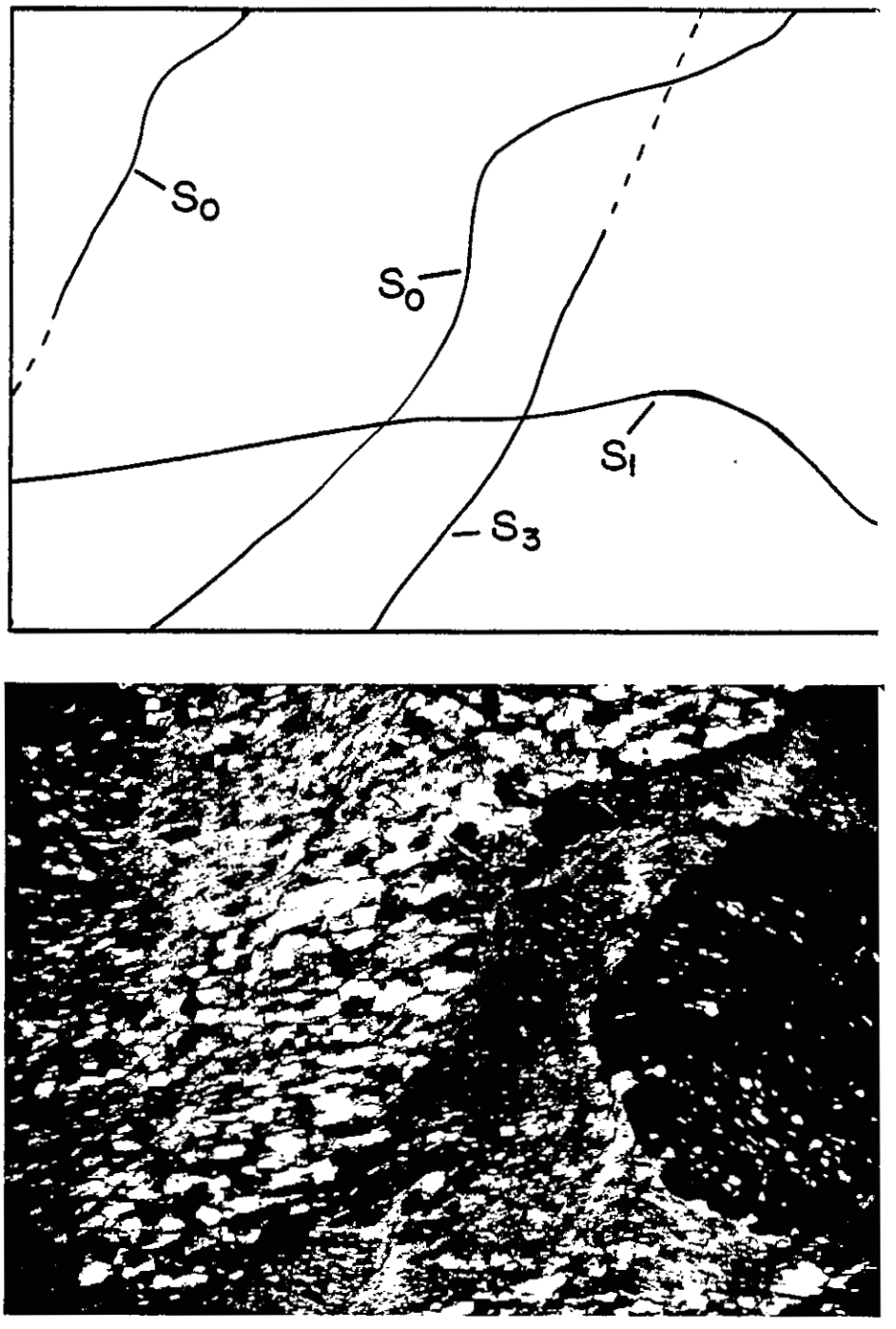

Figure 10. Photomicrograph of S_0, S_1, and S_3 in garnet schist of the Sevilleta formation. Note garnet with folded S_1 helicitic quartz inclusions. Orientations of S_0, S_1, and S_3 shown in sketch above.

Figure 11. Apparent S_1 transposition layers of white feldspar-rich rock within black amphibolite beds of the Sevilleta formation. Lens cap is 5 cm across.

Figure 12. Isolated F_1(?) fold noses in a thin-bedded quartzite of the Sevilleta formation. Isolated quartzite pod near base of sample may be an F_1 nose, whereas the more obvious fold noses above may be F_2 features. Smallest divisions on scale are mms.

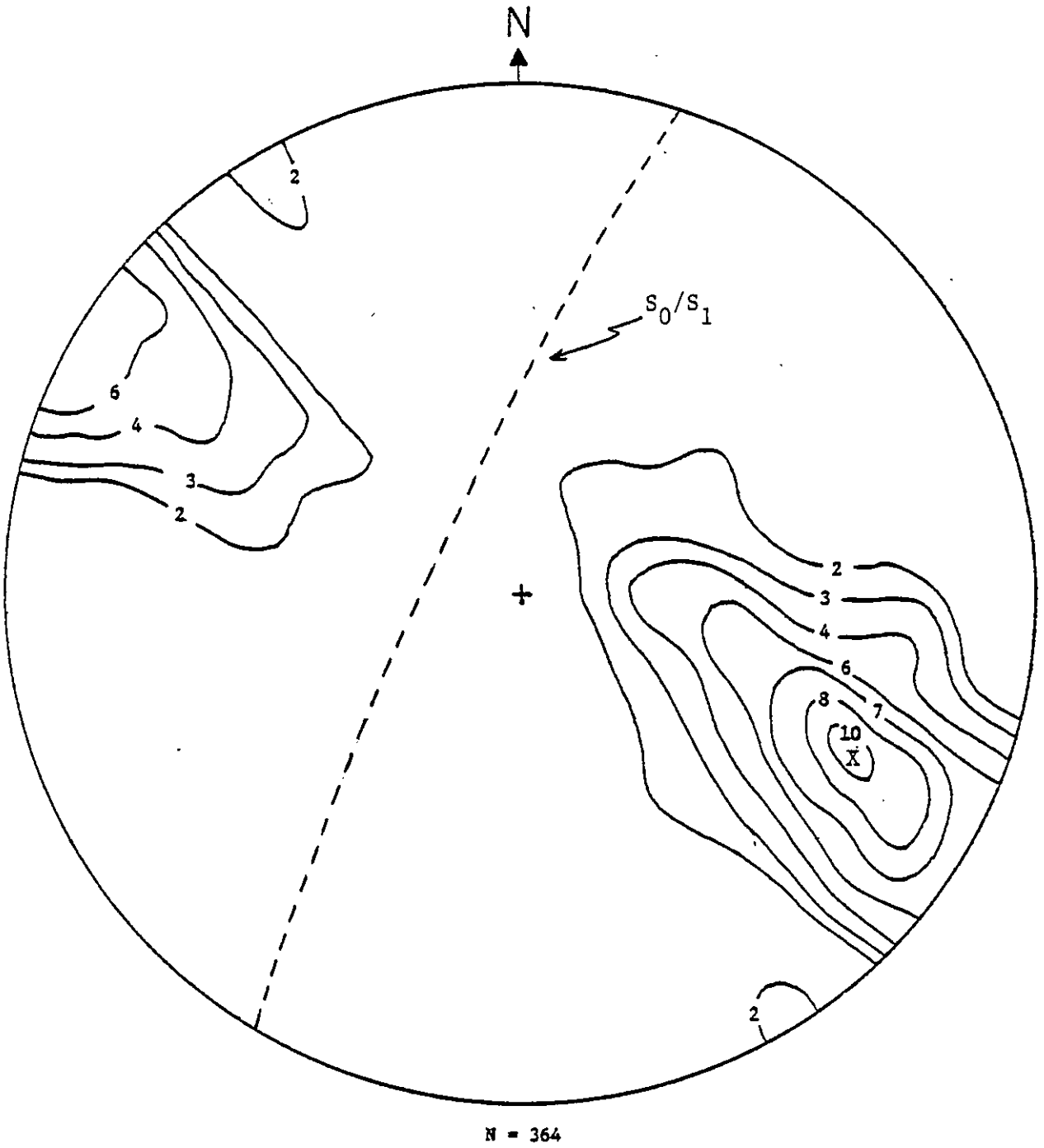

Figure 13. Contoured equal-area, lower hemisphere stereographic projection of poles to S_0/S_1. The pole maximum (X) corresponds to planes oriented at N25°E, 60°NW. Percentages as shown on contours. N = number of data points.

schists defined by alternating compositional layers of quartz-rich and mica-rich rock. Layers are spaced at about 0.5 to 2.0 mm, with quartz layers generally wider than mica layers. Muscovite, biotite, chlorite, hornblende, and commonly quartz crystals show a strong preferred orientation parallel to compositional layers. S_2 mica layers have clearly rotated and aligned discordant S_1 micas (fig. 14). In quartzites a preferred orientation of inequant crystals probably represents the S_2 cleavage. Some amphibolites show well developed S_2 hornblende alignments. The crenulated nature of S_2 is not apparent in most hand specimens. Instead, S_2 appears to be a well developed schistosity. Only in certain rocks is a regular compositional lamination of alternating light-colored, quartz-rich and dark, mica-rich layers seen. Rarely, cleavage lamallae on weathered schist surfaces appear as very thin, regularly spaced layers of raised relief. S_2 commonly cuts across S_0/S_1, although mesoscopic differences between S_1 and S_2 are so slight that in the absence of S_2, S_1 could be mistaken for S_2, or vice versa. In a few localities overprinting metamorphic differentiation along both S_1 and S_2 foliations is beautifully developed. In these rocks a strong S_1 mineralogical segregation has been partially rotated and destroyed by an incipient S_2 differentiated cleavage with local transposition (fig. 15).

A contoured stereogram of poles to S_2 (fig. 16) shows a pole concentration at S67°E, 20° which represents a concentration of S_2 planes at N23°E, 70°NW.

F_2 transposition textures are beautifully exhibited in the quartz vein-rich chlorite schist of the Blue Springs formation (see fig. 2). The orientations of veins, hooks, pods, and lenses of quartz indicate

Figure 14. Photomicrograph of Sevilleta schist showing micas aligned in S_2 crenulation cleavage. Note quartz-rich and mica-rich S_2 layers and discordant S_1 micas within quartz-rich layers. Field is 2.9 mm across.

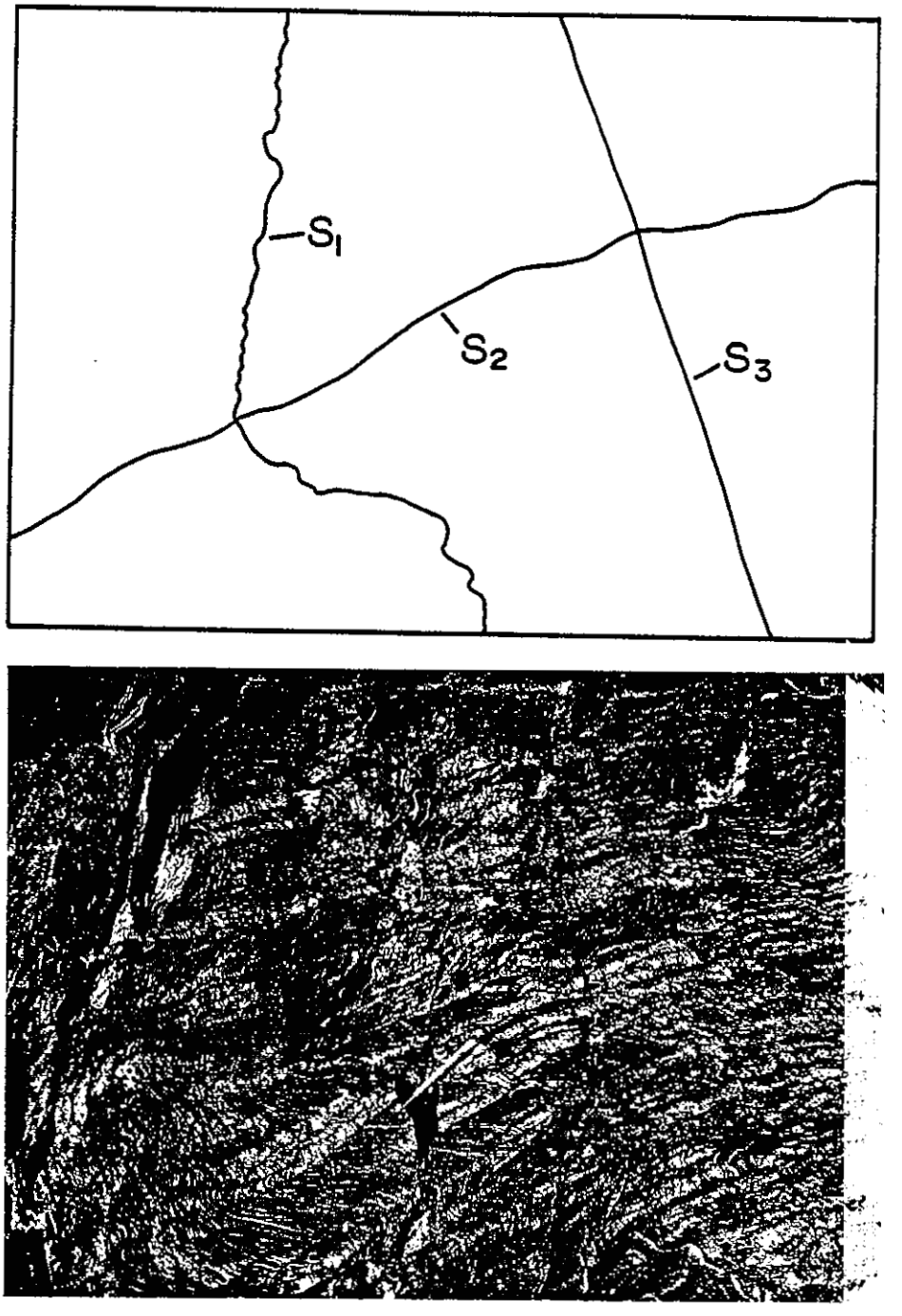

Figure 15. Micaceous quartzite from the Sevilleta formation with mineralogically segregated layers parallel to both S_1 and S_2. S_1 is parallel to folded thin layers which generally run vertically. S_2 overprints S_1 and is parallel to the blue pencil. Pencil is 15 cm long.

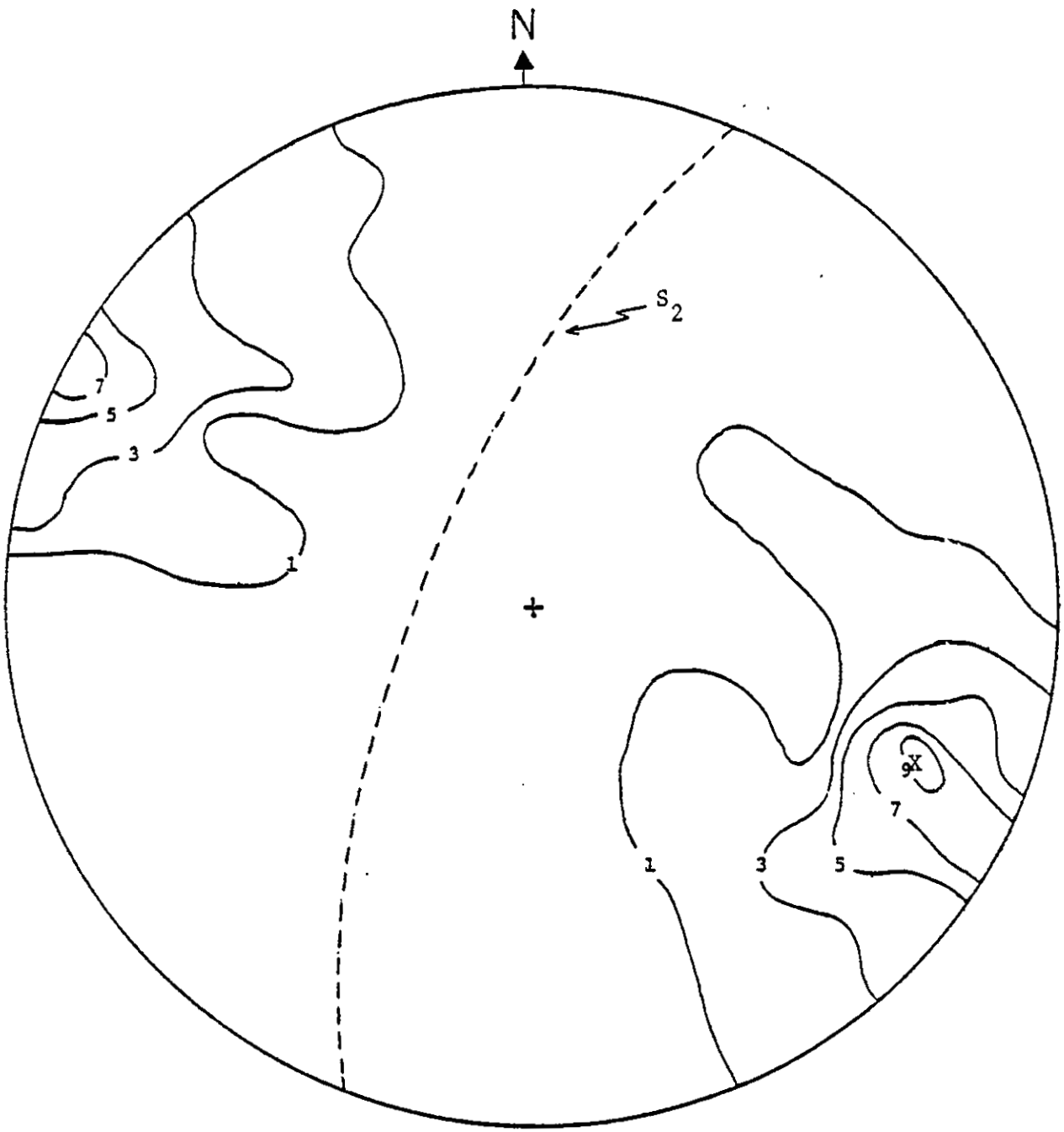

Figure 16. Contoured equal-area lower hemisphere stereographic plot of poles to S_2. Statistical S_2 plane maximum at N23° E, 70° NW. Percentages as shown on contours. X = pole maximum. N = number of data points.

that quartz veins have been stretched, broken, and locally rotated into S_2. There are other obvious transposition features within the quartzites, schists, and amphibolites of the Sevilleta, Sais, and White Ridge formations. The whole spectrum of the transposition process, from attenuated fold limbs through rotated and broken limbs, to isolated pods and fishhook fold noses, to new compositional layering can be found throughout the field area.

S_3 foliation. S_3 is a well-spaced planar fabric defined by kink fold hinges 0.5 to 2.0 cm apart in hand specimens of micaceous schist. Microscopically the S_3 fabric is formed by kink bands geometrically forming axial planes without having developed true mica cleavage planes. Only in the most schistose rocks are S_3 planes true crenulation cleavages (fig. 17). In less micaceous rocks S_3 is defined by synchronous mica extinction across folded micas as the section is rotated under doubly polarized light. S_3 clearly overprints S_2, with the angle between them generally greater than 60°. In one section two late, possibly conjugate, crenulations (S_{3A} and S_{3B}) cut S_2.

Figure 18 is a contoured stereogram of poles to S_3. Mean pole and plane orientations are at N25°E, 50°, and N65°W, 40°NE.

Lineations

Every S_0/S_1 surface in the southern Manzanos seems to show at least one intersection lineation. Extension lineations, generally biotite streakings, are scarce. Quartzites and metarhyolites generally

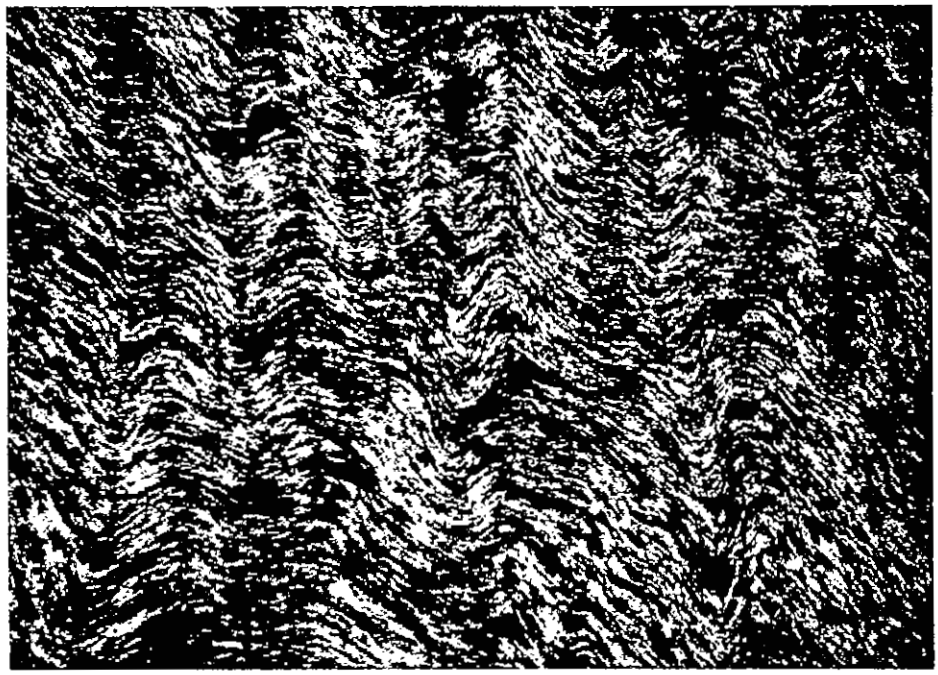

Figure 17. Photomicrograph of axial traces formed by S_3 foliation in Sais mica schist. S_3 is vertical. Kinked S_2 foliation is horizontal. Field is 2.9 mm across.

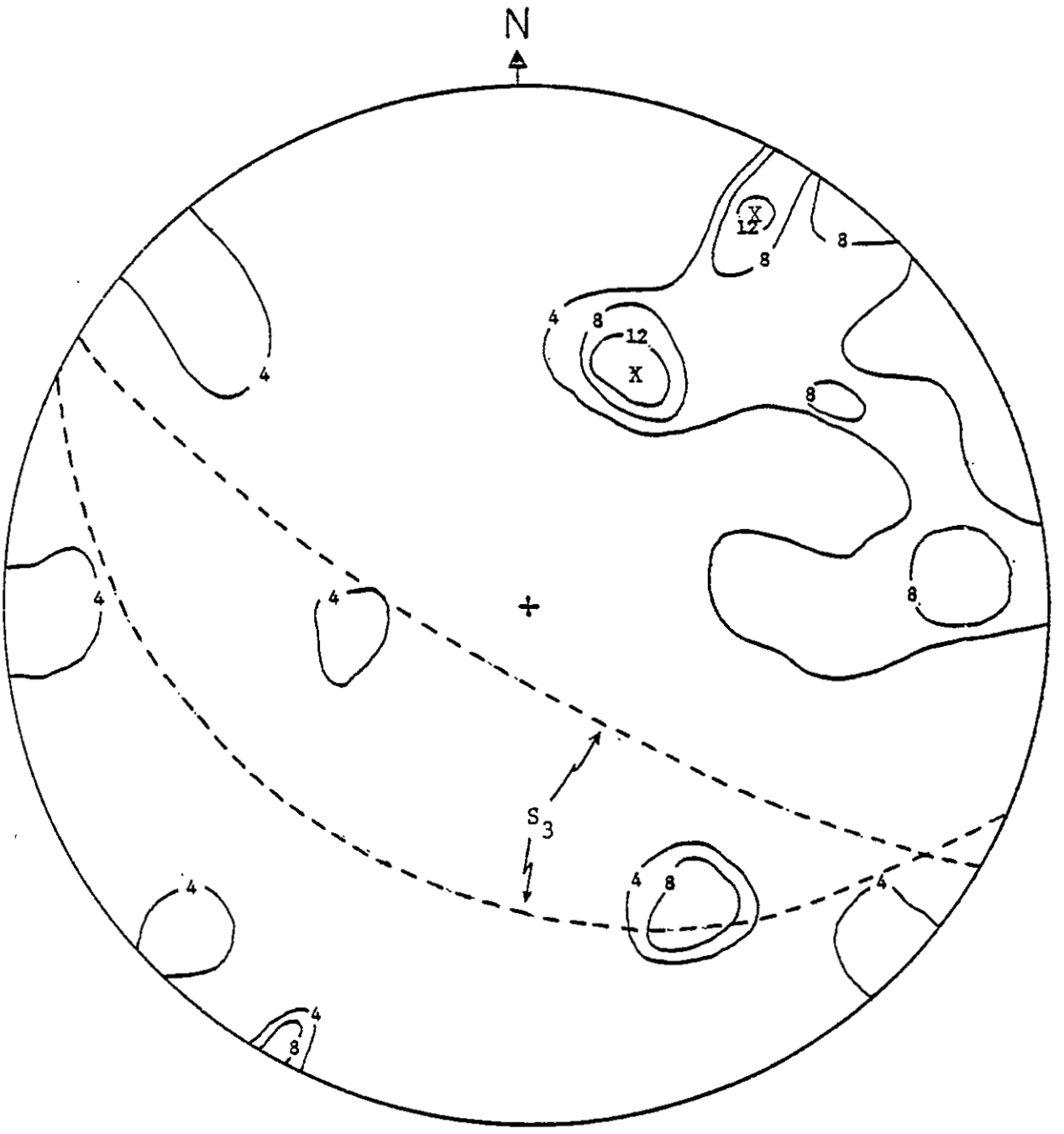

N = 25

Figure 18. Contoured equal-area, lower hemisphere stereographic plot of poles to S_3. Two statistical S_3 planes from double pole maxima at N65° W, 48° SW and N58° W, 12° SW. Double high may represent a conjugate kink set, although more data points are needed to be sure. Percentages as shown on contours. X = pole maximum. N = number of data points.

show only one intersection lineation, whereas schists commonly show two or three well defined lineations (fig. 19). On the S_0/S_1 surface, lineations may be distinct compositional bands, broad crenulations, fine crenulations, or very fine mica partings. Whether lineations are visible or not is more dependent on lithology than on location. In places it is possible to visually match a lineation with the intersection of S_0/S_1 and S_2; generally however it is not, and only attitudes and descriptions can be recorded.

The thinly laminated facies of the Blue Springs formation shows a very persistent lineation which appears to wrap around folded S_0/S_1 surfaces. This lineation has the look of a slickenside but lies in a plane oblique to the fold axis. Grambling (1982) reports that within a small mapped area in Trigo Canyon this same lineation is always contained within a plane normal to fold axes. This variation may be a function of the plunge of early fold axes.

A contoured sterogram plot of L_{10}, L_{20}, and L_{21} intersection lineations shows a strong statistical concentration about S44°W, 28° (fig. 20).

Minor Folds

F_1 Minor Folds. Rarely seen, but very distinctive, are small intrafolial F_1 isoclinal folds. This style most commonly is observed in thin-bedded quartzites and schistose quartzites of the Sevilleta formation (fig. 21). Unless the fold nose is clearly visible these folds may easily be overlooked. S_1 axial plane cleavage is parallel

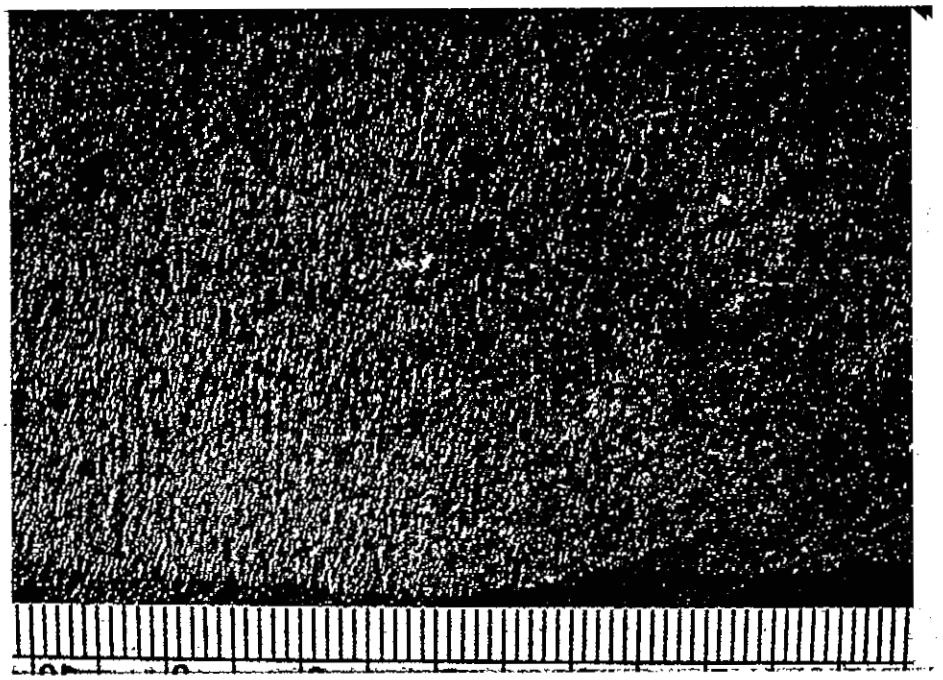

Figure 19. Crossing L_{21} and L_{31} intersection lineations on S_1 surface of Sais schist. Inclined line is parallel to L_{21}. Upright line is parallel to L_{31}. Numbered divisions on scale are cms.

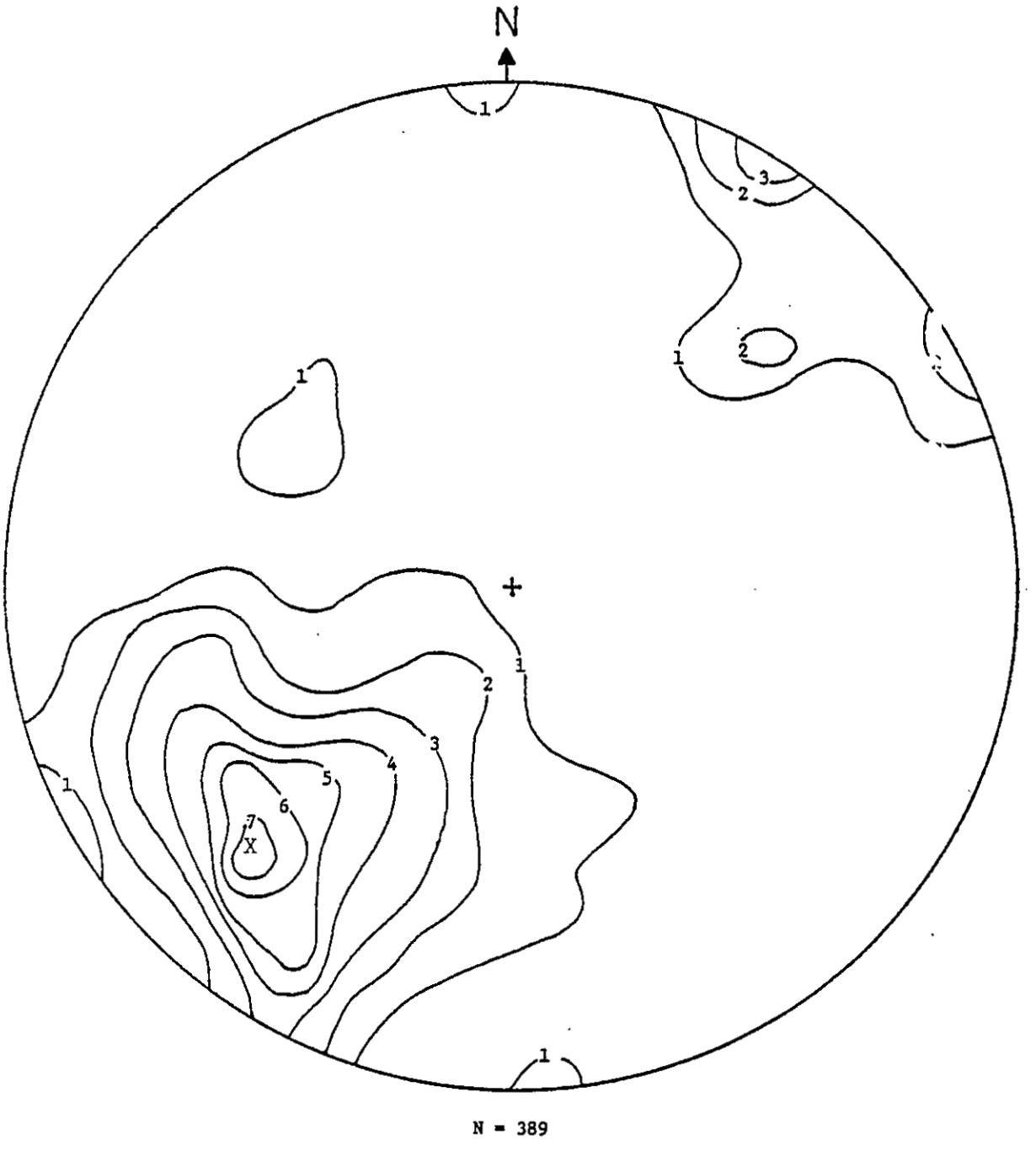

Figure 20. Contoured equal-area, lower hemisphere stereographic plot of L_{10}, L_{20}, and L_{21} intersection lineations. Statistical maximum (X) oriented at S44° W, 28°. Percentages as shown on contours. N = number of data points.

Figure 21. Isoclinal F_1 fold in thin-bedded quartzites of the Sevilleta formation. View south across Pipe Canyon. Picture is about 3.0 m across.

to compositional layering; F_1 fold axes (B_1^0) generally plunge southwest at about 30°.

F_2 Minor Folds. More common than F_1 folds, or perhaps more visible, are open to close to tight, typically asymmetric and disharmonic F_2 folds observed in all lithologies. Examples of these patterns are seen in hand samples of the colorfully laminated Blue Springs rocks (fig. 22). Minor folds in quartzites have larger wavelengths and amplitudes than those in schists. Most examples in quartzite layers are smoothly rounded around fold closures, whereas less competent beds contain abundant kinks, chevron folds, and parasitic folds. A spectacular folded outcrop of quartzites and schists occurs in Estadio Canyon. Two overturned, tight, F_2 antiforms 12 m high in hematitic quartzite seem to have formed with the intervening synform apparently sheared out (fig. 23). Fold axes trend N25°E and plunge 5°NE; axial planes are oriented at N24°E, 58°SE. Above the quartzite, garnet schist and thin-bedded quartzites contain numerous disharmonic F_2 folds, some with similarly absent synforms.

A very revealing outcrop located near the gold mine one kilometer north of Monte de Abajo Canyon in schists and quartzites of the Sevilleta formation shows F_1 isoclinal folds with axes bearing from S20°W to S10°E and F_2 open folds with axes bearing from S55°W to S40°W; F_1 folds plunge from 45° to 59°, F_2 folds plunge from 42° to 54°. Outcrops such as this, in which both F_1 and F_2 folds are visible, are rare.

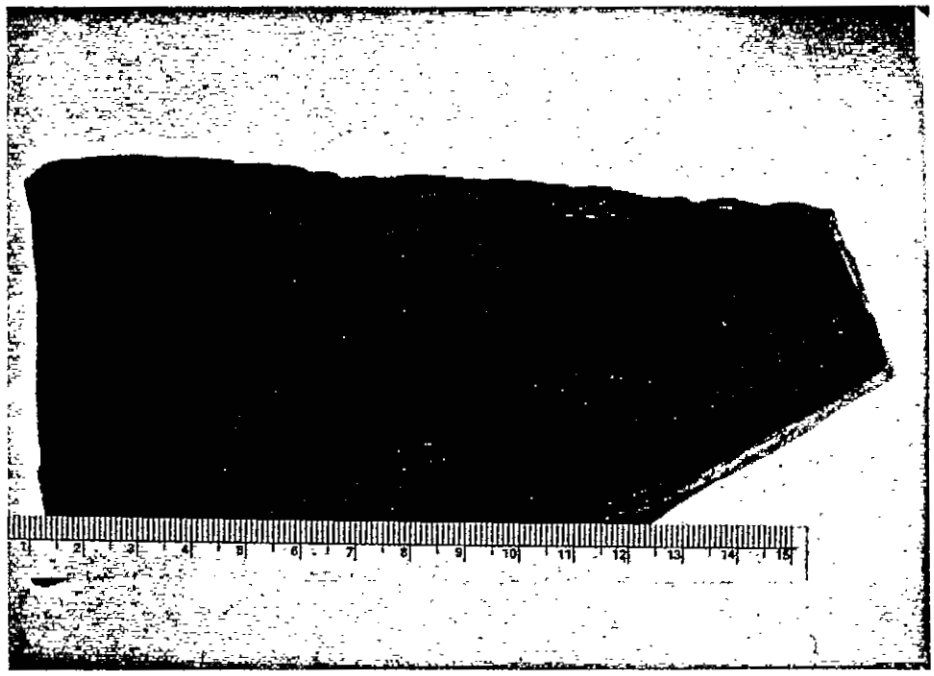

Figure 22. Disharmonic F_2 folds in sample of laminated Blue Springs formation. Scale in cm.

Figure 23. Tight, overturned F_2 antiforms with sheared-out intervening synform in Estadio Canyon. View to the north. Geologist on fold nose in center of photo is 1.7 m tall.

The contoured equal-area plot of B_2^0 fold axes shows a strong statistical grouping at S45°W, 35° (fig. 24).

F_3 Minor Folds. F_3 mesoscopic folds are areally insignificant with respect to F_2 folds. Scarce, small (0.5 to 2.0 cm in wavelength) kink bands form sharp, angular, generally symmetric chevron folds in schists and thinly bedded quartzites (fig. 25). Fold shape remains fairly constant throughout different layers, defining similar type (Class 2) folds, although in very schistose rocks thicknesses of individual layers remain constant, defining parallel folds (Class 1); Ramsay, 1967). F_3 folds commonly die out over distances of tens of centimeters. Broad, smooth F_3 folds have formed in less micaceous rocks such as thin-bedded quartzite.

Major Folds

F_1 Major Folds. No map-scale F_1 folds have been recognized.

F_2 Major Folds. Stark (1956) believed that the major structure in the area was an overturned, gently plunging syncline whose axis followed the center of the Sevilleta formation. Evidence supporting this fold included bedding-cleavage vergence data, minor folds, and exposures of the Blue Springs and White Ridge rocks on either side of the Sevilleta. S_0/S_1-S_2 vergence data do not consistently nor convincingly designate synform towards Stark's proposed fold axis, although vergences consistently point synform to the west along some east-west traverses through the Sevilleta amphibolitic terrain. S_0/S_1-S_2 relationships are poorly exposed within the metarhyolite

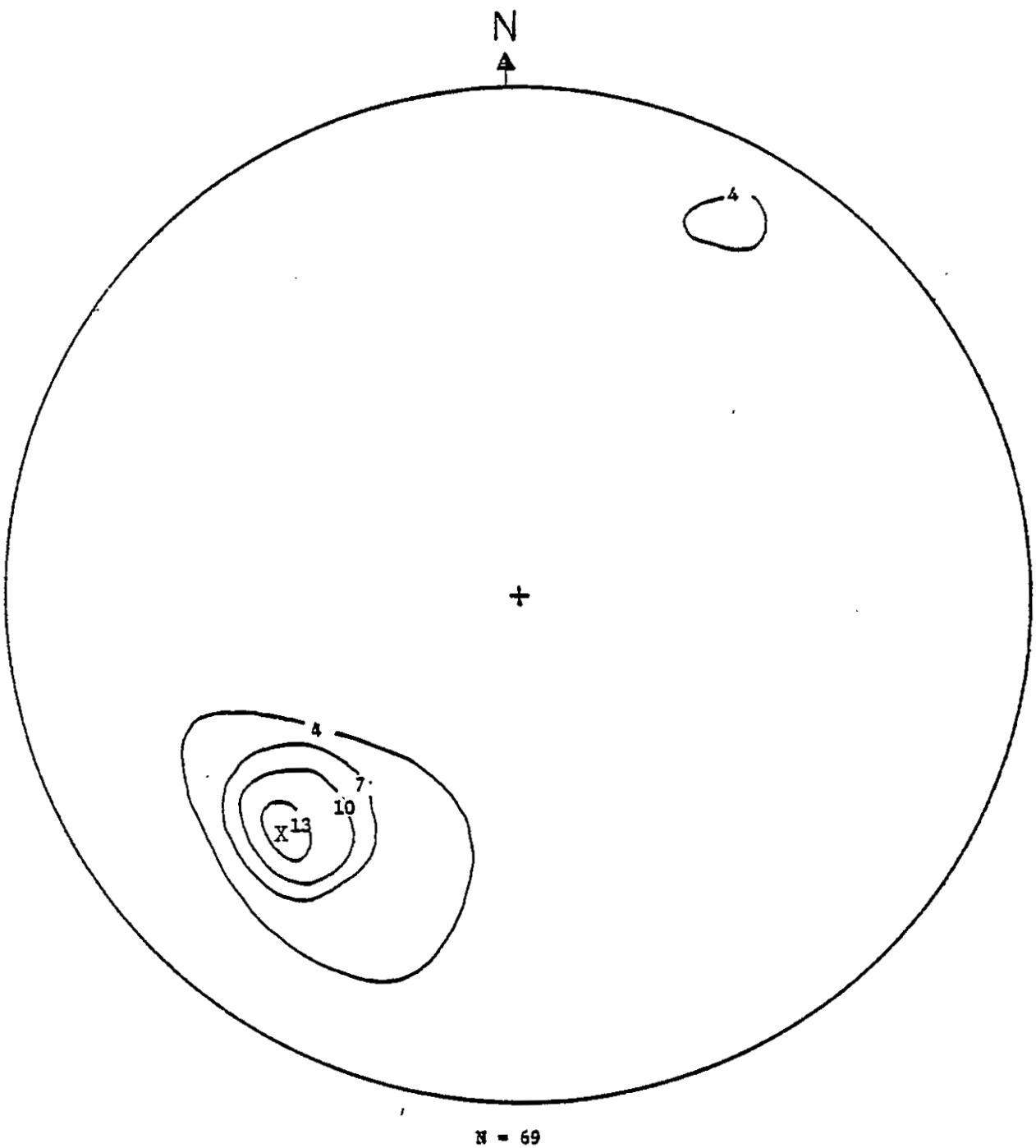

Figure 24. Contoured equal-area, lower hemisphere stereographic projection of B_2^0 fold axes. Statistical maximum (X) at S45°W, 35°. Percentages as shown on contours. N = number of data points.

Figure 25. F_3 chevron folds in Sevilleta schist. Scale is in cm.

terrain; most data are taken on the thin, infolded metasedimentary beds within the metarhyolite. A detailed examination of Stark's large synform is found in the discussion section.

The west-central map area contains 2 - 3 km^2 of extremely complex amphibolitic terrain. Beds of amphibolite and schist pinch out along strike, S_0/S_1 is folded and ranges from vertical to horizontal. Several large southwest-plunging F_2 antiforms and synforms infold amphibolites and quartzites into a monotonous repetitive sequence. Transposed bodies of garnet schist sit within amphibolite folds and bedded quartzites and as elongate pods.

Characteristically, most rocks outside of this deformed area in the amphibolitic terrain are steeply dipping. As one stands on a ridge looking along strike across a canyon to the next ridge, one commonly sees the dip direction of S_0/S_1 switch from east to west over a distance of less than 200 m but rarely are fold noses of any of these large F_2 folds seen.

The northwestern part of the map area contains a region of intense deformation and mineralization within the Sevilleta metarhyolite. Numerous southwest-plunging folds defined by schist, quartzite, and amphibolite beds commonly die out along plunge. Much of this area is strongly brecciated, with copper oxides coating fracture surfaces. Shallow prospect pits dot the area, including a small operating gold mine. The folded metasediments and amphibolites are probably minor folds on a large F_2 fold.

The eastern part of the map area is dominated by a large, overturned, southwest-plunging F_2 synform cored by laminated Blue Springs formation. The fold is tight, although the coincidence of

topography and fold plunge lend it an isoclinal map expression. The overturned western limb dips steeper than the eastern limb. S_0/S_1-S_2 vergences are not all consistent with the observed geometry. Numerous, smaller, southwest-plunging, disharmonic F_2 folds occur north of the large synform (fig. 26). A particularly well exposed overturned antiform in sections 17 and 18 presents some geometric problems. The chlorite schist unit of the Blue Springs clearly folds around the major synform, yet the adjacent gray quartzite which forms the antiform strikes off to the north without seeming to reappear outside the schist on the western limb. This anomaly will be addressed in the discussion section.

F_3 Major Folds. No map scale F_3 folds are recognized.

Faults

The Paloma fault is a relatively poorly-defined and poorly dated structure which separates Sevilleta and White Ridge rocks from the other Precambrian rocks to the east. The fault runs from the southern map area northeast through Manzano Peak, paralleling compositional layering much of the way. Although it is well constrained in the southern area, the fault is difficult to trace north of the Priest pluton. Near Estadio Canyon, in the southern map area, thin, folded, garnet schist beds can be traced to the fault where the beds appear to be truncated. A slice of garnet schist is juxtaposed against the fault on the ridge north of Estadio Canyon. Half a kilometer north the fault intersects a second garnet schist bed which parallels the fault for two kilometers

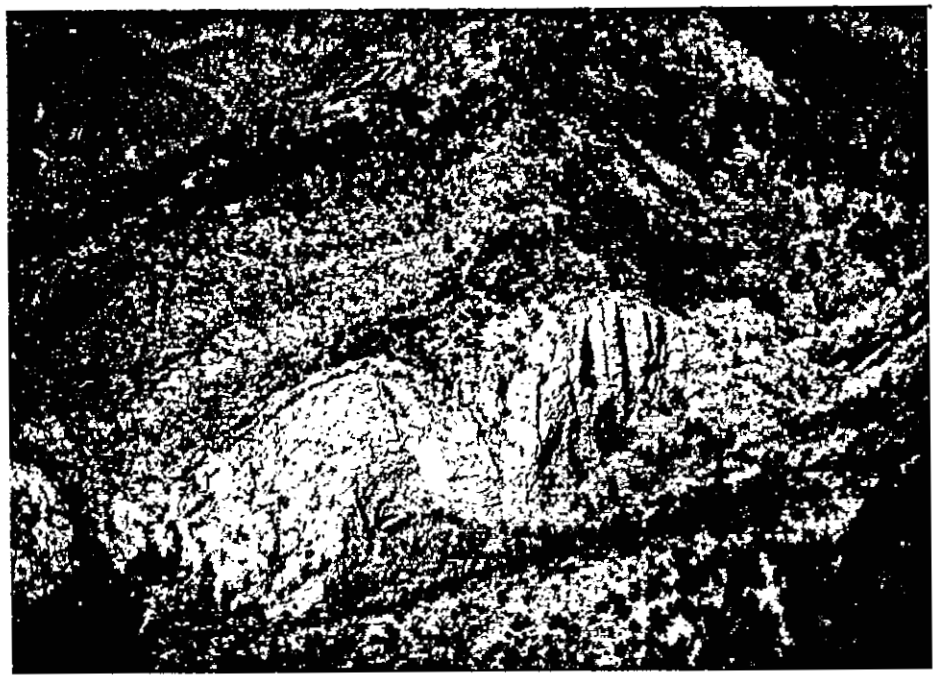

Figure 26. Aerial photograph looking south of large, southwest-plunging F_2 folds in Sais quartzite, about 1.5 km northwest of Pine Shadow Spring. Wavelength of folds is 150 m.

northward. The Paloma appears to be parallel to S_1 foliation from this schist intersection northward. The fault trace on topography indicates that the fault plane dips steeply to the west. Slip, separation, and timing of movement(s) are unknown, although Stark (1956) states that it is a Laramide age reverse fault. Stark's evidence is based on the Paloma's relationship to the better understood Montosa fault to the east.

The Montosa fault is a west-dipping reverse fault which separates Precambrian from Paleozoic rock. Slip is unknown along the Montosa but must be a minimum of 2000 m since eroded Precambrian rocks are exposed on the upthrown block at over 3000 m elevation, whereas Permian rocks sit at 1000 m elevation on the downthrown block. Paleozoic strata are commonly overturned into drag folds along the fault (fig. 27). Fault breccia generally is seen in quartzites adjacent to the fault. Stark's Laramide age for the Montosa is demonstrated in the Los Pinos Mountains, where the fault cuts Cretaceous limestones but is overlain by undisturbed Tertiary volcanics. Stark notes that the Paloma and Montosa faults merge 5.5 km south of Capilla Peak and continue northward as the Montosa thrust. Stark assumes that they are contemporaneous since they join and have somewhat similar styles. However, the Paloma could very well be older than the Montosa, although evidence constraining the Paloma's age more precisely is totally absent. It is not clear where the Paloma lies in the northern map area. Orientations of White Ridge, Blue Springs and Sais rocks are parallel in this area. Judging from its last known location near the Priest intrusion, the fault lies between the resistent unit of the White Ridge and the Blue Springs schist to the east.

Figure 27. Aerial photograph looking north of Precambrian rocks to west separated from Paleozoic rocks to the east by the Montosa fault. Fault is buried on slope east of central canyon. Note overturned Madera Group sediments along eastern fault boundary.

Summary

Table 2 summarizes the geometry of the structure in the southern Manzanos. Figure 28 illustrates some outcrop-scale fold interference patterns between these three folding events.

Table 2. Summary of geometry of folding events in the southern Manzano Mountains.

EVENT	DESCRIPTIONS
F_1	S_1-strong schistosity generally parallel to bedding(S_0); may be the dominant foliation in some outcrops; strong transpositional layering. Isoclinal, intrafolial F_1 folds commonly plunge southwest; closures rarely seen in outcrop. L_{10} generally indistinguishable from L_{20}.
F_2	S_2-strong crenulation cleavage, dominant in most outcrops; generally oriented at N30°E, vertical; local transposition seen in schistose lithologies, common F_2 folds are open to close to tight, symmetric or asymmetric, commonly disharmonic, and southwest plunging. L_{20} is dominant in most outcrops, parallel to B_2^0.
F_3	S_3-geometrically formed, non-penetrative cleavage seen locally in schistose rocks. F_3 folds are small kinks in schists, broad folds in more quartzose rocks. There are probably two S_3 cleavages present (S_{3A} and S_{3B}); they may be conjugate but one is dominant. S_3 is generally northwest striking and steeply dipping.

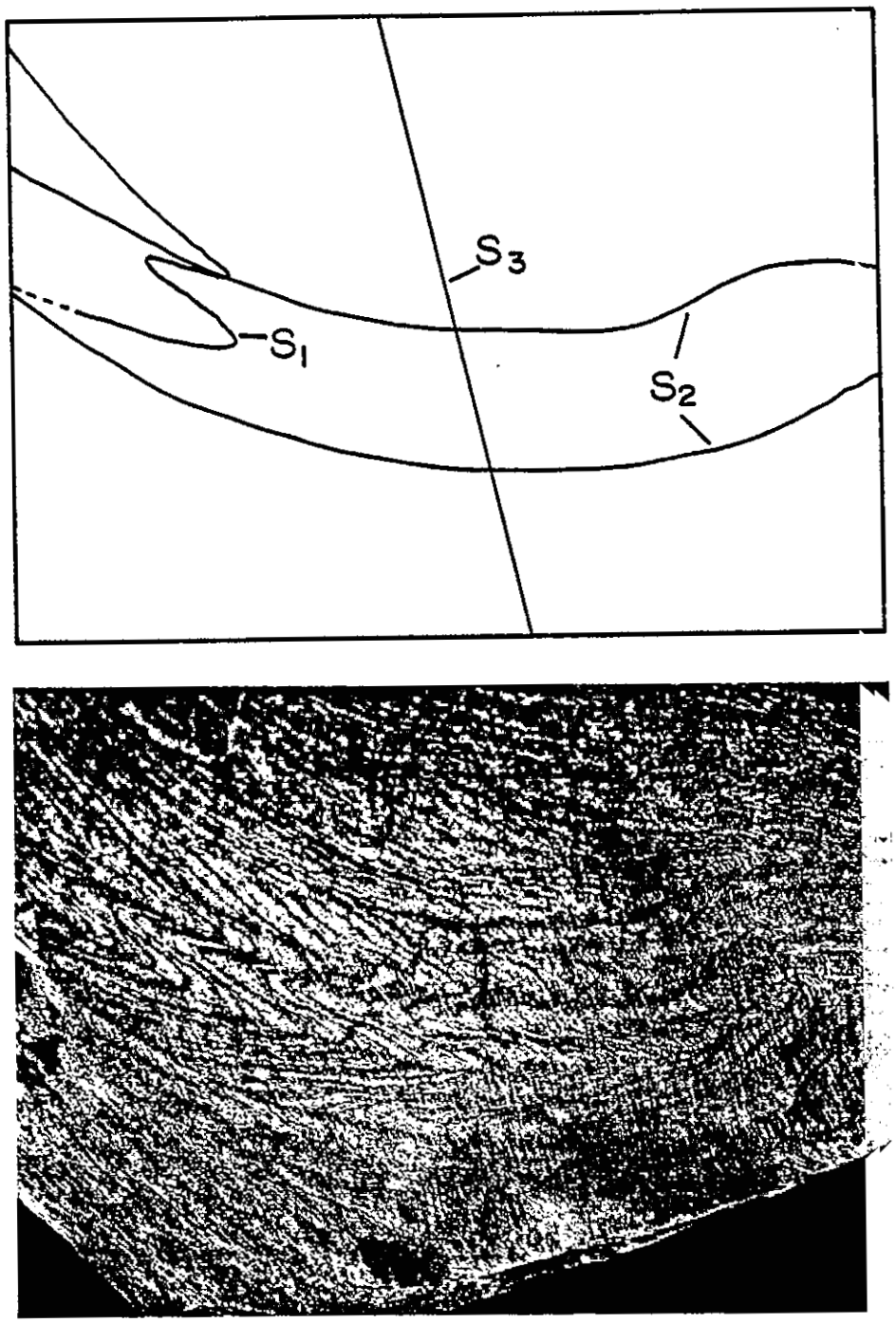

Figure 28. Overprinting fold relationships between F_1, F_2, and F_3 in micaceous quartzite of the Sevilleta formation. Orientations of S_1, S_2, and S_3 are as shown in sketch above. F_2 folds are tight. F_3 fold is broad. Picture is 25 cm across.

STRUCTURAL ANALYSIS

Introduction

Because geometrical analysis is relatively independent of the mechanism of deformation, it can be an extremely useful device in simply deformed terrains. In areas with complex tectonic histories the methods of analysis still may be applied, although assumptions made become less reliable and results less unique and consequently less revealing. The methods used in this study are based loosely on those of Turner and Weiss (1963) and Holcombe (personal commun., 1982).

There are several generations of interfering fold systems on both a mesoscopic and macroscopic scale in the southern Manzanos. In the study area the mesoscopic interference pattern appears similar to a Ramsay Type 3 pattern (Ramsay, 1967). This pattern is not exceedingly complex, although such factors as topography, transposition, minor folds, non-cylindrical folding, and complex stratigraphy can result in very complex patterns.

Multiple folding is especially obvious in low- to medium-grade metamorphic rocks such as in the Manzanos. Characteristic of these terrains are non-cylindrical folds, non-linear lineations, complicated outcrop patterns, and extensional lineations parallel to fold axes. (Hobbs and others, 1976).

β-Plots. The S_0/S_1 maximum defines a plane that strikes N20°E to N30°E and dips around 60° NW (fig. 13). Poles to S_0/S_1

define a great circle with a β_2 girdle axis at S30°W, 15° (fig. 29). S_0/S_1 is folded around a gently plunging fold axis contained in a nearly vertical axial surface. Fold limbs are steep, suggesting tight to close folding. The high proportion of northwest-dipping S_0/S_1 planes implies that folds are overturned to the southeast. Judging from the scarcity of gently dipping, northwest-striking planes, F_2 fold noses are not common.

The stereographic plot of poles to S_2 shows a diffuse pattern of steeply-dipping N20°E- to N30°E- striking cleavage planes with a statistical maximum at N23°E, 70°NW (fig. 16). Even though the S_2 pole pattern is similar to that of S_0/S_1, it does not appear to define a girdle. Instead most S_2 planes have dips greater than 50°. The statistical maximum of northwest-dipping S_2 planes again suggests that F_2 folds are overturned to the southeast.

The plot of S_3 poles (fig. 18) shows scattered points with a statistical maximum corresponding to planes oriented at N65°W, 40°NE.

Figure 30 shows L_{10}, L_{20}, and L_{21} intersection lineations on a contoured equal-area plot. Data points are scattered around a strong statistical maximum at S44°W, 28°. A weak girdle along the great circle N50°E, 90° suggests that lineations have been folded around a northwest-southeast-trending F_3 axis.

A similar pattern for B_2^0 fold axes has a statistical maximum of folds plunging at S45°W, 35°, and a weak S_3 girdle along a plane at S45°W, 80°NW (fig. 31).

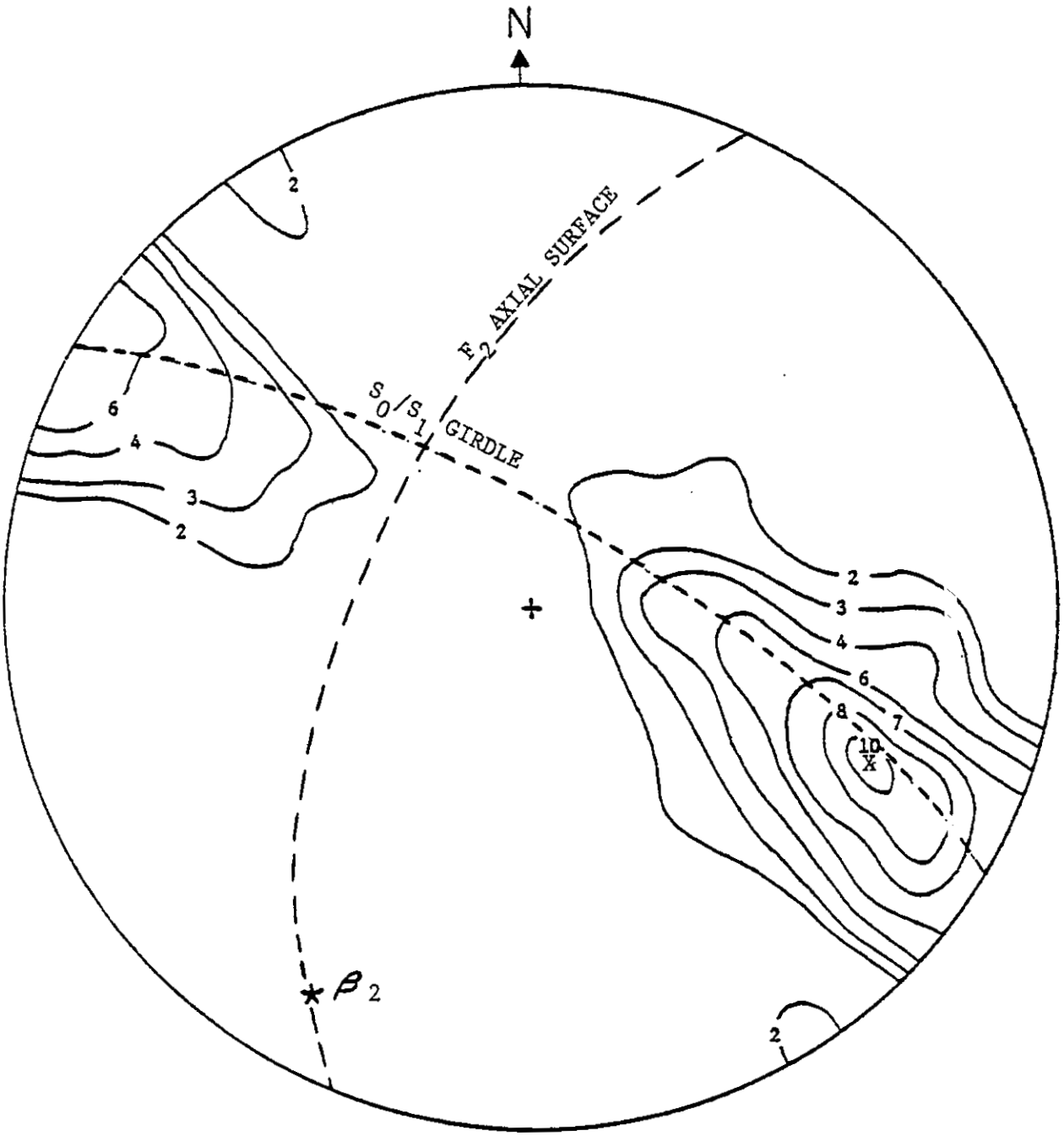

Figure 29. Contoured equal-area, lower hemisphere stereographic projection of poles to S_0/S_1. S_0/S_1 girdle defines β_2 axis at S30°W, 15°. S_0/S_1 statistical pole maximum (X) at S65°E, 25°. F_2 axial surface at N25°E, 64°NW is defined as the plane normal to the S_0/S_1 pole maximum. Percentages as shown on contours. N = number of data points.

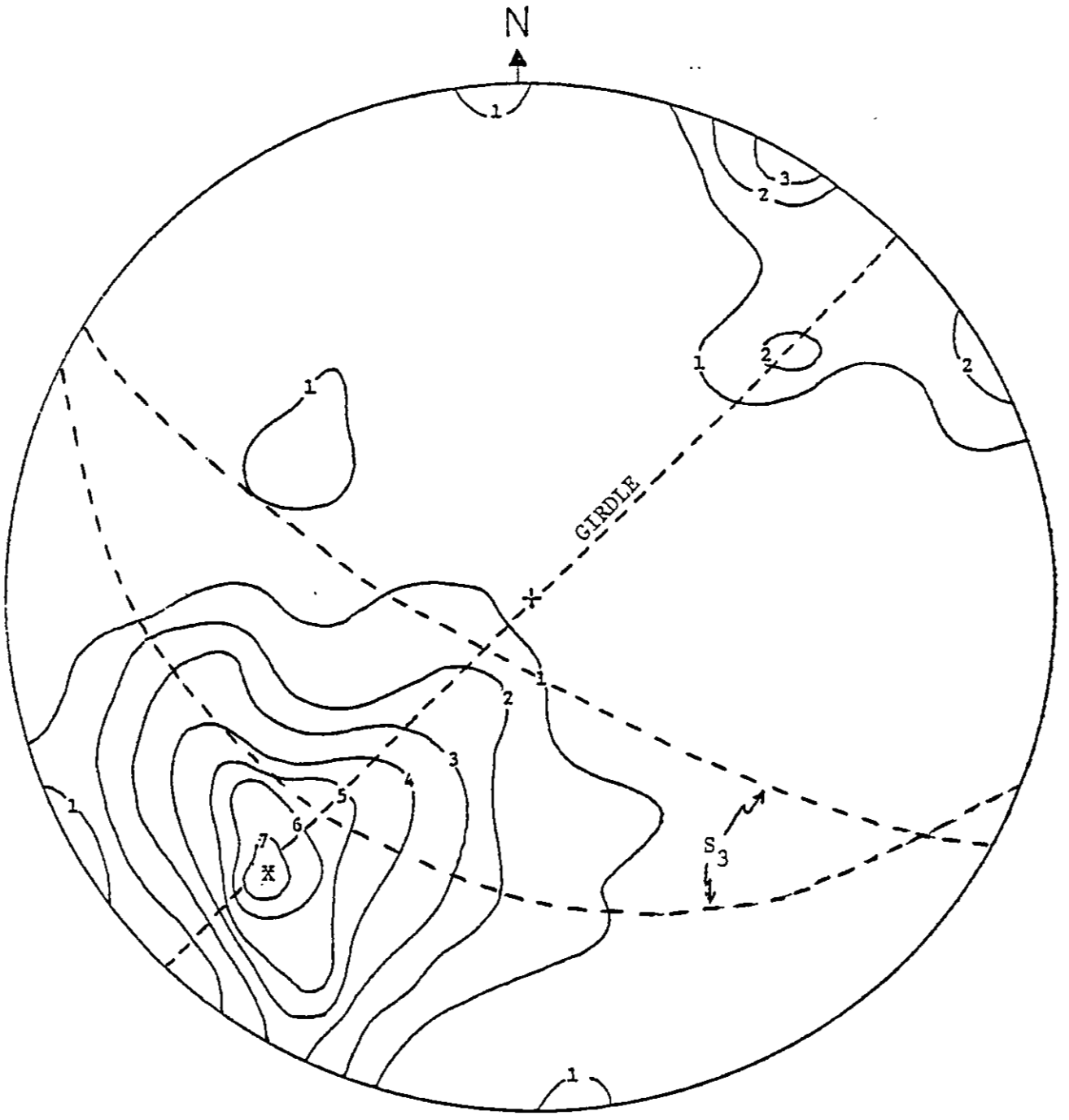

Figure 30. Contoured equal-area, lower hemisphere stereographic projection of L_{10}, L_{20}, and L_{21} intersection lineations. Weak girdle along great circle N46°E, 90°. X = lineation statistical maximum. N = number of data points. Girdle may be due to rotation around S_3 axes.

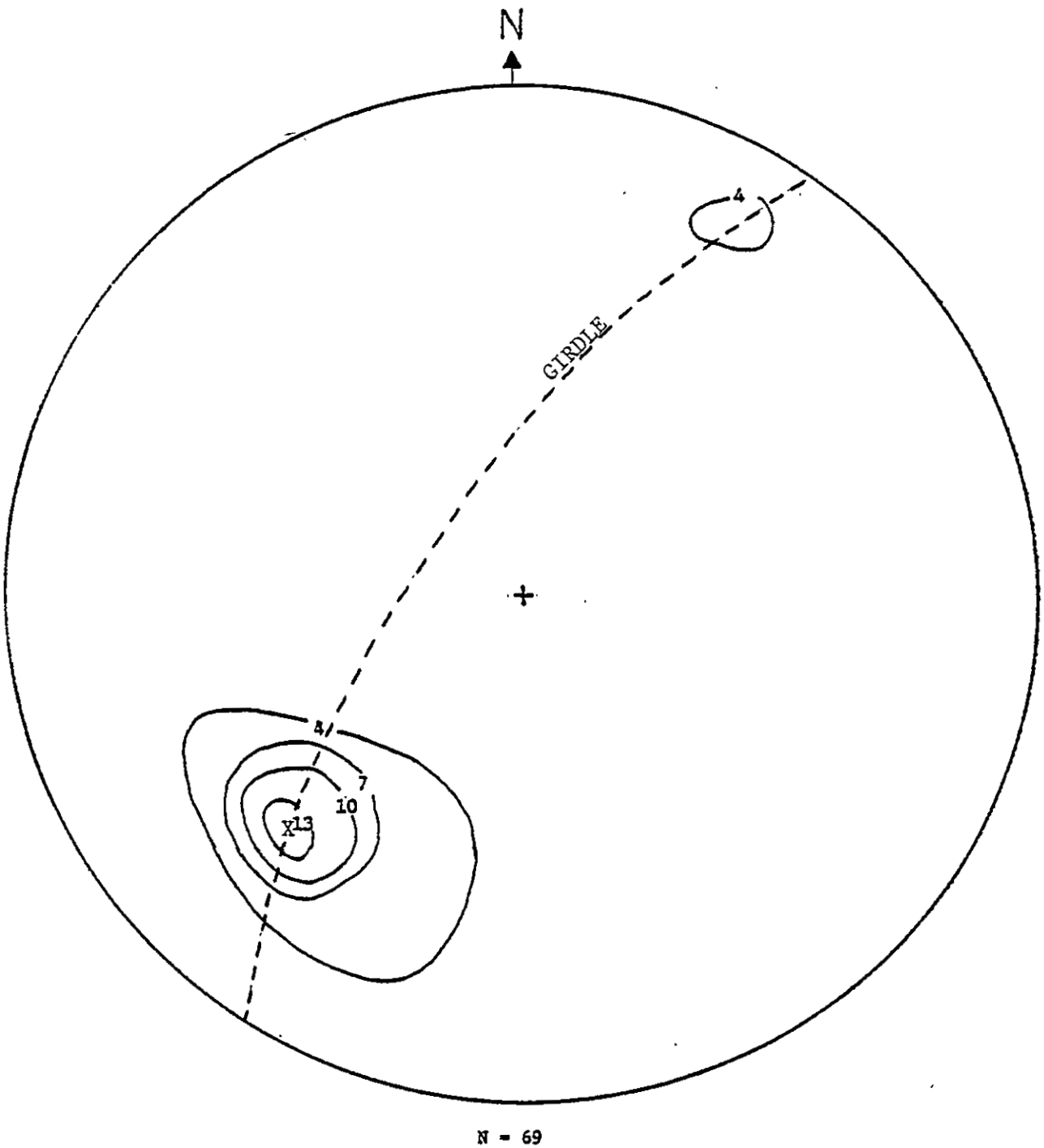

Figure 31. Contoured equal-area, lower hemisphere stereographic projection of B_2^0 fold axes. Statistical maximum (X) at S45°W, 35° and weak girdle at N35°E, 73°NW. N = number of data points.

Discussion

The S_0/S_1 and S_2 pole patterns are a classical example of those formed by an axial plane foliation cutting compositional layering (fig. 32). The similar patterns indicate in a general sense that S_0/S_1 and S_2 are nearly parallel on the limbs of F_2 folds. The greater scatter of S_2 points may reflect cleavage fanning, cleavage refraction, or the presence of S_1 planes mistakenly recorded as S_2. S_0/S_1 is folded around a gently southwest plunging $_2$ as demonstrated by a pole girdle, whereas S_2 poles show no such well-defined girdle. Both B_2^0 and intersection lineation data are consistent with southwest-plunging F_2 folds. The lineation plot is useful only in a general sense since it does not differentiate between L_{10}-L_{20} and other intersection lineations. In order to learn more about the relation between lineations and cleavages, another approach was taken. Data for every station in which S_0/S_1-S_2 and at least one lineation were measured were plotted individually on an equal-area stereonet. For each station the calculated S_0/S_1-S_2 intersection (L_C) was compared to each of the measured intersection intersections (L_M). Plots were then compiled for all S_2 and lineations in which L_C and L_M were congruent. The modified S_0/S_1 and S_2 contoured plot (fig. 33) is essentially identical to the original plot. The new lineation plot (fig. 34) is similar to the original lineation plot, although the new plot shows less scatter, especially in the northwest quadrant. This agreement between plots confirms the idea that both F_1 and F_2 are southwest-plunging folds with axial planes overturned to the southeast.

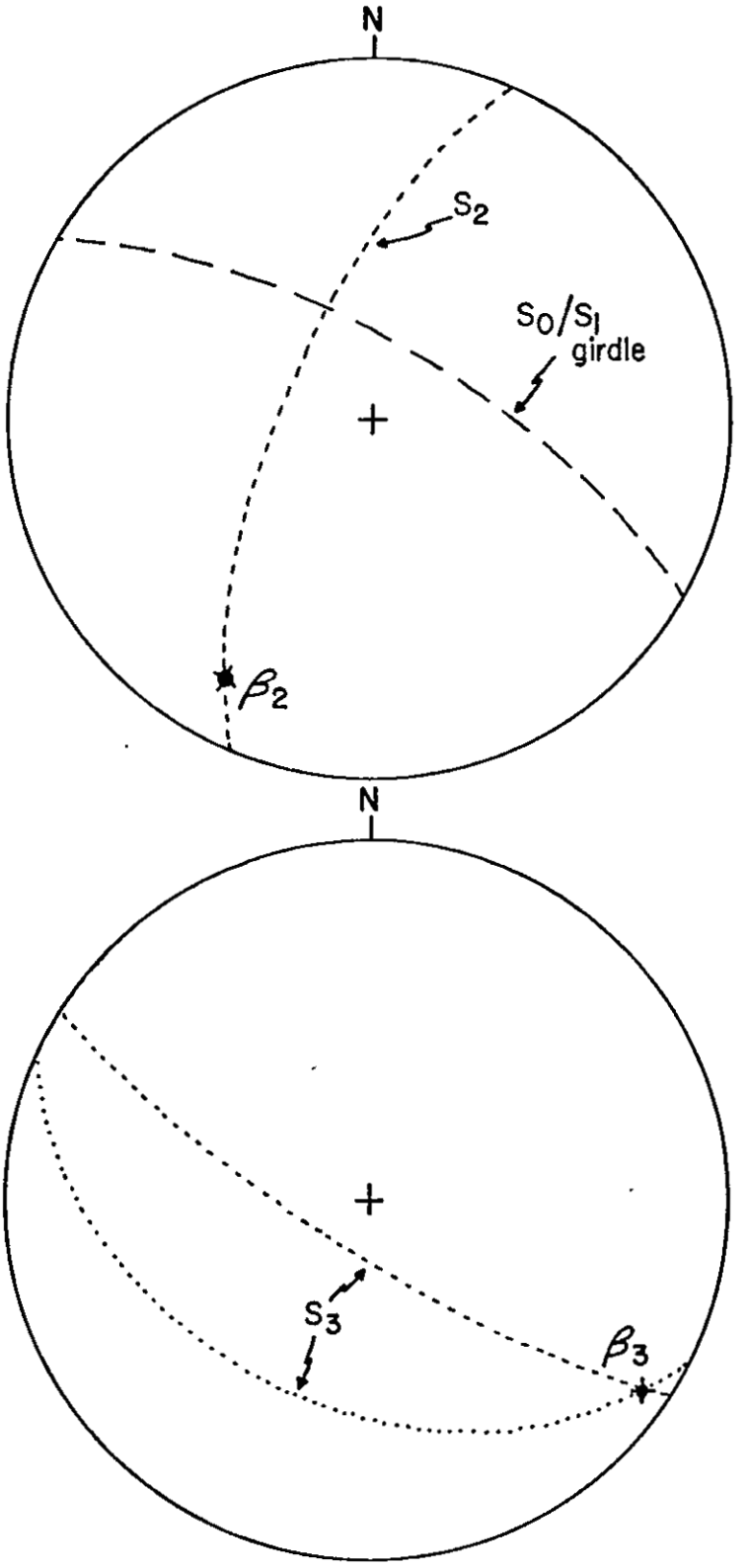

Figure 32. Synoptic diagrams showing orientations of S_0/S_1 girdle, S_2 axial surface, β_2, S_3 plane, and β_3.

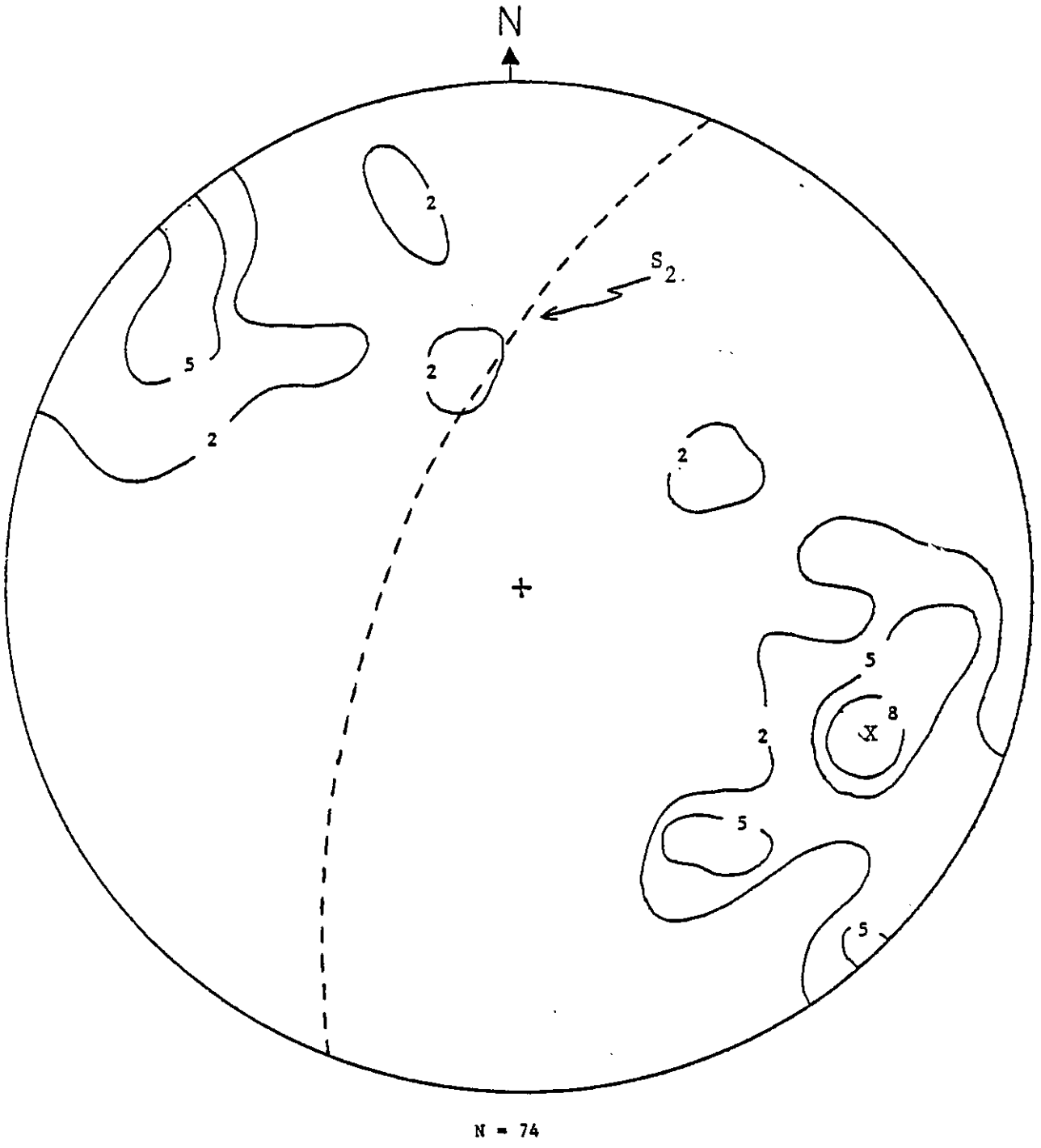

Figure 33. Contoured equal-area, lower hemisphere stereographic projection of selected poles to S_2. See text for discussion. Percentages as shown of contours. X = statistical pole maximum. N = number of data points.

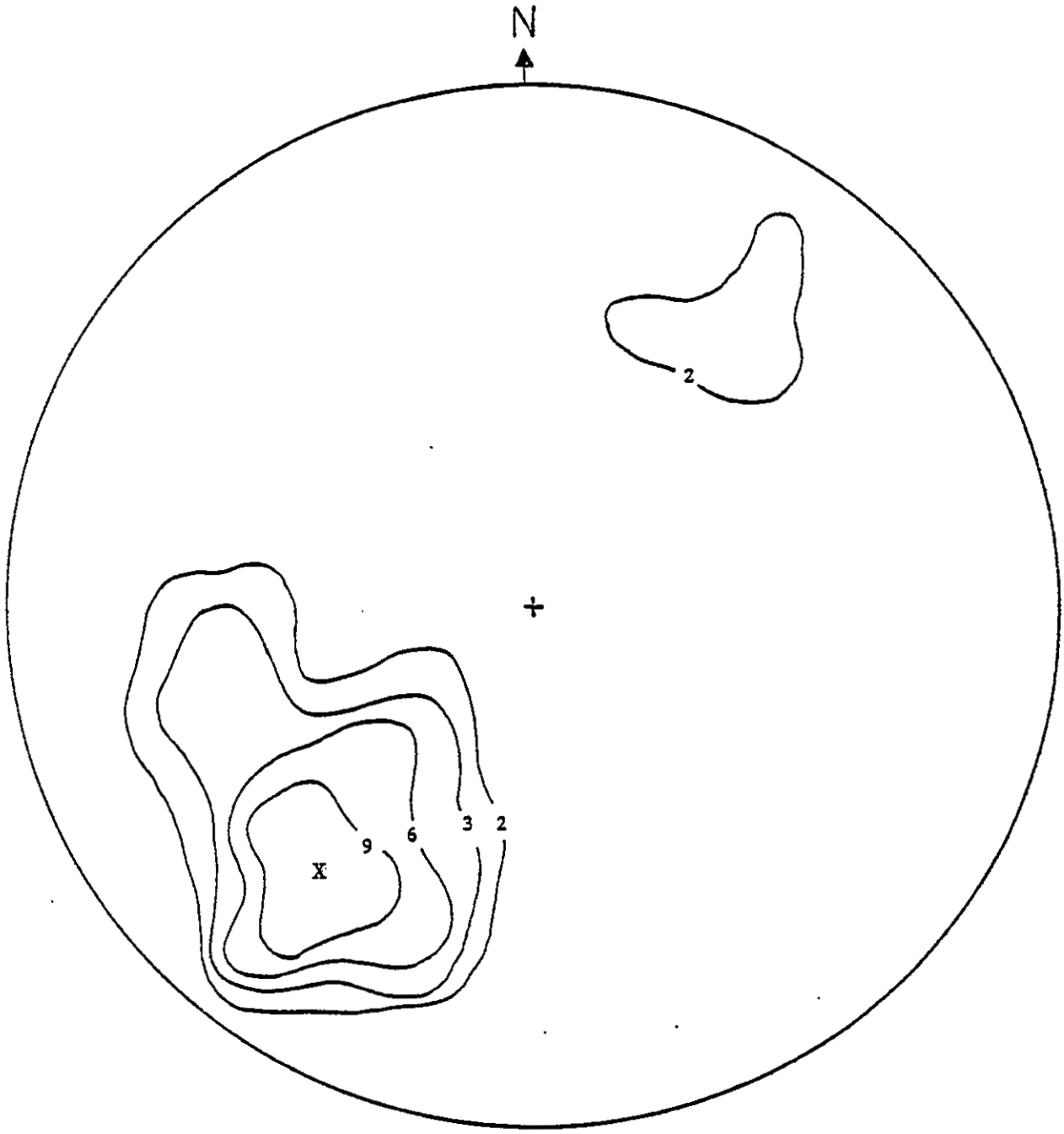

Figure 34. Contoured equal-area, lower hemisphere stereographic projection of selected intersection lineations. See text for discussion. Percentages as shown on contours. X = statistical maximum. N = number of data points.

Numerous trends were recognized while plotting data of individual stations for the previous analysis. In many cases none of the L_M corresponded with the L_C. At some of these stations three intersection lineations were recorded. Three possibilities for this lack of agreement are:

1) The cleavage measured was S_2 but none of the lineations were L_{21}; but rather S_3 intersections;
2) The cleavage was S_1 but none of the lineations were L_{10};
3) Measurements were imprecise due to steep dips and/or nearly co-planar planes.

In several locations the L_C corresponded with what was clearly recorded as a crenulation lineation. Since S_2 is a crenulation cleavage, these lineations are probably L_{20} rather than L_{10}.

At one locality S_0/S_1 and S_2 both strike northwest and dip northeast, whereas L_M and L_C are coaxial at S30°W, 30°. The intersection lineation has remained at the familiar southwest orientation whereas the dominant cleavage has been folded to a N40°W orientation. Perhaps locally the S_1 cleavage is dominant and lineation measured is L_{10}. If so, L_{10} and L_{20} are approximately coaxial in this area.

In many areas S_2 stubbornly strikes northeast in spite of any folding of S_0. In these cases either the dominant cleavage is S_2, which cuts folded S_0/S_1 layering, or the cleavage is S_1 in an area of F_1 fold noses folding a discrete S_0, and S_2 is weakly developed. The former is favored since layering appears to be a schistosity and no large F_1 closures are recognized. In other areas a different layering-cleavage relationship is recognized. S_0/S_1

commonly switches from dipping northwest to southeast. While plotting individual stations it became apparent that the dip of S_2 was following layering as it changed dip direction. Unless an unrecognized folding event is folding S_2 , the cleavage measured must be S_1, which is folded with S_0 by F_2.

At one station two cleavages and three lineations were recorded. Overprinting criteria were not discernible. The stereoplot of the data matched each of the L_C with an L_M. A fine mica lineation plunged steeply west, and a broad crenulation lineation plunged gently southwest. The obvious interpretation is that the mica lineation is L_{01}, and the crenulation lineation is L_{20}. If this is so, then F_1 and F_2 fold axes are not coaxial in this area.

The most important point to be noted from the preceeding case studies is that the relative development of the S_1 and S_2 fabrics is variable over the study area. In the absence of a strong S_2, S_1 can effectively mimic S_2. Since this is a local effect, it is probably not significant in the preceding geometrical analysis.

Strain

The geometry and kinematics of strain are poorly understood in the Manzanos. No initially spherical bodies are recognized in the rocks. Some constraints can be put on the strain that folds have undergone by the shapes of the folds and the development of penetrative axial-plane cleavage. In interlayered sequences, folds are generally controlled in their distribution and wavelength by the competent layers (Hobbs and others, 1976). Thus, the large disharmony between folded layers in the

Manzano area can result in inappropriate strain analyses. In addition, the thicknesses of both F_1 and F_2 fold layers have probably been modified by transposition and flow during deformation. According to Ramsay (1967), rocks in which a penetrative axial-plane cleavage has developed have undergone a minimum of about 50 percent shortening. Fold morphology and transposition features suggest much larger shortening during both F_1 and F_2, but shortening can not be more precisely quantified without good strain markers.

Assuming S_1 was horizontal, isoclinal F_1 folds formed with principal strain axes as shown in Figure 35. A major component of horizontal shear is required to form recumbent isoclinal folds and extensive transposition layering.

F_2 orientation and geometry suggests shortening is a N60°W-S60°E direction with yielding to the southeast. D_2 principal strain axes superimposed on the F_1 geometry are shown in Figure 36. This figure assumes coaxial F_1 and F_2 folding, which would yield a Ramsay Type 3 (Ramsay, 1967) interference pattern. If F_1 and F_2 are not coaxial, or given noncoaxial strain, the interference pattern will be different. Armstrong and Holcombe (1982) interpret the F_1 and F_2 folding events in the Precambrian rocks of the Pedernal Highlands as noncoaxial with steeply plunging L_{10} and more gently plunging L_{21}, giving a Type 2 (Ramsay, 1967) interference pattern. The exact relation between F_1 and F_2 axes is uncertain in the southern Manzanos.

F_3 chevron folds were probably formed by slip along layers, as in a flexural-slip model. This fold type forms with the maximum compressive stress acting parallel to layering (Ramsay, 1967, p. 44).

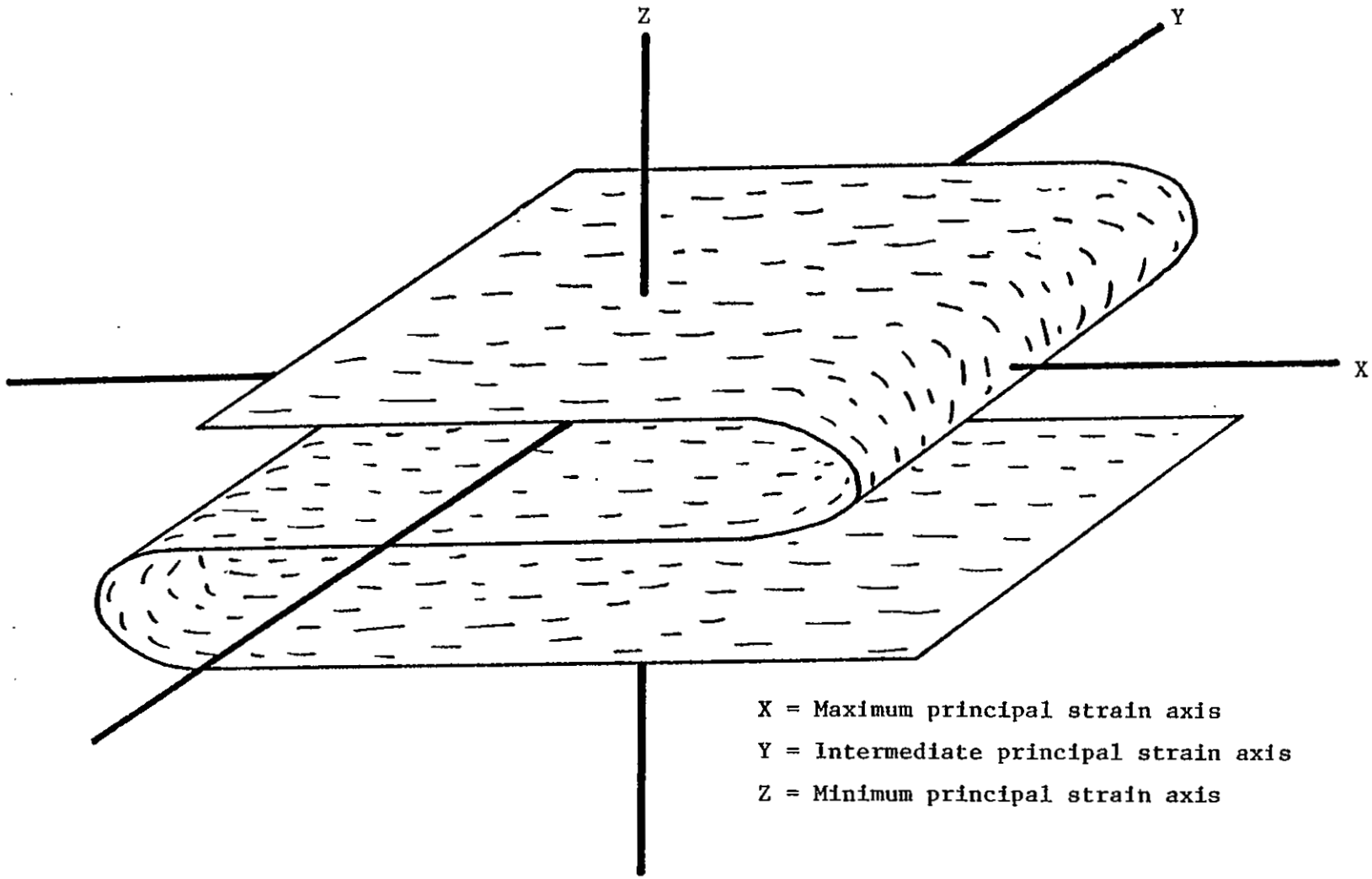

Figure 35. Theoretical principal strain axes for F_1 deformation.

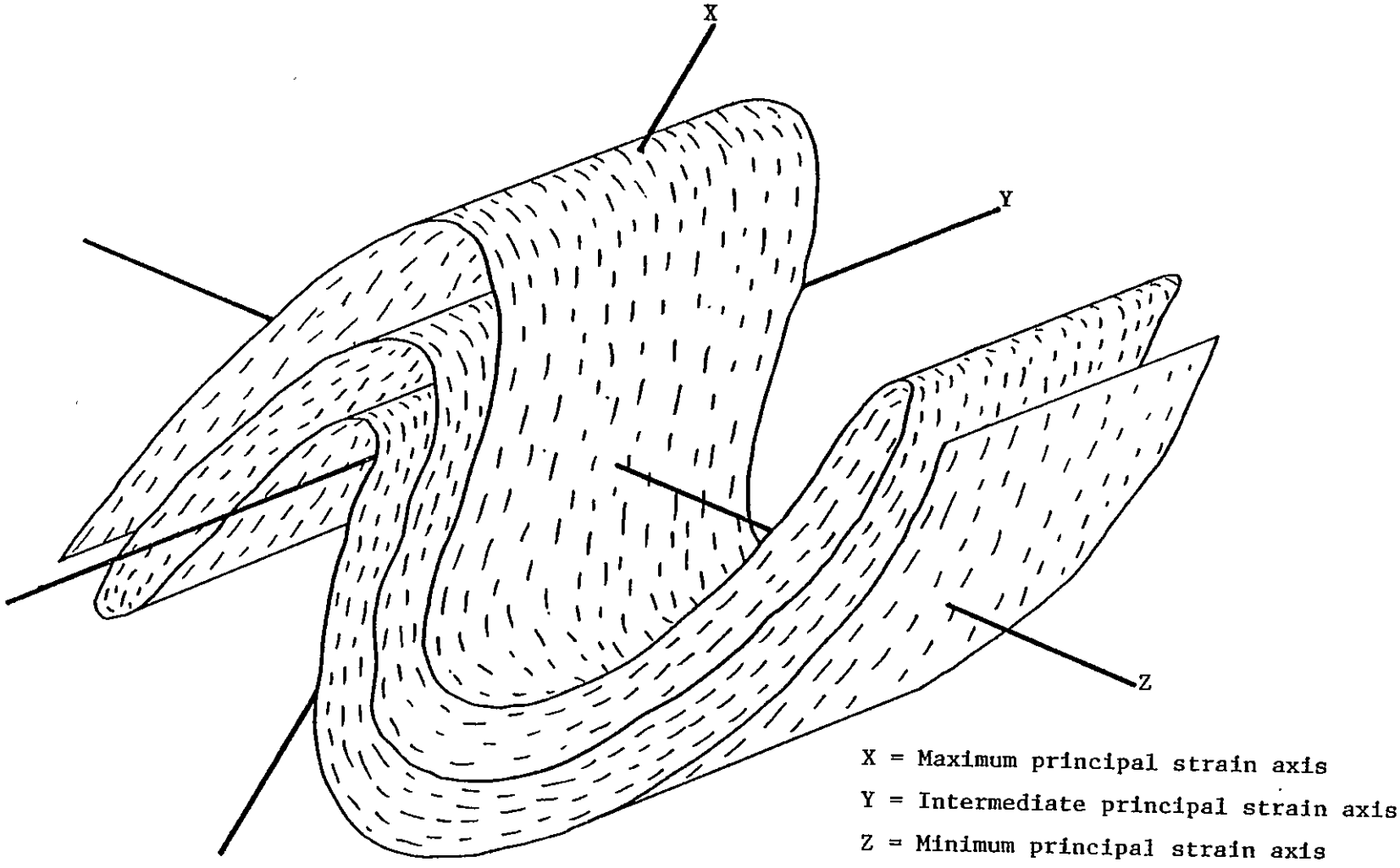

Figure 36. Theoretical principal strain axes for F_2 deformation superimposed on a coaxial F_1 fold geometry. See text for discussion on relative orientations of F_1 and F_2 fold axes.

Shortening in schists associated with F_3 folds is no more than 40 or 50 percent.

Problems

A number of factors complicate a structural analysis of the southern Manzano rocks. Cleavage styles are dependent on lithology, strain parameters, pre-existing structures, and the deformational environment, thus there is no guarantee that a particular axial plane foliation will consistently have a unique style. The dominant cleavage (either S_1 or S_2) in one area need not be dominant in a nearby area. Similarly, fold morphology is dependent on a combination of lithology, bed thickness, and viscosity contrast. Fold styles may vary considerably over the map area. On a larger scale an interpretation of major structures is inhibited by the extremely varied topography, polyphase folding, transposition layering, discontinuous igneous structures, and nearly vertical, coplanar S_0/S_1 and S_2 axial-plane foliations.

Hobbs and others (1976) comment that in many areas second or third generation folds reflect the prominent outcrop map pattern. F_1 isoclinal folding with regional transposition may be eclipsed in map pattern. In addition, this problem of F_1 recognition may be compounded by an accepted, but potentially incorrect, stratigraphy, which unwittingly assumes isoclinal fold limbs to be different stratigraphic layers.

Conclusions

The map area can be divided into eastern and western structural domains, separated by the Paloma fault. The western region consists mainly of complex Sevilleta rocks, whereas the eastern region contains less complex, more continuous metasedimentary rocks.

The thinly laminated siliceous member of the Blue Springs formation is a distinctive lithology, and as such is probably stratigraphically correlative from the eastern to the western exposures. Stark (1956) thought that the thin quartzites and schists east of the western Blue Springs were correlative with the much thicker White Ridge sequence to the west. This is possible and if true strongly supports his idea of a large synform between the two units. However, the western lithologies are much more similar to the Sais units than to the Blue Springs. Whereas excellent crossbed data for the eastern domain indicates that the Blue Springs is younger than the Sais, no convincing stratigraphic data exists for relative ages between:

1) the western Blue Springs and the adjacent metasediments to the east;
2) the eastern units and any western units;
3) the Sevilleta and anything else.

The only stratigraphic evidence for Stark's large synform is between two outcrops of Blue Springs which are separated by a fault with unknown displacement. A worrisome note is the occurrence of different lithologies on either side of the synformal axis; metarhyolite on the west and amphibolite-metasediments to the east. In support of a possible synform three ways of producing such a lithologically

asymmetric structure are:

1) The Sevilleta contained a facies change from dominantly rhyolite to the west to dominantly amphibolite to the east, which has been folded;
2) Pre-synformal layers are actually transpositional layers such that later lithologically symmetric folds are not required;
3) A pre-synformal fault separates the Sevilleta from other units.

The third idea requries less of a special case than the first two, although evidence of extensive transposition does exist. Either situation, or a combination of the two, would make many of the mapped geometrical incongruities easier to accept. The potential for structural and stratigraphic complexities through a process of folding either a transposed terrain or a sequence of stacked thrust sheets is enormous.

The extremely complex amphibolitic region in the west-central map area is poorly understood due mainly to poor exposure plus inconsistent and indecipherable tectonite fabrics. One cannot project structures above or below the ground with any certainty. On a broad scale this area may represent a large minor fold region of some larger fold. The locally shallow dips may occur where the fold noses of parasitic folds happen to intersect topography. Two other possibilities for relating this area to some larger structure are that it may be an inflection point or some type of shear zone. In any case, infolded amphibolites, quartzites, and schist beds represent a transposed, structurally thickened section due to tight, upright F_2 folds.

The structural domain east of the Paloma fault is better understood than the western domain. A more rigorous analysis is permitted due to shallowly dipping beds plus the absence of metavolcanic rocks.

Inconsistencies in S_0/S_1 - S_2 vergences with the overturned fold geometries may be due to either the presence of many unrecognized F_2 minor folds, of S_1 readings which locally were unwittingly deemed S_2. The geometric problem noted earlier of tracing Sais units around the large synformal nose to the western limb may be explained by any of the following ideas:

1) The gray quartzite does indeed reappear on the western limb, but has changed into the thinner, red quartzite adjacent to the schist;

2) A fault runs between the chlorite schist and the red quartzite on the western limb. This requires that either the fault is folded around the synform and separates different strata from the schist on either limb of the fold, or the fault is post-folding and separates the red quartzite from all rocks to the east. In support of a folded fault is the fact that in Pipe Canyon the contact between the red quartzite and chlorite schist is itself folded. Although it is possible that folding in Pipe Canyon is post-synform and post-faulting, it is very unlikely, since F_2 was apparently the final substantial deformational event;

3) The compositional layers are themselves transposed layers such that there is no requirement for lithologic symmetry around F_2 folds. This seems unlikely owing to the well preserved, consistent crossbeds in the Sais quartzites. Crossbeds

indicate that the Sais underlies the Blue Springs, which suggests that the sequence east of the Paloma fault is an orignal stratigraphic sequence, barring the existence of unrecognized bedding-plane thrust faults.

The first idea is the least objectionable, although all three are entirely speculative and unsupported by field data.

It is not known why the eastern domain is less deformed than the western. Certainly, thickness and competence of strata are factors. Thin-bedded Sevilleta schists, amphibolites, and quartzites are undoubtedly more receptive to folding than are massive White Ridge and Sais quartzites. If the Paloma fault has substantial offset, deformational environments may have been different on either side of the fault.

Summary of Structure

Geometrical analysis of this area is complicated by problems associated with varying deformational intensity, varying lithology, and a complex deformational history.

The region west of the Paloma fault is structurally complex due to original igneous structures, an early strong transpositional episode with isoclinal folding (F_1), and later close to tight folding and local transposition (F_2). The map shows an intricate pattern of folds and pinched beds within the thinly bedded amphibolites, quartzites, and schists of the Sevilleta formation.

Well-defined, large, disharmonic, southwest plunging, tight F_2 folds suggest less intense deformation in the eastern structural domain. This difference may be due to regional variations in stress and strain

across the Paloma fault, and rheological differences between the thin-bedded Sevilleta rocks and the more competent Sais and White Ridge rocks.

Geometrical incongruities in several areas raise the possibility of the existence of unrecognized Precambrian-age bedding-plane thrust faults. Regional F_1 transposition effects may also contribute to mappable inconsistent geometries.

Small local F_3 chevron and broad folds probably reflect only very minor large-scale D_3 deformation.

A generalized block diagram for the northern half of the map area illustrates the major structures (fig. 37).

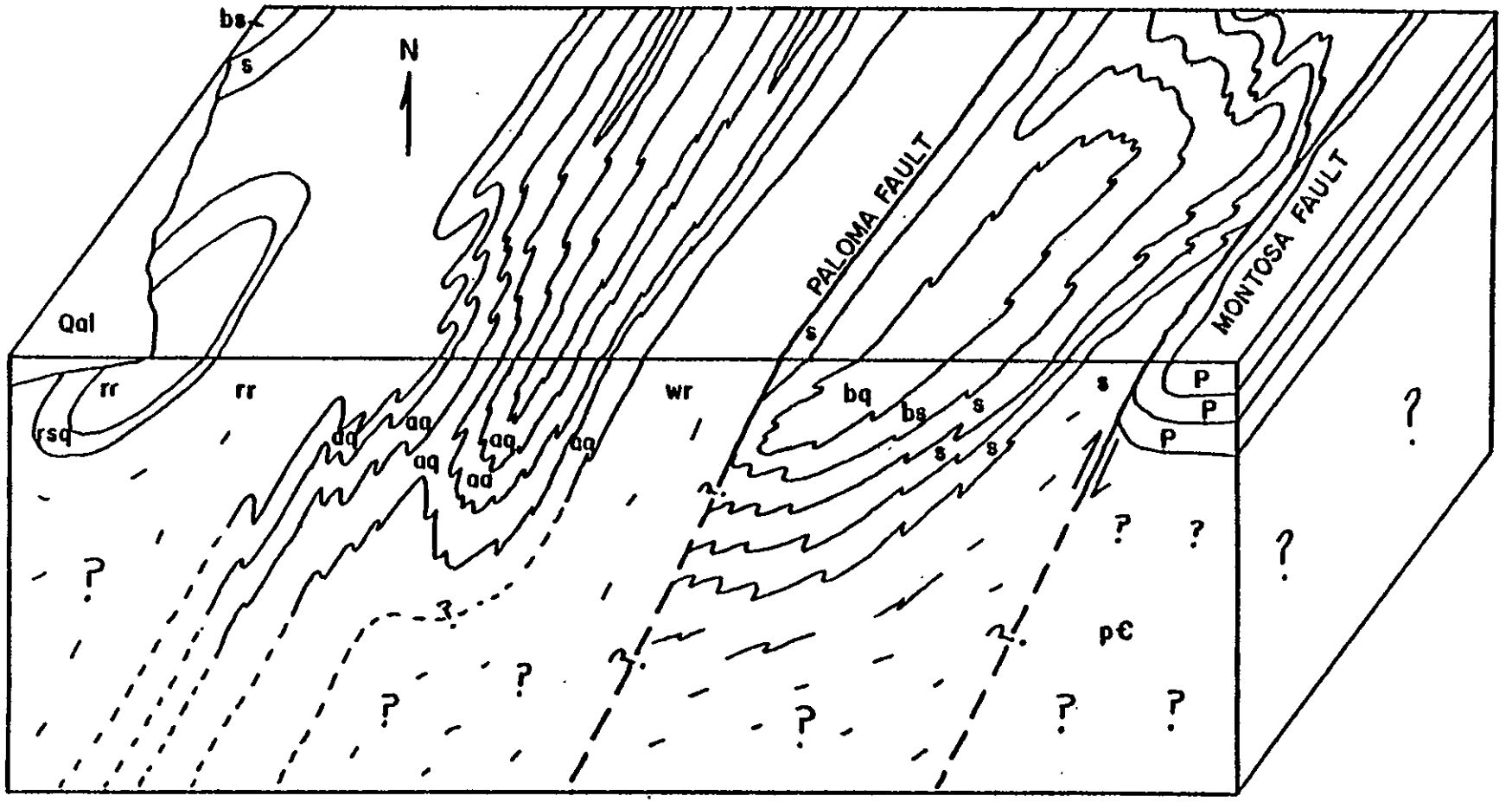

Figure 37. Generalized block diagram of northern map area showing major structural features. r = Sevilleta rhyolitic terrain, a = Sevilleta amphibolitic terrain, wr = White Ridge, s = Sais, b = Blue Springs, P = Paleozoic.

METAMORPHISM

Mineral Paragenesis with Deformation

Most minerals are clearly spatially associated with one of the S-surfaces, although some ambiguous textures exist. S_1 deformation was accompanied by alignment and/or growth of muscovite, chlorite, biotite, and quartz crystals. All three micas do not necessarily occur together in all S_1 cleavages, but all are seen within S_1.

The S_2 differentiated cleavage has rotated and recyrstallized muscovite, biotite, chlorite, quartz, and opaques parallel to S_2. Muscovites are generally small (0.05 to 0.11 mm long); S_2 chlorites are up to 0.6 mm long and commonly show deformation lamallae. Quartz grains commonly are elongate parallel to S_2. Porphyroblasts of biotite, garnet, staurolite, and chloritoid are all syn- or post-tectonic to F_2. Two types of biotite porphyroblasts are recognized. Dark brown, blocky, strained, subhedral, moderately poikioblastic crystals with quartz inclusions, 0.3 to 0.4 mm long lie consistently inclined 30° to 60° to S_2. These biotites are unaffected by S_2, are all aligned, but not with any visible cleavage. These biotites are post-S_2 and probably post-S_3, and may be aligned parallel to the biotite mineral streaking, which is probably L_{31} seen in hand specimen. The second biotite types are large (0.5 to 0.9 mm long), light brown, anhedral, extremely poikiloblastic web-like crystals forming helicitic and mimetic textures over S_1 and S_2 by selectively replacing muscovite and biotite crystals (fig. 38). The absence of

visible strain textures makes their relationship to S_3 uncertain, but they are certainly post-S_2 and probably post-S_3.

Garnet porphyroblasts are generally euhedral to subhedral, are up to 2.0 mm across, and contain helicitic S_2 and S_3 structures. Garnets grew post-S_2 and S_{3A}; their growth relative to S_{3B} is uncertain.

Staurolite porphyroblasts are up to 2.0 cm long, form poikiloblastic web-like structures with helicitic and mimetic structures identical to those of the biotite described above. These crystals are post-tectonic to S_2, and uncertain in age with respect to S_3 (fig. 38).

Chloritoid porphyroblasts are euhedral to subhedral, up to 3.0 cm long, and commonly twinned. Some crystals lie randomnly oriented over S_2 with S_2 micas abutting against porphyroblasts and gently warping around the chloritoids (fig. 39). Other chloritoids overgrow S_2 but contain helicitic and mimetic textures defined by quartz inclusions. One revealing porphyroblast has overgrown and preserved a small S_{3A} fold, but shows strain lamallae parallel to S_{3B}. This is excellent evidence that chloritoid grew after S_{3A} and before S_{3B}. The gentle S_2 warping around chloritoids is probably related to late compression (F_3), rather than very late F_2 syn-tectonic growth; although Fisher and Ehlers (1982) have shown experimentally that it may be possible for a growing porphyroblast to displace the matrix.

Biotite alignments without any associated fabric element suggest a preferred orientation of crystallographic axes rather than of grain dimensions. The mechanism of alignment was probably oriented growth

Figure 38. Photomicrograph of post-tectonic, helicitic, mimetic biotite and staurolite porphyroblasts in Sais schist. Staurolite may be syn-tectonic to S_3. Field is 2.9 mm across.

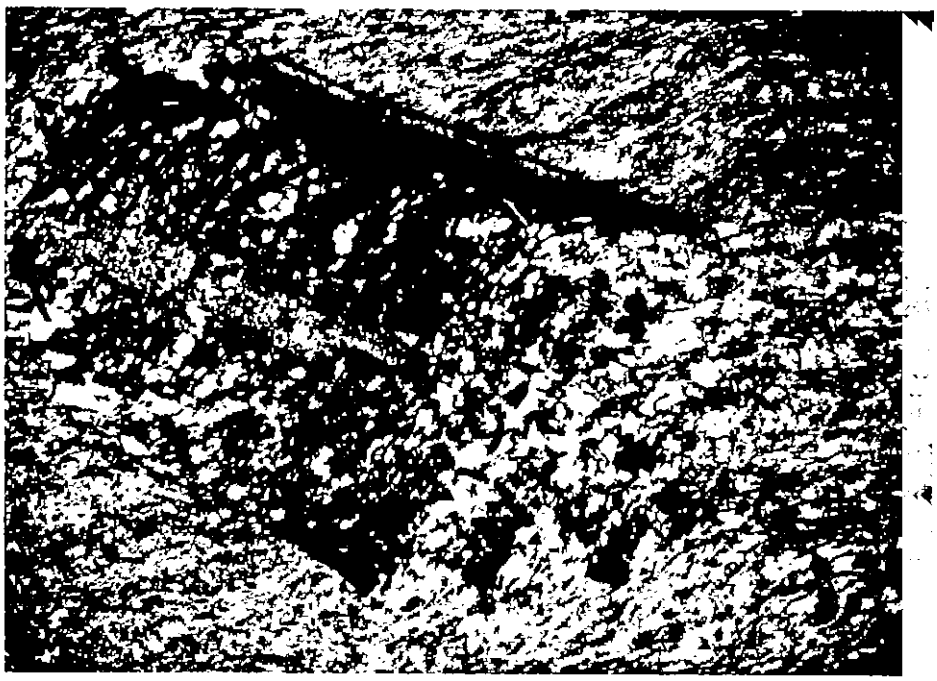

Figure 39. Photomicrograph of twinned, helicitic chloritoid porphyroblast in Sevilleta schist. Field is 5.0 mm across.

with respect to stress with elastic strain only, rather than rotation into parallelism.

There appears to have been a strong period of biotite, garnet, chloritoid, and staurolite porphyroblastic crystal growth post-dating F_2 deformation (Table 3). Helicitic and mimetic textures over both S_2 and S_3 demonstrate this. The relationship between heating and deformation in metamorphic belts generally is such that the major fabric-forming event predates the thermal maximum (Yardley, 1981). Yardley notes that this pattern is due in part to the changing mechanical behavior of rocks during a regional heating and cooling sequence. During heating, dehydration reactions liberate large volumes of fluids, leading to extensive ductile deformation under a given tectonic stress. During cooling, under similar stress and temperature, but lacking the free fluid component, rocks will behave more rigidly. The Manzano deformation-metamorphism pattern is consistent with Yardley's findings, although its applicability is questionable since it is not known if porphyroblast growth occurred during the waning stages of F_3 tectonism.

Mineral Assemblages and Reactions

Previous workers have generally agreed that peak metamorphic conditions in the southern Manzano rocks were within the upper greenschist or lower amphibolite facies (Reiche, 1949; Stark, 1956; Beers, 1976; Condie and Budding, 1979; Grambling, 1982), based mainly on mineral assemblages.

Table 3. Timing between deformation and mineral growth in pelitic schists of the southern Manzano Mountains, N.M. Question marks mean timing uncertain with respect to F_3. They may be pre-, syn-, and/or post-F_3.

MINERAL	F_1	F_2	F_3
Muscovite	---	---	
Chlorite	---	---	-?- -----
Biotite	---	---	-?- -----
Garnet			-?- -----
Chloritoid			-?- -----
Staurolite			-?- -----

Only schists located more than one kilometer from the Priest intrusion were considered for regional metamorphic analysis. Table 4 lists common mineral assemblages seen in pelitic schist and amphibolitic schist.

The only regional variation in metamorphic mineral occurrences is recognized in a sequence of pelitic schists in the Sevilleta amphibolitic terrain. In a 5- to 20-m thick bed, large (up to 3.0 cm), poikiloblastic, twinned chloritoid porphyroblasts are common in the northern schist, whereas a kilometer along strike to the south abundant, cruciform staurolite porphyroblasts occur. No thin sections from rocks removed from the Priest intrusion contained both chloritoid and staurolite, although the transition zone was not extensively sampled. Petrogenetic textures may suggest that both chloritoid and staurolite are in equilibrium with biotite, muscovite, and chlorite over the scale of a thin section, since all are in contact without any obvious partial reaction textures.

Assemblages from the Blue Springs rocks contain at most two Thompson AFM mineral phases (Thompson, 1957), all of which plot on or below the garnet-chlorite tie line (fig. 40). In contrast, Sevilleta rocks contain two, three, or four AFM phases, and Sais schists have at most three AFM phases. Possible reasons for "too many" AFM phases in Sevilleta rocks are metastable garnet, retrograde chlorite, disequilibrium, or internal H_2O buffering. In some Sevilleta schists, garnet has grown syn- or post-staurolite, as garnets contain twinned staurolite inclusions. This suggests that garnet is not an early phase which is metastably present due to relatively large amounts of Ca or Mn. Chlorite textures are commonly ambiguous. Certainly there

Table 4. Common mineral assemblages in pelitic schists and mafic schists.

Formation	Sample #	Stl	Ctd	Gt	Bi	Chl	Mu	Qtz	Opq	Plag	Hbl	Tour	Ap	Mt	Ep
Eastern Blue Springs	27		X	X	X	X	X			X					
	36)					X	X	X	X	X					
	40)					X	X	X	X						
Sais schist	28)	X			X	X	X	X	X						
Sevilleta	29)		X	X	X	X	X	X	X						
Amphibolitic Terrain	3)	X		X	X	X	X	X	X						
	30)		X	X	X	X	X	X							
	32)		X	X		X	X	X							
	9)						X	X		X				X	
	10)				X	X	X	X	X	X	X		X		X

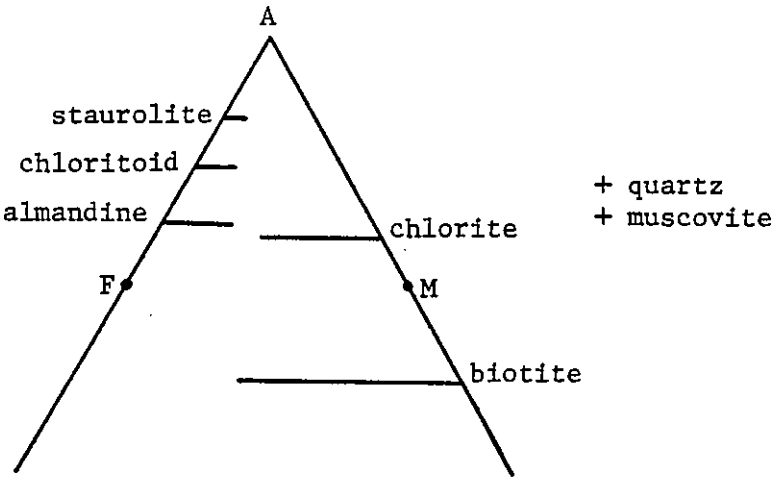

a. Sevilleta schists

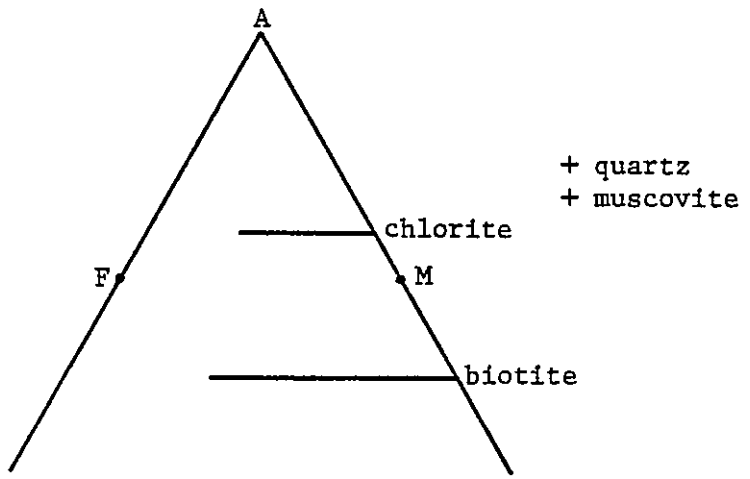

b. Blue Springs schists

Figure 40. Thompson AFM projections showing mineral phases present in Sevilleta versus Blue Springs schists. No tie line assemblages are implied.

are large retrograde chlorite porphyroblasts which overgrow everything, but smaller chlorites which appear in equilibrium with biotite and staurolite are also present. Petrogenetic textures show no obvious disequilibrium in the assemblages chlorite-biotite-staurolite-muscovite and chlorite-biotite-chloritoid-muscovite, over the scale of a thin section. No reaction rims were seen around any chloritoid, staurolite, biotite, garnet, or chlorite porphyroblasts. One would normally expect internal H_2O buffering in massive, relatively impermeable rocks rather than permeable pelites. Fluids can diffuse relatively rapidly along schistosity surfaces in metapelites. Thus internal fluid buffering is not a likely candidate for explaining the extra phase in the Sevilleta rocks. In short, thin section observations directly suggest none of the extra phase-forming mechanisms listed above, and the factors responsible are unknown. Perhaps detailed chemical studies of mineral phases would help resolve this.

The growth of staurolite, and chloritoid at low grade, is controlled by the bulk composition of the rock (Winkler, 1979). Albee (1972) notes that typical aluminous rocks will contain chloritoid and then staurolite with increasing temperature, whereas less aluminous rocks will not contain either mineral until the assemblage garnet-chlorite-muscovite becomes unstable. In pelitic schists the stable coexistence of biotite with either chloritoid or staurolite is not recognized if garnet + chlorite (+ muscovite + quartz) is stable. Chloritoid forms at low metamorphic grades under the special conditions of a large Fe/Mg ratio and a relatively high Al content. This chemistry should preclude the growth of chloritoid in biotite-bearing rocks, although this is clearly not the case in the Sevilleta schists.

According to Albee (1972), under the proper conditions the garnet-chlorite tie line may break early in the sequence, allowing chloritoid-biotite coexistence. These conditions must have been met in the Sevilleta rocks.

The variation along strike of chloritoid in the north to staurolite in the south suggests a lateral variation in temperature and/or pressure during regional metamorphism, with higher temperatures in the south. It is unlikely that this mineralogic variation is due to variations in rock composition. The higher temperature to the south may be related to the intrusion of the post-tectonic Priest quartz monzonite. Relative timing of peak metamorphic conditions and intrusion is unknown. Both probably occurred post-F_3 based on mineral textures and foliations. Contact metamorphic textures adjacent to the pluton grade into regional metamorphic textures away from the pluton.

The appearance of staurolite marks the transition from low to medium-grade metamorphism. A number of staurolite-in reactions have been proposed (Winkler, 1979):

1) chloritoid + O_2 = staurolite + magnetite + quartz + H_2O at about 545°C, 5 kb (Ganguly and Newton, 1969)
2) chloritoid + (andalusite or kyanite) = staurolite + quartz + H_2O at 545 ± 20°C, 4-8 kb (Hoschek, 1967)
3) chloritoid + quartz = staurolite + almandine + H_2O at about 560± 15°C, above 4 kb (Ganguly, 1969)
4) chlorite + muscovite = staurolite + biotite + quartz + H_2O at 540°C, 4 kb (Hoschek, 1969)
5) chlorite + muscovite + almandine = staurolite + biotite + quartz + H_2O (Carmichael, 1970) No P-T given.

Reactions (1) through (4) occur around 550°C and are not overly sensitive to changes in pressure (Hirschberg and Winkler, 1968), making the staurolite-in reaction a good geothermometer. It should be noted that these reactions are sensitive to changes in oxygen and water fugacities; data for which are not available. Petrogenetic textures and assemblages allow us to eliminate some of the above reactions from consideration. Reaction (1) is unlikely since magnetite is not abundant in staurolite-bearing rocks. Neither andalusite nor kyanite is present in chloritoid rocks, thus eliminating reaction (2) unless all andalusite or kyanite was consumed. Although almandine is seen with staurolite inclusions, reaction (3) need not be precluded if there were more than one period of garnet growth. Staurolite and biotite show synchronous growth, a texture suggestive of either reaction (4) or (5). With either (4) or (5) we would require a second chloritoid-out reaction, evidence of which is absent. AFM topology does not help in choosing a reaction since the only apparent change with increasing temperature is chloritoid-out, staurolite-in. There is also the added complication of an extra AFM phase.

The fact that chloritoid and staurolite are not seen coexisting in any rock, removed from the Priest intrusion, may be due to either sampling techniques, the outcrop width of the univariant assemblage containing chloritoid + staurolite (+ other phases), problems in recognizing very small chloritoid crystals, or some combination of the above.

Electron microprobe data for garnet-biotite pairs for three Sevilleta pelitic schists, using the technique of Ferry and Spear (1978; D. Codding, personal commun., 1982) are given in Tables 5 and 6. The

SAMPLE	MINERAL	FeO	MgO	MnO	CaO	Na_2O	K_2O	ZnO	TiO_2	Al_2O_3	SiO_2	Total
SMZ-29	Garnet(R)	30.72	0.88	9.39	-	-	-	-	0.04	22.26	38.46	101.75
	Chlorite	32.20	8.32	0.41	-	-	-	-	0.05	24.16	22.68	87.82
	Chloritoid	25.01	1.52	0.92	-	-	-	-	-	41.48	24.65	93.58
SMZ-30	Garnet(R)	38.58	1.33	2.02	2.23	-	-	-	0.05	21.03	36.64	101.87
	Biotite	24.54	6.58	0.02	0.01	0.17	8.43	-	1.63	19.80	34.67	95.83
SMZ-37	Garnet(R)	39.30	1.61	1.57	1.34	-	-	-	0.04	20.73	36.33	100.92
	Garnet(C)	38.05	1.75	1.81	2.22	-	-	-	0.09	20.63	36.25	100.81
	Biotite	22.41	7.64	0.01	0.00	0.19	8.57	-	1.52	19.90	34.55	94.80
	Chlorite	32.86	8.49	0.21	-	-	-	0.43	0.07	20.52	22.52	85.10
SMZ-55	Garnet(R)	35.27	2.30	3.22	2.35	-	-	0.27	0.03	20.95	36.53	100.92
	Biotite	22.72	9.61	0.04	0.00	0.26	8.53	-	1.49	19.68	33.46	95.89
	Chlorite	29.19	14.25	0.00	0.01	0.04	0.05	-	0.14	23.42	23.03	90.18
	Staurolite	14.42	1.63	0.15	0.01	-	-	0.28	0.44	54.72	26.76	98.40

(R) = garnet rim

(C) = garnet core

Table 5. Electron microprobe data for pelitic schists in the southern Manzano Mountains, N.M. (from Codding, 1982, personal commun.; Grambling, 1982, personal commun.).

Table 6. Garnet-biotite geothermometry calculations for three Sevilleta pelitic schists. Error is about ± 50°C (calculations using method of Ferry and Spear (1978); see Appendix I).

SAMPLE	AT 4 KB(°C)	AT 6 KB(°C)	ASSEMBLAGE
SMZ-30	478	485	Gt-Bi-Chl
SMZ-37	466	472	Gt-Bi-Chl
SMZ-55	533	541	Gt-Bi-Stl-Chl

530-540°C ±50°C temperature derived for the staurolite-bearing rock agrees very well with the temperatures obtained from the above mineral assemblages. The lower temperatures derived from the other two schists may be due to P_{H_2O} less than P_{Total} during metamorphism. Low P_{H_2O} would tend to stabilize staurolite at lower temperatures.

No recognized differences in metamorphic pressure and temperature occur across the Paloma fault.

Summary

Pelitic schists indicate upper greenschist - lower amphibolite facies metamorphism with a peak temperature between 465°C and 560°C. Pressure is less well constrained but 3 to 6 kb is probably a good estimate based on mineral assemblages and the presence of staurolite (fig. 41). A mineralogic change from chloritoid to staurolite schists along strike probably indicates a slightly higher temperature to the south. Chloritoid-out and staurolite-in reactions are poorly constrained because of lack of data on mineral chemistry. Garnet-biotite geothermometry data yield an anomalously low temperature of 466°C for some schists, suggestive of local conditions of P_{H_2O} less than P_{Total}.

Dynamic metamorphism

Schistose rocks generally show good granoblastic textures. In contrast, quartz-rich rocks commonly show mortar textures and lobate

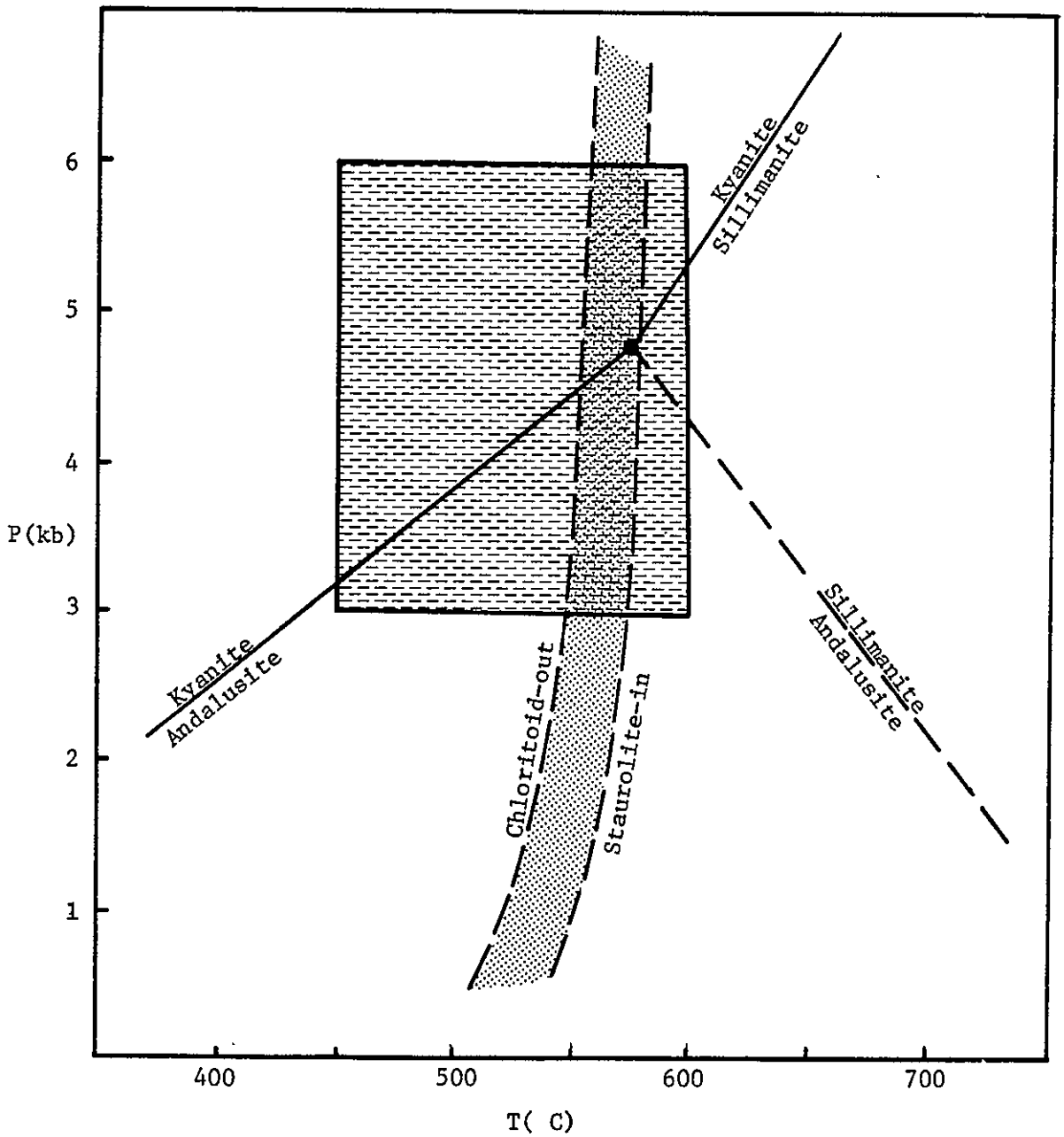

Figure 41. Possible P-T field for southern Manzano rocks (shaded region), based on garnet-biotite geothermometry and mineral assemblages. Stippled area is chloritoid-staurolite facies boundary from Bailey and Macdonald, 1976. K-A-S curves as a reference only.

quartz boundaries, strain ribbons, and nearly mylonitic textures in some samples (fig. 42). In places, small crystals of quartz seem to have grown between larger strained grains. Textural heterogeneity due to a variety of quartz grain sizes, shapes, and boundary types was observed in several quartzites.

A puzzling note is the fact that pre-thermal-peak cataclastic textures exist in quartzites. Microprobe data, and mineral assemblages and textures indicate that peak metamorphism of about 500°C occurred after F_2 and F_3 deformation. Quartz anneals readily at temperatures of 300°C. It is not clear how the pervasive strain textures seen in quartzites could persist through a 500°C thermal event. It seems unlikely that the extreme flattening and elongation of quartz grains could be formed in a non-penetrative event that did not affect schist fabrics, but that is the conclusion to which we are led. The question remains unresolved; perhaps future detailed petrographic studies will answer it.

Contact metamorphism

Intrusion of the Priest quartz monzonite into the Sevilleta, White Ridge, Blue Springs, and Sais metaclastics was accompanied by thermal metamorphism best seen in adjacent schists. The more aluminous Sevilleta schists show the most modified mineralogy. Two pelitic schists within a few hundred meters of the pluton have the assemblages:

sillimanite-staurolite-biotite-chlorite-muscovite-quartz-opaques

garnet-staurolite-chloritoid-biotite-chlorite-muscovite-quartz-opaques

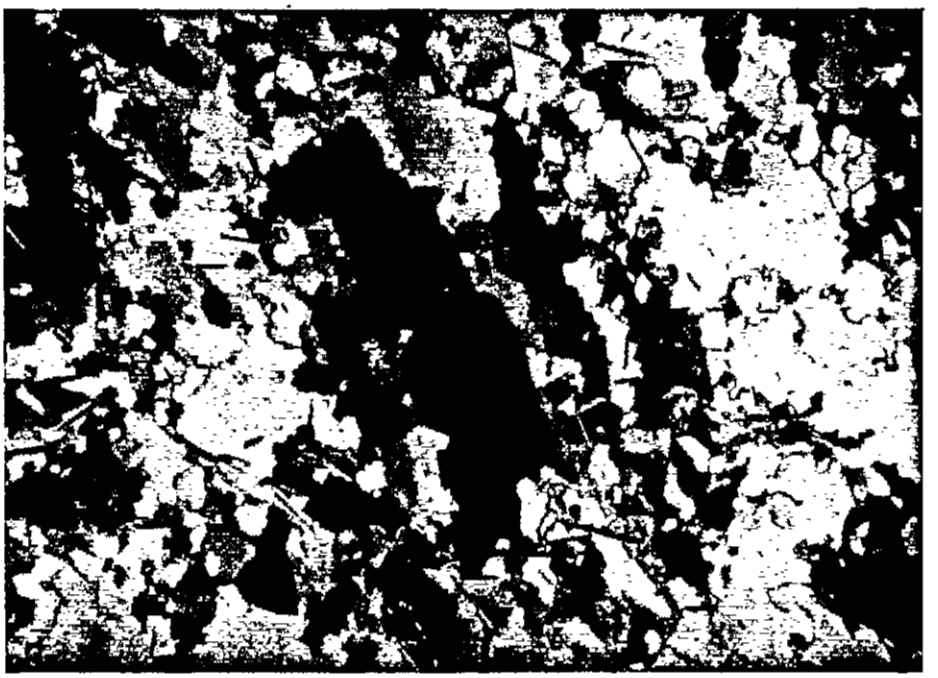

Figure 42. Photomicrograph of strained quartz grains with lobate disequilibrium boundaries in a White Ridge quartzite. Field is 2.0 mm across.

The only aluminum silicate observed in the map area is sillimanite found in some pelitic schists adjacent to the intrusion (fig. 43). Other nearby Sevilleta pelitic schists are tourmaline-bearing with assemblages of:

garnet-biotite-chlorite-muscovite-quartz-opaques

In many samples muscovite crystals are larger and more numerous than in typical pelitic schists of the area.

The laminated siliceous facies of the Blue Springs is drastically altered near the Priest intrusion. Hand specimens are dark, nearly massive looking, fine-grained rocks. In thin section the rock is well-foliated, extremely fine-grained, and composed of 50 percent quartz (0.05 mm across), 40 percent biotite, plus muscovite, sericite and opaques. The high proportion of fine-grained biotite imparts the dark color.

Rare quartz-plagioclase pegmatite dikes associated with the Priest intrusion cut country rock. One such dike 4.0-to 6.0-cm wide, which cuts pelitic schist, has formed a beautiful gradational quartz-tourmaline contact zone within the schist. Tourmaline crystals are poikiloblastic and up to 2.0 cm across.

Table 7 summarizes the relations between fabric development, deformation, and metamorphism in the southern Manzano Mountains.

Figure 43. Photomicrograph of contact metamorphic assemblage of garnet-fibrolite-biotite-staurolite-chlorite-quartz-muscovite in pelitic Sais schist adjacent to the Priest quartz monzonite. Field is 2.0 mm across.

Table 7. Summary chart of fabrics and metamorphism during deformation

D_1

S_1 Strong, penetrative, axial plane schistosity; generally parallel to bedding, although observed cutting S_0 locally; associated with a regional transposition layering; locally may be the dominant axial plane cleavage; in thin section appears to be spaced cleavage in some specimens; the question of whether S_1 is the earliest penetrative fabric is unresolved; folded by S_2; oriented at around N25°E, 60°NW.

L_{10} Intersection lineation seen locally, but generally indistinguishable from other lineations, may plunge 30°-50° southwest

F_1 Rarely seen, small, intrafolial, isoclinal folds visible only in thin-bedded quartzites and micaceous quartzites; no noses of map-scale F_1 folds are recognized; mesoscopic folds generally plunge gently southwest

M_1 Synkinematic metamorphism; growth and alignment of muscovite, biotite, and chlorite associated with S_1 development; greenschist facies; no large porphyroblasts recognized. Note: M_1, M_2, and M_3 may not be distinct metamorphic events. Instead, slow heating with successive deformations may have culminated after F_3.

D_2

S_2 Strong, well-developed, penetrative, axial-plane crenulation cleavage; overprints S_1 in schists by rotating micas into compositional, mica-rich layers; parallel to quartz grain elongation in quartzites; hand specimens locally show a metamorphic differentiation of mica-rich versus quartz-rich layers; local transposition in schists; the dominant cleavage in most outcrops, although may be confused with S_1 due to differing intensity of S_2 over map area; commonly nearly coplanar with S_1; oriented at around N25°E, 70°NW

L_{21} The dominant intersection lineation, generally a compositional banding or a crenulation lineation; parallel to F_2 fold axes at S45°W, 35°

F_2 Abundant, commonly disharmonic, symmetric to asymmetric, open to tight folds; seen in all lithologies; style depends on thickness and ductility contrast of strata; many map-scale closures recognized; strong statistical maximum of B_2^0 at S45°W, 35°

M_2 Synkinematic metamorphism; growth and alignment of muscovite, biotite, chlorite, quartz, and opaque crystals parallel to S_2; greenschist facies; no large porphyroblasts, some moderate sized biotites and chlorites; both cataclastic and granoblastic textures observed

D_3

S_3 Weak, non-penetrative, non-planar kink cleavage; two kink sets recognized (S_{3A} and S_{3B}); S_{3A} is dominant; generally near vertical, northwest striking

L_3 Uncommon; generally recorded as an intersection of aligned kink axes on S-surfaces generally plunges to the east

F_3 Not common; chevron kink folds in schists and some thin-bedded quartzites, and locally as broad folds in competent rocks; kinks are a few centimeters in wavelength; no F_3 map-scale fold noses recognized; at most, F_3 broadly warps rocks around a northwest axis

M_3 May be post-kinematic metamorphism; growth of large porphyroblasts of garnet, biotite, chloritoid, and staurolite; represents the thermal peak of regional metamorphism at upper greenschist to lower amphibolite facies; garnet, biotite, chloritoid, and staurolite show excellent mimetic and helicitic textures over S_1 and S_2; may have occurred between S_{3A} and S_{3B}; possibly coeval with post-tectonic granite intrusion

GEOCHRONOLOGY

Bolton (1976) performed Rb-Sr whole rock analyses on four samples of Sevilleta metarhyolite and one amphibolite, and six samples of Priest quartz monzonite. The five Sevilleta rocks defined an isochron of 1660±50 m.y. with an initial $^{87}Sr/^{86}Sr$ ratio of 0.7021±0.0022. Without the amphibolite sample an isochron of 1700±58 m.y. with a low initial $^{87}Sr/^{86}Sr$ ratio of 0.6995±0.0008 was derived for the metarhyolites. Priest rocks defined a 1470±30 m.y. isochron with an initial $^{87}Sr/^{86}Sr$ ratio of 0.7054±0.0012.

The Sevilleta date is the oldest isochron age for a siliceous metaigneous rock in central New Mexico (Condie and Budding, 1979). Recent U-Pb zircon data for metavolcanics in central New Mexico by Bowring and Condie (1982) have yielded similar ages.

The Priest date agrees well with a date of 1445±40 m.y. for the Sandia granite (Brookins and Majumdar, 1982) and other post-tectonic Precambrian granitic plutons in central New Mexico.

TECTONICS

Constraints

Ideas concerning tectonic mechanisms in the Proterozoic abound in the modern literature. Some of these disregard the detailed field observations which should form the foundation of any regional tectonic interpretation. In spite of the relatively small exposure of Precambrian rock in the Manzano Mountains, a number of geological constraints can be placed on the Precambrian deformational environment. These are lithologic, structural, and temperature-pressure constraints. They may be used to test Precambrian tectonic models for this area.

The general litho-stratigraphy in the southern Manzanos consists of a thick sequence of both thin-bedded and massive, shallow-water sandstones and shales overlain (or possibly underlain) by a bimodal assemblage of rhyolites and basalts. Precambrian granitic plutons intrude these supracrustal rocks. Thin, discontinuous beds of what may have been chert and conglomerate are present locally.

Structural constraints include style, orientation, and timing of deformational events. F_1 was an episode of regional transposition and isoclinal folding with formation of a penetrative axial plane schistosity. The original orientation of S_1 is not known, but because B_1^0 and B_2^0 are approximately coaxial, S_1 was probably horizontal.

F_2 formed open to tight folds, local transposition, and a strong crenulation cleavage. S_1 dips steeply to the northwest and strikes N30°E; B_2^0 plunges about S40°W. F_2 folds are common, range in wavelength from centimeters to kilometers, and are overturned slightly to the southeast.

F_3 was a mild deformational event which formed broad folds and kink folds. S_3 is not a penetrative fabric, and cuts across S_1 and S_2 at a high angle.

The third constraint concerns limits of metamorphic temperature and pressure which presumably reflect depth of burial of rocks and geothermal gradient. The highest grade Manzano rocks show a metamorphic thermal peak of about 500°C at 4 kb approximately synchronous with F_3 deformation. F_1 and F_2 do not seem to preserve evidence of syn-tectonic porphyroblastic growth. Grambling (1981) has calculated that average metamorphic geotherms and pressures were 47°C/km and 4.3 kb in the early Proterozoic, and 35°C/km and 6.0 kb in the late Proterozoic. Reasonable values for the 1.6-b.y.-old Manzano rocks might be 40°C/km and 5kb. Assuming the Manzano rocks lay in an average geothermal gradient, peak thermal metamorphism occurred at a crustal depth of about 13 km. Unfortunately, this gives depth for F_3 only, since the absolute timing between F_1, F_2 and F_3 is unknown.

Interpretations of Constraints

A lithologic assemblage of thick, shallow-water sandstone and shale suggests an environment of deposition similar to modern stable, lagoonal or deltaic continental shelves, or large, stable intracontinental

basins. Interpretation of volcanic and plutonic rocks is less precise since it is known that in modern times an assemblage of igneous rock can be formed in a number of different tectonic environments. In the western United States bimodal basalt-rhyolite suites and small allochthonous granitic bodies are common post-orogenic eugeoclinal rocks. In the San Juan Mountains of Colorado an early Miocene switch from intermediate rocks to dominantly basalt-rhyolite volcanics coincides with the onset of Rio Grande rifting (Lipman and others, 1970). This is characteristic of much of Cenozoic volcanism in the western U.S. interior (Lipman and others, 1970). In terms of relating bimodal volcanism to a specific tectonic geometry, very little is known. All one can say with reasonable certainty is that some thermal event causes magmatic differentiation of crust or mantle-derived rocks.

An interpretation of structural constraints is also somewhat nebulous since we have no equivalent of F_1 deformation in Phanerozoic rocks of the southwest, and because structural signatures are also non-unique criteria for tectonic geometry. We can give a number of generalities based on deformation style, which any theory must account for. Isoclinal folding and regional transposition of S_0 parallel to S_1 suggests a compressional stress regime with extreme shortening and/or shearing. From deep seismic studies Brown and others (1981) have postulated the existence of pervasive heterogeneity and horizontal layering in the middle and lower crust. They present a mechanism of crustal layering and thickening due to stacking of thrust sheets during episodes of continental collision. This is one preferred method for forming a horizontal S_1 fabric. Bedding faults and lithologic anomalies would accompany the S-fabric in this process. A second method

of horizontal compression, forming large-scale recumbent folds and nappes, could result in deformation similar to F_1. Again, geometric complexities through bedding-plane and similar faults might accompany folding. These two mechanisms are not mutually exclusive; in fact one might expect a combination of the two during some type of tectonic event involving extreme crustal shortening. A third setting for F_1 deformation in the deep crust by shearing along the mantle-crust boundary is not favored here due to the relatively low temperature-pressure conditions thought to exist during F_1 deformation. Hobbs and others (1976) state that regions with strong S_1 and many mesoscopic folds, but not large F_1 folds, may represent a series of F_1 thrust nappes. The southern Manzanos may be such an area.

It is not known whether fold generations represent separate episodes or successive responses during a single episode of orogeny. Hobbs and others (1976) note that multiple deformation may be due to either:

(1) A single episode with a complex response of the rocks; e.g. schistosity development followed by conjugate crenulation cleavage with continuous flattening;

(2) A changing tectonic setting of either:

  (a) change in type of orogeny;

  (b) change in direction of displacement;

  (c) change in rate of displacement.

Ramsay (1967, p. 519) states that successive deformations in one orogenic cycle are common and probably account for most of the examples

of polyphase folding. He does not attempt to separate Precambrian from Phanerozoic deformation belts.

Hobbs and others (1976) note that two common sequences of fold styles are almost invariably recognized in multiply deformed terrains. They are:

(1) F_1 - tight to isoclinal slaty cleavage or a schistosity as axial plane foliation

F_2 - one or more folds with crenulation cleavage as axial plane foliation; more open than F_1, but may be very tight; axial plane foliation can pass from an obvious crenulation cleavage to a schistosity which may mimic S_1

F_3 - one or more folds which lack axial plane foliation; commonly kink or chevron folds in rocks with prior foliation, and open folds with rounded hinges and curved limbs in more competent rocks

(2) F_1 - recumbent folds with schistosity parallel to axial planes

F_2 - as in (1) above, with steeply dipping axial surfaces

F_3 - as in (1) above

The similarities between the geometry of the Manzano fold sequences and these common styles are remarkable. It is also of interest that F_1 folds are commonly recumbent. This common deformation sequence argues for similar deformation mechanisms in operation over a very large area, perhaps during much of Precambrian time.

The role of volatile metamorphic fluids may play a significant role in style and apparent intensity of deformation. As Yardley (1981) has pointed out, with heating, dehydration reactions release large volumes of fluids which most certainly allow more extreme ductile deformation for a given set of stress parameters. A changing deformational history need not reflect changes in regional stresses. F_2 structures of tight folds and local transposition suggest a more moderate episode of deformation than F_1. If F_1 and F_2 are about coaxial, and assuming that the same tectonic geometry is responsible for both F_1 and F_2, either the center of strain was farther removed during F_2, the tectonism itself had waned, or the mechanical behavior of the rocks had changed. Since the absolute timing of F_1 and F_2 is not known, the above assumption is of low certainty. Van Schmus and Bickford (1981) state that Proterozoic rocks of the western U.S. show two distinct episodes of orogeny at 1.78-1.69 b.y. and 1.68-1.61 b.y. Since the Sevilleta amphibolites were emplaced between 1.65 and 1.75 b.y. and the undeformed Priest pluton at 1.43 to 1.50 b.y. (Bolton, 1976), there exists the possibility that F_1 and F_2 represent these two regional orogenic events in central New Mexico.

Whereas F_3 deformation is relatively insignificant with respect to strain magnitude, the S_3 orientation does indicate a new strain regime with the maximum principal strain axis having rotated from an F_2 orientation of north-northeast to west-northwest. F_3 also represents the time of maximum mineral growth. The tectonic significance of these occurrences is unknown, but may be related to granitic intrusion.

P-T constraints apply only to metamorphism around D_3. With the available data we can set only the most general limits on F_1 and F_2 conditions. Regional P-T were lower than F_3 conditions, since F_3 is a prograde event. Also, conditions were such that both ductile folds and brittle textures formed during deformation. Peak temperatures and pressures of around 500°C, 4 kb have been reported for many of the Proterozoic terrains in central and northern New Mexico (Cavin and others, 1982; Grambling, 1979; Grambling and Codding, 1982). This suggests that a very widespread, relatively constant set of regional metamorphic conditions existed over this area, and that all these Precambrian uplifts show similar erosional levels.

Models

Tectonic models of Precambrian mountain-belt formation are divided into uniformitarian and non-uniformitarian or actualistic. They differ mainly on the timing of the onset of buoyancy-powered subduction. Uniformitarianists interpret rocks as indicating that modern-type tectonics were operating as early as the Archean (Burke and Kidd, 1978; Windley, 1979), whereas actualists propose alternative mechanisms in the Archean with gradual phasing in of modern-day tectonics during the Proterozoic (Kroner, 1981; Hargraves, 1981; Goodwin, 1981).

Condie has proposed two entirely different uniformitarian models for the evolution of the southwestern United States. His early model (Condie and Budding, 1979) compared Precambrian rocks of New Mexico with Phanerozoic eugeocline, miogeocline, and continental-rift assemblages. Similarities between the Precambrian and rift rocks led him to conclude

that Precambrian rocks of central and south-central New Mexico developed in an incipient rift or multiple-rift system. In order to explain the observed rock assemblages, structural settings and igneous geochemistry he postulated an active subduction zone lying to the west with consequent back-arc spreading in the southwestern United States. In support of this model he stated that evidence of major compressive polyphase deformation such as nappes and complex fold interference patterns are not observed in the Precambrian of New Mexico. Major folds were interpreted as passive drape features. This model is incompatible with observed structure in the Manzano Mountains. At least three episodes of deformation are recognized in the Manzanos. The first two (F_1 and F_2) represent radical shortening of competent strata, most likely in a compressive stress field. Furthermore, every Proterozoic terrain in New Mexico that has recently been mapped and analyzed in detail has shown comparable polyphase deformation (Grambling, 1982; Holcombe and Callender, 1982; Grambling and Codding, 1982; Cavin and others, 1982; R. Miller, personal commun., 1982). Extension is clearly not the proper stress environment for such areas.

Condie's recent model (Condie, 1982) is based on the following observations: (1) Precambrian supracrustal rocks young from north to south; (2) Precambrian granitic plutons intrude these rocks; (3) sequences of bimodal volcanics are overlain by quartzite-shale assemblages; and (4) geochemical and Sr-isotope data suggest "a variably depleted upper mantle source for basalts and a short-lived (100 m.y.) lower-crustal source for granite and felsic volcanic magmas (Condie, 1982, p. 37)." In order to explain these general observations Condie proposed a model of southward-migrating arcs with successive basin

closures and Andean-type orogenies accreting 1300 km of continental crust between 1.8 and 1.1 b.y. ago. Condie notes that a serious shortcoming of this model is the absence of, or only minor amounts of, calc-alkalic volcanics, graywacke, and chert commonly associated with contemporary convergent plate boundaries. Aside from this, the four regional constraints above are well accomodated by this model. On a local scale however there are some inconsistencies between this model and the geology of the southern Manzanos. Primarily there is the incongruity of forming northeast-striking tight and isoclinal folds in a north-south compressive regime. This is not a problem in the Picuris, Truchas, and Rio Mora areas to the north where F_1 and F_2 fabrics trend east-west (Holcombe and Callender, 1982; Grambling, 1979; Grambling and Codding, 1982), although this trend may not be due to S_2 (J. Grambling, personal commun., 1982). Two ways to accomodate this model to the Manzanos are to call upon either local stress conditions during both F_1 and F_2, or post-orogenic basement block rotation. Local anomalous stress may have required only an irregular boundary which was maintained throughout both F_1 and F_2. Post-orogenic basement block fracture and rotation is possible but would have required 40° to 60° of rotation of the whole Sandia-Manzanos-Los Pinos block. A total lack of field evidence insures that this remains unresolved. A second inconsistency between field data and Condie's model concerns the stratigraphic relations between quartzite-schist and metavolcanic assemblages. If Stark's stratigraphy is valid, and the limited available data suggests that it is, then the quartzite-schist is overlain by bimodal volcanics, not underlain by them. Perhaps this is

not particularily damaging to the model since it is not known what lies above the metavolcanics if the metaclastics do not.

The notion of intensity of deformation decreasing with time, as observed in the Manzanos, is remarkably suited to Condie's accretionary model. As the suture zone migrates south, repeated collisiors should produce successively weaker overprinted fabrics assuming successive orogenies are about equal in severity. A necessary corollary is that tectonite fabrics will not be correlative by style along a line perpendicular to the orogenic belt. This effect would greatly complicate regional syntheses of deformation.

Several authors have recently suggested that Precambrian tectonic styles may have been different than modern Wilson-cycle plate tectonics (Kroner, 1982; Hargraves, 1982; Goodwin, 1982). The generally agreed upon major constraint on a tectonic mechanism is that the Earth's mean heat flow has decreased through time. Actualistic models state that a hotter earth precluded buoyancy-powered subduction. Lacking subduction, a process of crust-mantle delamination followed by intracortinental orogenesis is preferred by most theorists. Deformational features are likely to be similar to those of colliding continents, but rock assemblages, which are the thorns in uniformitarianists sides, may be different. Actualistic interpretations may better apply to the observed geology of the southern Manzano mountains. The model favored here is one similar to Condie's (1982) but lacking the subduction zone and back-arc basin. In this model a hot spot or "hot line" migrated southward, causing successive continental delamination and intracontinental ensialic orogeny. S_1 forms by stacked thrust sheets and/or recumbent folds and nappes or some mechanism as yet unrecognized.

S_2 forms during either a pulse within the same strain field as S_1, or as a later distinct event. S_3 and associated thermal metamorphism form later, perhaps during granitic intrusion, in a new stress field under higher temperatures. This scheme is consistent with field data from the southern Manzanos, but is also speculative.

CONCLUSIONS

1. A simple stratigraphic sequence of Sais, Blue Springs, White Ridge, and Sevilleta rocks as previously described (Stark, 1956) does not exist. Instead, this area consists of at least two distinct structural-stratigraphic terrains separated by bedding-plane faults. The western terrain mainly consists of thin, structurally complex metavolcanic and metaigneous units. The eastern terrain contains thicker, more competent metaclastics which outwardly appear less deformed. Similar lithologies in both terrains may or may not be stratigraphically correlative.
2. Previous estimates of stratigraphic thicknesses of units are high due to tectonic thickening during multiple deformations.
3. The earliest recorded deformation (D_1) was a strong, penetrative, S_1-schistosity-forming event with recumbent isoclinal folding and associated regional transposition of bedding (S_0) parallel to S_1.
4. S_1 locally appears to be a spaced cleavage, implying that it cuts an earlier S-fabric, but this issue remains unresolved.
5. Although small, isoclinal F_1 fold noses are seen in outcrop, no map scale F_1 closures are recognized. The reason is unknown, although it is likely that D_1 transposition with later F_2 deformation have made major F_1 folds unrecognizable.
6. D_2 formed a well-developed, penetrative, axial-plane crenulation cleavage (S_2) which is manifest in schists as a metamorphic differentiation of mica-rich versus quartz-rich layers. S_2 is

the dominant cleavage in most outcrops, although it may be mistaken for S_1 locally.

7. Abundant, commonly disharmonic, open to tight F_2 folds exhibit a wide range of styles due to the relative thickness and ductility contrast of beds.

8. F_2 folds are upright, generally plunge gently southwest, and are overturned slightly to the southeast. Numerous map-scale F_2 structures are recognized.

9. D_3 was a weak, non-penetrative event which formed chevron folds in schists and broad folds in quartzites. No major F_3 fold closures are recognized.

10. Peak thermal metamorphism (M_3) in the upper greenschist to lower amphibolite facies was post-kinematic. Porphyroblasts of garnet, biotite, chloritoid, and staurolite have overgrown tectonite fabrics. Mineral assemblages and garnet-biotite geothermometry yield peak metamorphism at about 500°C, 3-6 kb.

11. A trend along strike from chloritoid-bearing schists to staurolite-bearing schists suggests a higher temperatures in the southern map area. This lateral variation may be related to anomalously high temperatures around the Priest quartz monzonite during its emplacement. If so, M_3 porphyroblast growth is coeval with the Priest pluton thermal event.

12. Both cataclastic (strain) and granoblastic (equilibrium) quartz grain textures are seen. Non-annealed quartz strain textures imply that extensive strain occurred after the thermal metamorphic peak; but M_3 is clearly post-F_3. This apparent inconsistency remains unresolved.

13. Similarities in deformational styles and peak metamorphic conditions between the Manzano rocks and other Proterozoic terrains in north-central New Mexico argue for widespread, relatively constant tectonic mechanisms and geothermal gradients. Furthermore, Hobbs and others (1976) note that the fold styles seen in the Manzanos are common in most multiply deformed terrains. This also suggests similar deformation mechamisms over large areas.

14. Proterozoic rocks of the western U.S. show two distinct orogenic events at 1.78 - 1.69 b.y. and 1.68 - 1.61 b.y. (Van Schmus and Bickford, 1981). These dates are consistent with D_1 and D_2 in the Manzano Mountains.

15. An actualistic tectonic model for the evolution of supracrustal Proterozoic rocks in this area is proposed in which a southward-migrating "hot-line" causes successive continental delamination and intracontinental orogeny. In this model S_1 forms either by stacked thrust sheets or recumbent thrust nappes during compressional orogeny. S_2 forms by local horizontal west-northwest compression during either a pulse within a long-lived event or as a later distinct event. S_3 and later thermal metamorphism form later under a new stress field in response to both local and regional granitic intrusions.

REFERENCES CITED

Albee, A. L., 1972, Metamorphism of pelitic schists: reaction relations of chloritoid and staurolite: Geological Society of America Bulletin, v. 83, p. 3249-3268.

Armstrong, D. G. and Holcombe, R. J., 1982, Precambrian rocks of a portion of the Pedernal Highlands, Torrance County, New Mexico: in Grambling, J. A., Wells, S. G. and Callender, J. F., eds. New Mexico Geological Society Guidebook 33, p. 203-210.

Bauer, P. W., 1982, Precambrian geology and tectonics of the southern Manzano Mountains, New Mexico: in Grambling, J. A., Wells, S. G., and Callender, J. F., eds., New Mexico Geological Society Guidebook 33, p. 211-216.

Beers, C. A., 1976, Geology of the Precambrian rocks of the south Los Pinos Mountains, Socorro County, New Mexico (M.S. thesis): New Mexico Institute of Mining and Technology, Socorro, 238 p.

Birch, F., 1980, Geophysical evaluation of basin hydrologic characteristics in the central Rio Grande, Part I: Gravity models of the Albuquerque-Belen Basin: preliminary unpublished report, University of New Mexico.

Blount, W., 1982, Contact between Sais quartzite and lower metaclastics of Oja da Casa, New Mexico: in Grambling, J. A., Wells, S. G., and Callender, J. F., eds., New Mexico Geological Society Guidebook 33, p. 26.

Bolton, W. R., 1976, Precambrian geochronology of the Sevillita

Metarhyolite and the Los Pinos, Sepultura, and Priest plutons of the southern Sandia uplift, New Mexico (M.S. thesis): New Mexico Institute of Mining and Technology, Socorro, 45 p.

Bowring, S. A. and Condie, K. C., 1982, U-Pb Zircon ages from northern and central New Mexico (Abs.): Geological Society of America Abstracts with Programs, Rocky Mountain section, v. 8, p. 304.

Brookins, D. G. and Majumdar, A., 1982, The Sandia granite, New Mexico: biotite metamorphic and whole rock Rb-Sr ages: Isochron/West, n. 33, p. 19-21.

Brown, L. D., Oliver, J. E., et al., 1981, Deep crustal structure: implications for continental evolution, in W. S. Fyfe, ed., Evolution of the Earth, p. 38-52.

Burke, K. and Kidd, W. S. F., 1978, Were Archean continental geothermal gradients much steeper than those of today?: Nature, v. 272, p. 240.

Carmichael, D. M., 1970, Intersecting isograds in the Whetstone Lake area, Ontario: Journal of Petrology, v. 11, p. 147-181.

Cavin, W. J., Connolly, J. R., Woodward, L. A., Edwards, D. L., and Parchman, M., 1982, Precambrian stratigraphy of the Manzanita and North Manzano Mountains, New Mexico: in Grambling, J. A., Wells, S. G., and Callender, J. F., eds., New Mexico Geological Society Guidebook 33, p. 191-196.

Condie, K. C., 1982, Plate-tectonics model for Proterozoic continental accretion in the southwestern United States: Geology, v. 10, p. 37-42.

Condie, K. C., and Budding, A. J., 1979, Geology and geochemistry of

Precambrian rocks, central and south-central New Mexico: New Mexico Bureau of Mines and Mineral Resources Memoir 35, 58 p.

Ferry, J. M. and Spear, F. S., 1978, Experimental calibration of the partitioning of Fe and Mg between biotite and garnet: Contributions to Mineralogy and Petrology, v. 66, p. 113-117.

Fisher, A. B. and Ehlers, E. G., 1982, Porphyroblasts and "crystallization force": an experimental analog: Geology, v. 10, p. 394-399.

Ganguly, J., 1969, Chloritoid stability and related parageneses: theory, experiments, and applications: American Journal of Science, v. 267, p. 910-944.

Ganguly, J. and Newton, R. C., 1969, Thermal stability of chloritoid at high pressure and relatively high oxygen fugacity: Journal of Petrology, v. 9, p. 444-466.

Goodwin, A. M., 1981, Precambrian perspectives: Science, v. 213, p. 55-61.

Grambling, J. A., 1979, Geology of Precambrian metamorphic rocks of the Truchas Peaks area, north-central New Mexico (Ph.D. thesis): Princeton, New Jersey, Princeton University, 209 p.

Grambling, J. A., 1981, Pressures and temperatures in Precambrian metamorphic rocks: Earth and Planetary Science Letters, v. 53, p. 63-68.

Grambling, J. A., 1982, Precambrian structures in Canon del Trigo, Manzano Mountains, central New Mexico: in Grambling, J. A., Wells, S. G., and Callender, J. F., eds., New Mexico Geological Society Guidebook 33, p. 217-220.

Grambling, J. A. and Codding, D. B., 1982, Stratigraphic and structural

relationships of multiply deformed Precambrian rocks in the Rio Mora area, New Mexico: Geological Society of America Bulletin, v. 93, p. 127-137.

Greenwood, H. J., 1976, Metamorphism at moderate temperatures and pressures, in Bailey, D. K. and Macdonald, R., eds., The evolution of the crystalline rocks: New York, Academic Press, p. 187-260.

Hargraves, R. B., 1981, Precambrian tectonic style: a liberal uniformitarian interpretation, in Kroner, A., ed., Precambrain plate tectonics: Elsevier, New York, p. 21-56.

Hirschberg, A. and Winkler, H. G. F., 1968, Stabilitatsbeziehungen zwischen Chlorit, Cordierit und Almandin bei der Metamorphose: Contributions to Mineralogy and Petrology, v. 18, p. 17-42.

Hobbs, B. E., Means, W. D., and Williams, P. F., An outline of structural geology: Wiley, New York, 571 p.

Holcombe, R. J., and Callender, J. F., 1982, Structural analysis and stratigraphic problems of Precambrian rocks of the Picuris Range, New Mexico: Geological Society of America Bulletin, v. 93, p. 138-149.

Hoschek, G., 1967, Untersuchungen zum Stabilitatsbereich von Chloritoid und Staurolith: Contributions to Mineralogy and Petrology, v. 14, p. 123-162.

Hoschek, G., 1969, The stability of staurolite and chloritoid and their significance in metamorphism of pelitic rocks: Contributions to Mineralogy and Petrology, v. 22, p. 208-232.

Kroner, A., 1981, Precambrian plate tectonics, in Kroner, A., ed., Precambrian plate tectonics: Elsevier, New York, p. 57-90.

Lipman, P. W., Steven, T. A., and Mehnert, H. H., 1970, Volcanic history of the San Juan Mountains, Colorada, as indicated by potassium-argon dating: Geol. Soc. America Bulletin, v. 81, n. 8, p. 2329-2352.

Mallon, K. M., 1966, Precambrian geology of the northern part of the Los Pinos Mountains, New Mexico (M.S. thesis): New Mexico Institute of Mining and Technology, 88 p.

Myers, D. A. and McKay, E. J., 1974, Geologic map of the southwestern quarter of the Torreon 15-minute quadrangle, Torrance and Valencia counties, New Mexico: United States Geological Survey Miscellaneous Geological Investigations Map, I-820.

Ramsay, J. G., 1967, Folding and fracturing of rocks: McGraw-Hill, New York, 568 p.

Reiche, P., 1949, Geology of the Manzanita and North Manzano Mountains, New Mexico: Geological Society of America Bulletin, v. 60, p. 1183-1212.

Stark, J. T., 1956, Geology of the south Manzano Mountains, New Mexico: New Mexico Bureau of Mines and Mineral Resources Bulletin 34, 46 p.

Stark, J. T. and Dapples, E. C., 1946, Geology of the Los Pinos Mountains, New Mexico: Geological Society of America Bulletin, v. 57, p. 1121-1172.

Thompson, J. B., 1957, The graphical analysis of mineral assemblages in pelitic schists: American Mineralogist, v. 42, p. 842-858.

Turner, F. J. and Weiss, L. E., 1963, Structural analysis of metamorphic tectonites: McGraw Hill, New York, 545 p.

Van Schmus, W. R. and Bickford, M. E., 1981, Proterozoic chronology and evolution of the midcontinent region; North America, in A. Kroner, ed., Precambrian Plate Tectonics, Elsevier, New York, p. 261-296.

Windley, B. F., 1979, The Evolving Continents, Wiley, London, 385 p.

Windley, B. F., 1981, Precambrian rocks in the light of the plate-tectonic concept, in A. Kroner, ed., Precambrian Plate Tectonics, Elsevier, New York, p. 1-20.

Winkler, H. G. F., 1979, Petrogenesis of metamorphic rocks, 5th edition: Springer-Verlag, New York, 348 p.

Yardley, B. W. D., 1981, Effect of cooling on the water content and mechanical behavior of metamorphosed rocks: Geology, v. 9, p. 405-408.

APPENDIX I

Equal-area lower hemisphere stereographic projections

Contents:

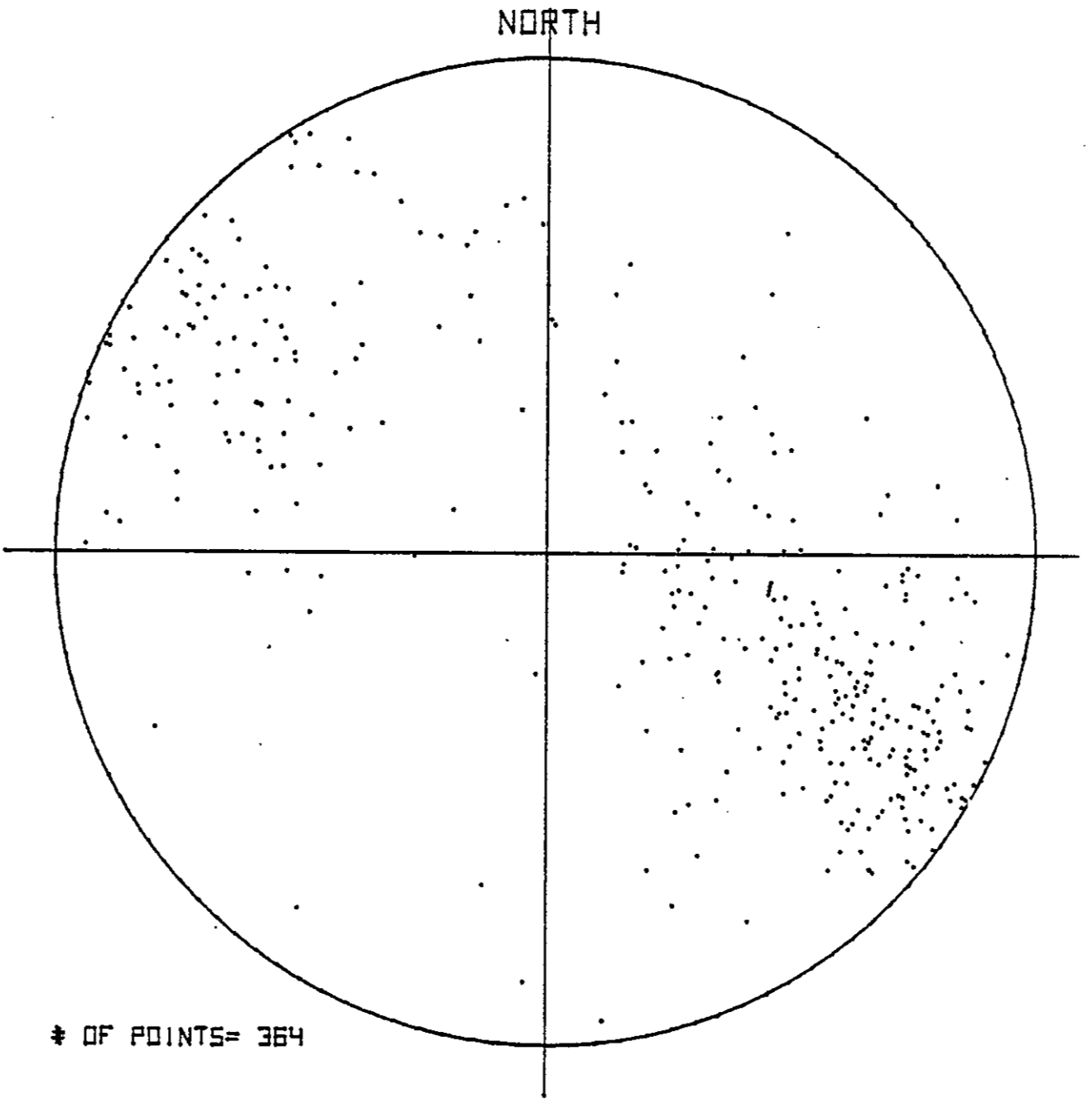

Equal-area plot of poles to S_0/S_1.

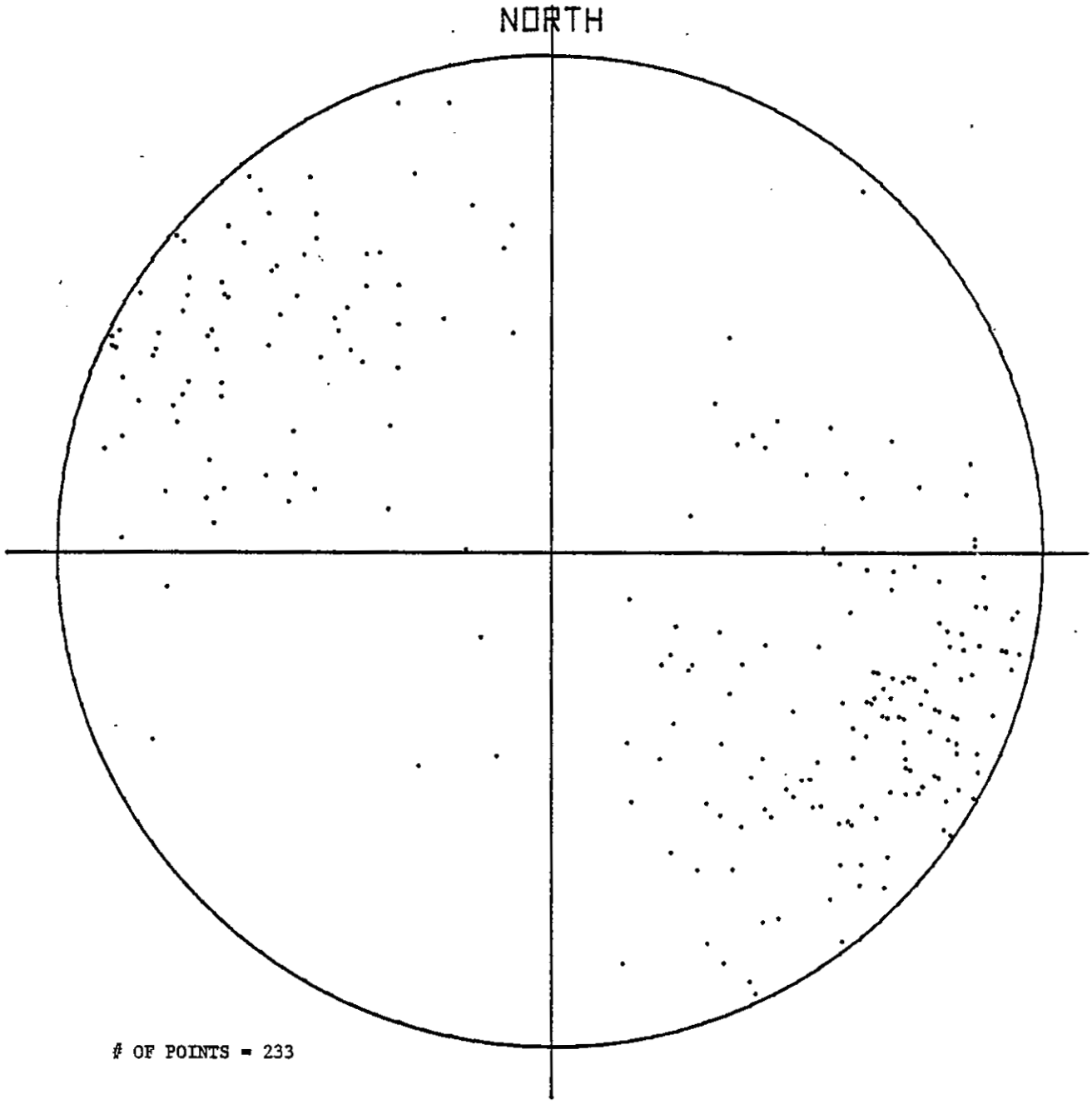

Equal-area plot of poles to S_2 planes.

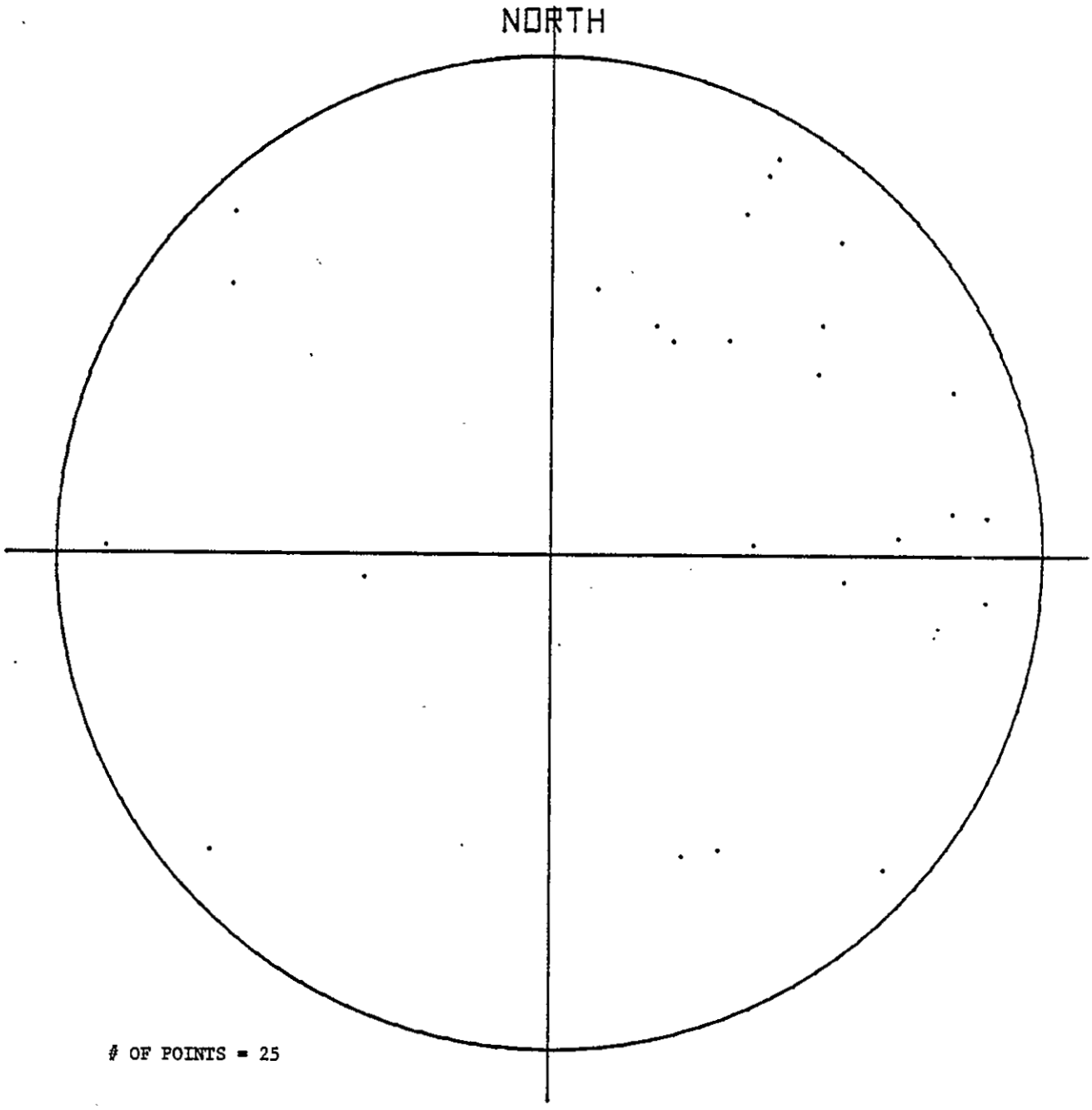

Equal-area plot of poles to S_3 planes.

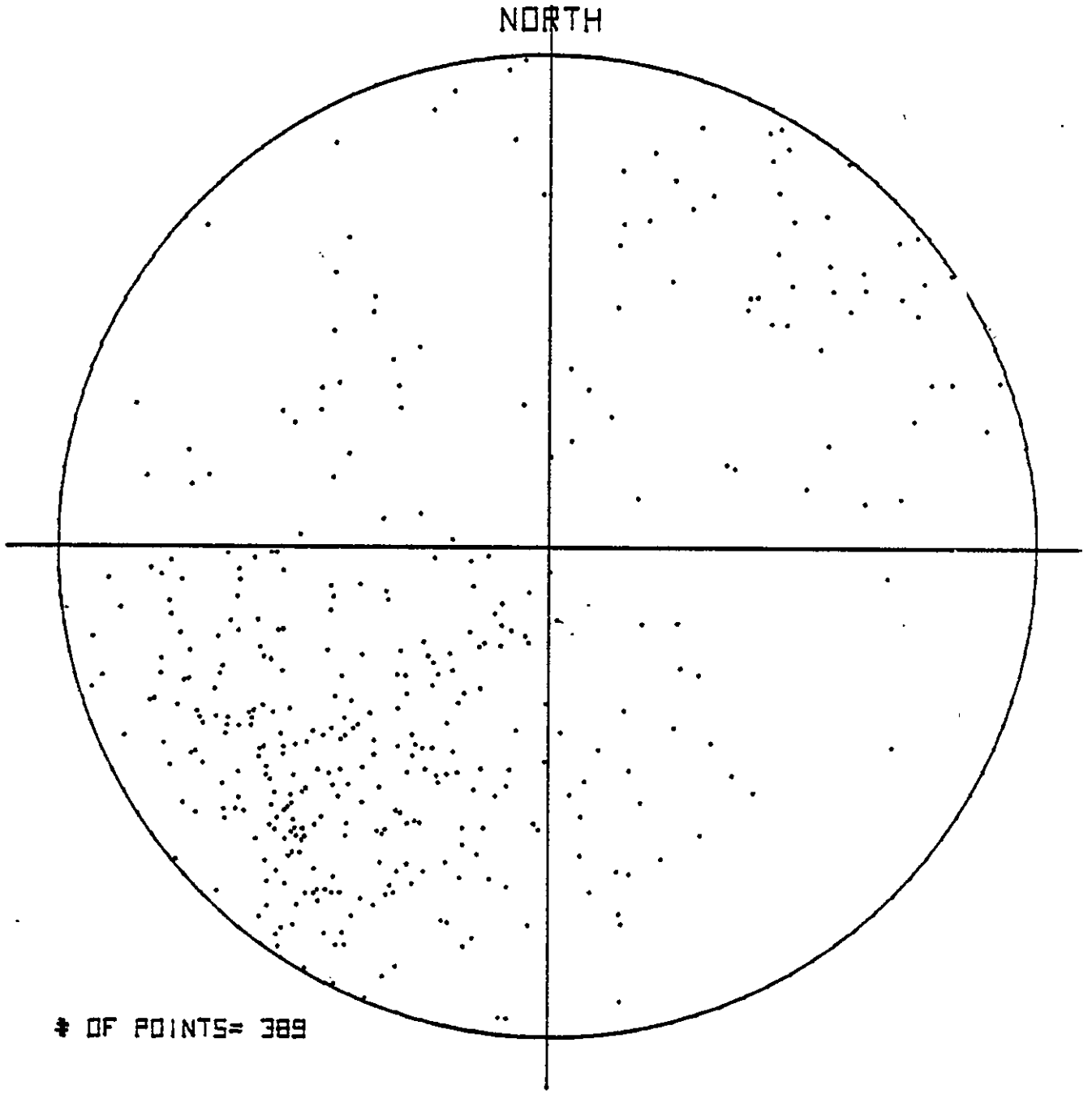

Equal-area plot of intersection lineations L_{10}, L_{20}, and L_{21}.

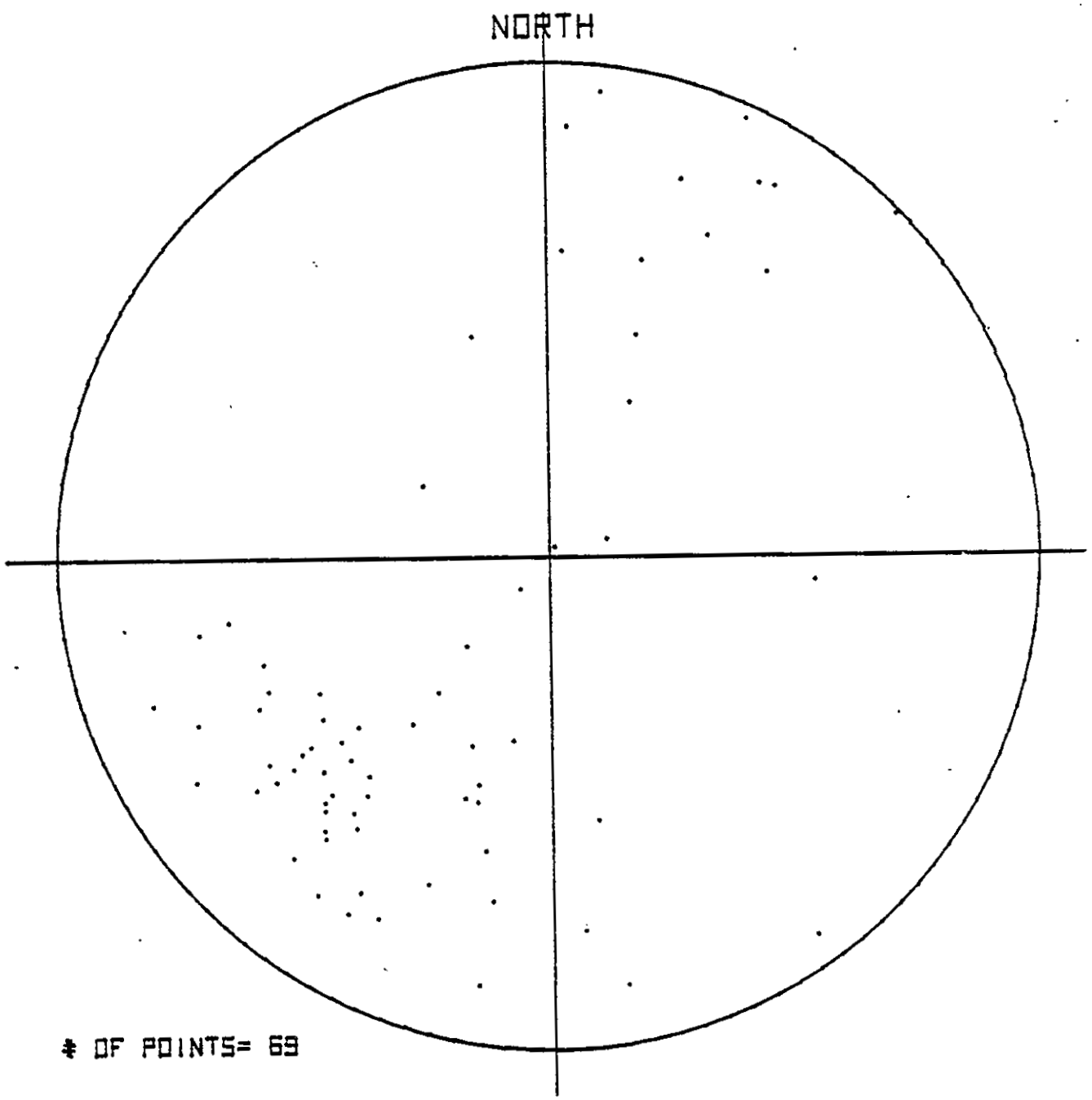

Equal-area plot of all B_2^1 fold axes.

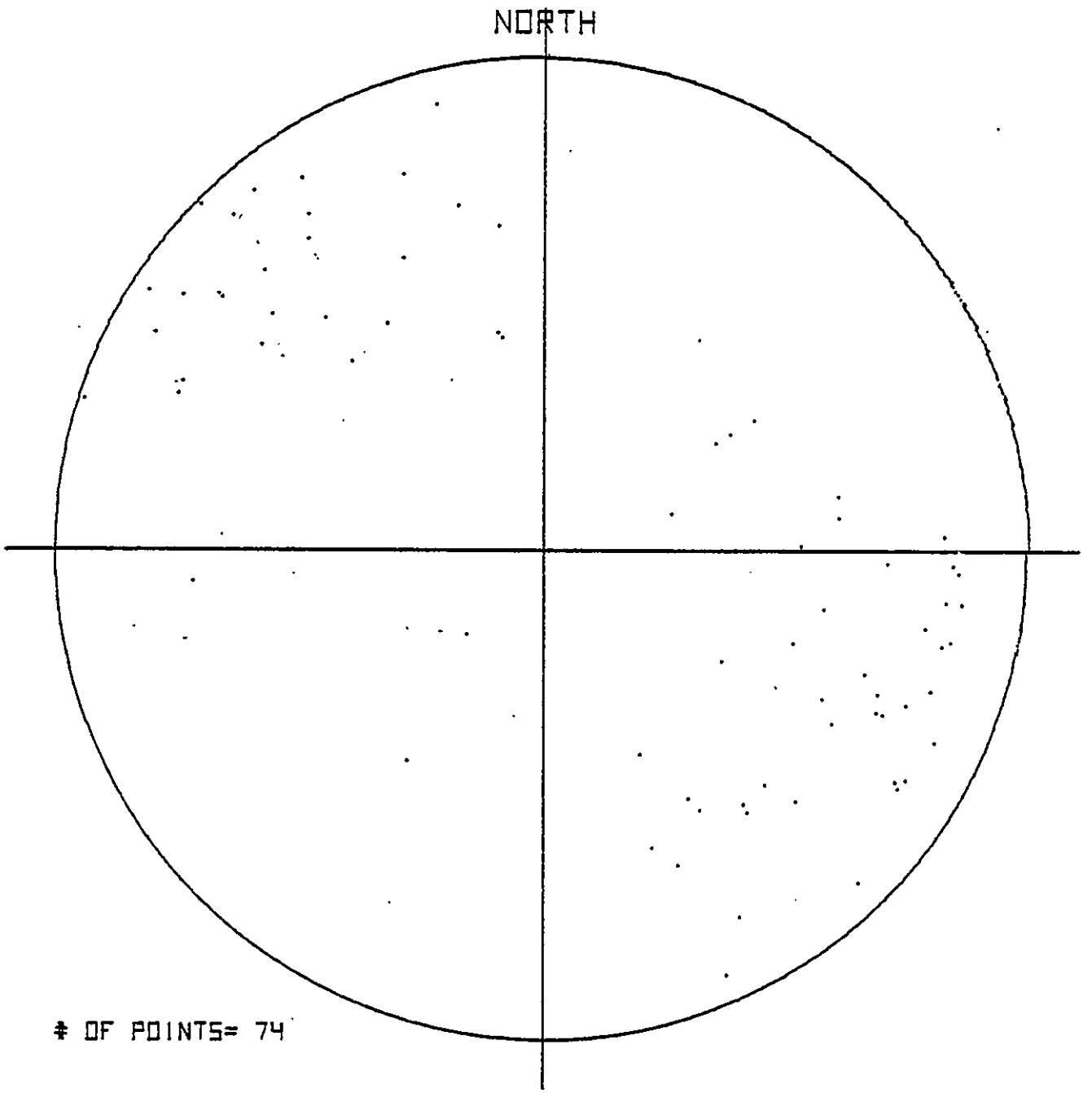

Equal-area plot of poles to selected S_2 planes.
See text for selection process.

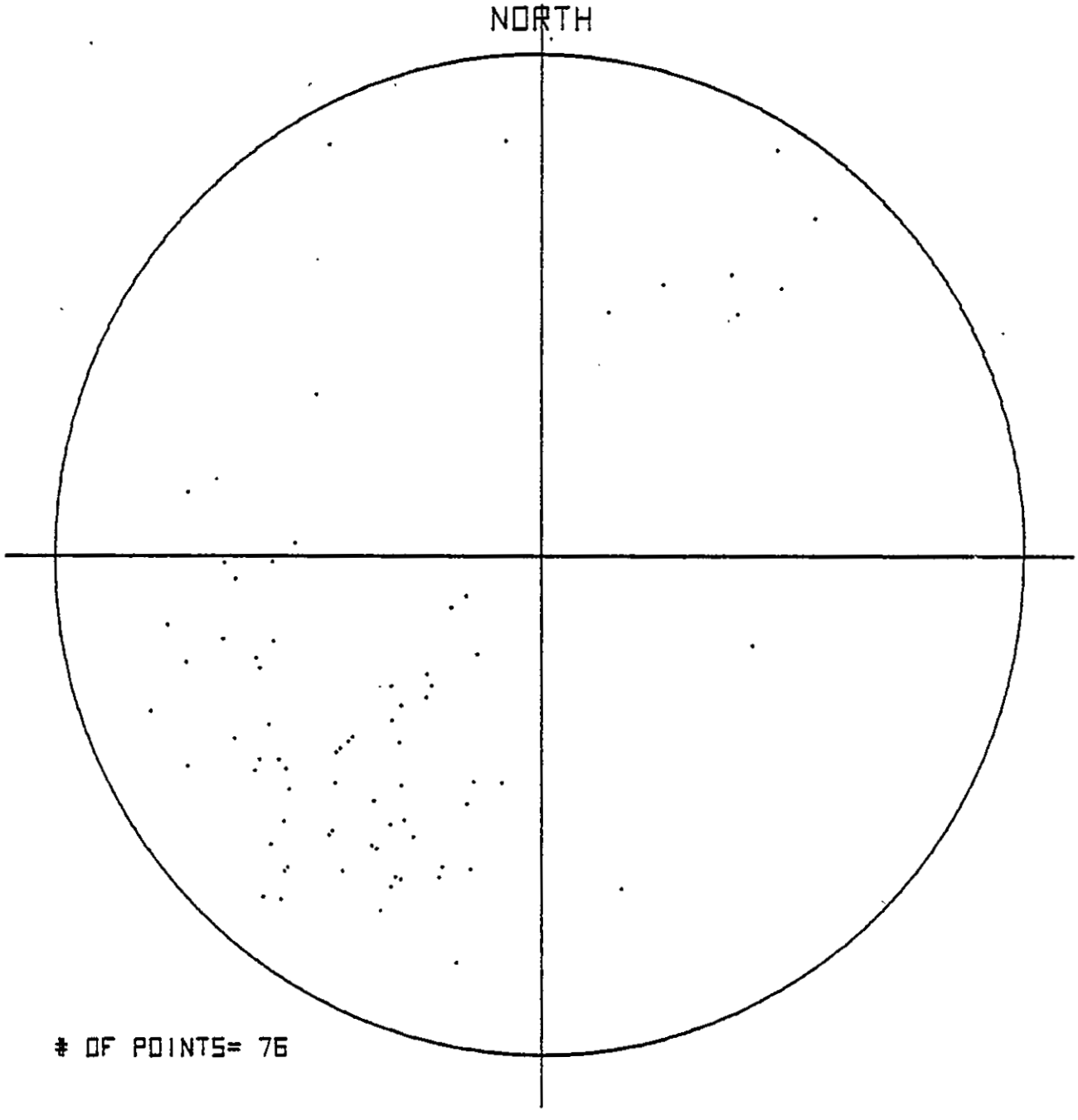

Equal-area plot of selected intersection lineations (L_{10} and L_{21}). See text for selection process.

APPENDIX II

Garnet-Biotite Geothermometry Calculations (from Ferry and Spear, 1978).

$$T\ (K) = \frac{12{,}454 + 0.057\ (P)}{4.662 - 3(1.9872)\ln K_D}$$

$$K_D = (Fe/Mg)_{Bi}/(Fe/Mg)_{Gt}$$

SAMPLE	Fe/Mi_{Bi}	Fe/Mg_{Gt}	K_D	P(kb)	T(°K)	T(°C)
SMZ-30	2.01	16.25	0.129	4	751	478
				6	758	485
SMZ-37	1.65	13.40	0.123	4	739	466
				6	745	472
SMZ-55	1.33	8.50	0.156	4	806	533
				6	814	541

GEOLOGIC MAP OF THE PRECAMBRIAN ROCKS OF THE SOUTHERN MANZANO MOUNTAINS, NEW MEXICO

PLATE 1

by
Paul W. Bauer
1982

106° 30' 34° 37' 15"
106° 27' 30"
106° 25' 20" 34° 36' 20"
34° 30'
106° 30'
106° 27' 30"

Base from U.S. Geol. Survey
Torreon Quad., 1:62,500, 1954

Map drafting by Judy Salas

SCALE 1:12,000

0 .5 MILE
0 .5 KILOMETER

CONTOUR INTERVAL = 40 ft.

108° 106° 104°
36°
34°
32°
Map area
NEW MEXICO

12.5°
T.N. M.N.

LEGEND

LITHOLOGIES

Qal — ALLUVIUM (QUATERNARY) - Unconsolidated silt, sand and gravel; pediment deposits

P — PALEOZOIC SEDIMENTS (MIDDLE PENNSYLVANIAN TO LOWER PERMIAN) - Includes sandstones, siltstones, shales, conglomerates, and limestones of the Sandia, Madera, Bursum, and Abo formations

PRECAMBRIAN LITHOLOGIES

East of Paloma Fault

pqm — PRIEST QUARTZ MONZONITE - Coarse-grained, biotite-quartz-feldspar phanerite with microcline phenocrysts

bq_1 — BLUE SPRINGS FORMATION-Thinly-laminated, very fine-grained, brightly colored quartzite

bs_1 — BLUE SPRINGS FORMATION - Dark, chlorite-muscovite schist with up to 40 volume percent vein quartz

sq_3 — SAIS FORMATION - Resistant, light-colored quartzites with interbedded schists

ss_2 — SAIS FORMATION - Quartz-muscovite schist; interlayered in sq_3

sq_2 — SAIS FORMATION - Purple, thin-bedded, crossbedded quartzites and thin schists

sq_4 — SAIS FORMATION(?) - Red massive, resistant, hematitic quartzite

ss_1 — SAIS FORMATION - Orange-weathering quarts-muscovite schist

sq_5 — SAIS FORMATION - Thin white quartzite; locally in SS_3

sq_1 — SAIS FORMATION - Blue-grey, vitreous, massive to thin-bedded, medium grained quartzite

ss_3 — SAIS FORMATION(?) - Chlorite-muscovite schist

West of Paloma Fault

bq_2 — BLUE SPRINGS FORMATION - Thinly-laminated, very fine-grained, brightly colored quartzite; correlative to bq_1

bs_2 — BLUE SPRINGS FORMATION(?) - Dark, chlorite-muscovite schist; may be correlative to bs_1

sq_8 — SAIS FORMATION(?) - Light colored, thin-bedded quartzite; may be correlative to sq_2-sq_3 and sq_4

ss_4 — SAIS FORMATION(?) - Quartz-muscovite schist; may be correlative to ss_1

sq_7 — SAIS FORMATION(?) - White to gray, resistant, massive quartzite; may be correlative to sq_3

sq_6 — SAIS FORMATION(?) Thin-bedded, reddish, schistose quartzite; may be correlative to sq_1

rsq — SEVILLETA FORMATION - Interlayered quartzites and schists; in the western felsic metaigneous terrain

ra — SEVILLETA FORMATION - Dark chlorite schists and amphibolites; commonly discontinuous along strike; in the western felsic metaigneous terrain

rr — SEVILLETA FORMATION - Pink or gray, blocky, somewhat schistose, porphyritic metarhyolite; in the western felsic metaigneous terrain

as — SEVILLETA FORMATION - Pelitic schists including chloritoid-garnet schists and staurolite-garnet schist; in the eastern amphibolitic terrain

aq — SEVILLETA FORMATION - Quartzites and local reddish metarhyolite; in the eastern amphibolitic terrain

aa — SEVILLETA FORMATION - Variety of mafic metaigneous rocks; includes chlorite-hornblende schist and amphibolite, metadiorite; commonly discontinuous along strike; in the eastern amphibolitic terrain

wq_3 — WHITE RIDGE FORMATION - Orange-weathering, generally thin-bedded schistose quartzite

wq_2 — WHITE RIDGE FORMATION - White to gray, medium-grained, thin-bedded, very resistant orthoquartzite

ws_1 — WHITE RIDGE FORMATION - Coarse-grained garnet-muscovite schist

wq_1 — WHITE RIDGE FORMATION - Light-colored, medium-grained, massive thin-bedded, hematitic, vitreous quartzite

POSSIBLE CORRELATION OF PRECAMBRIAN ROCK UNITS

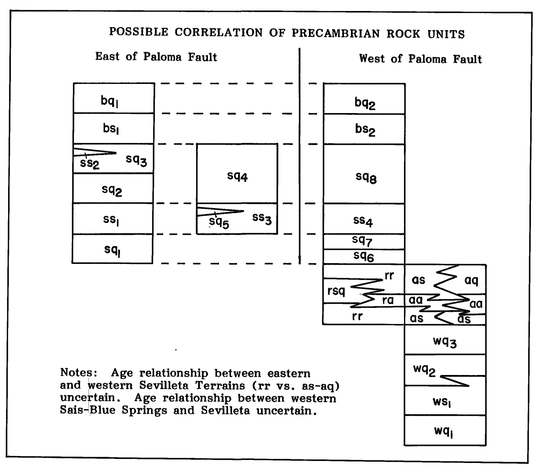

Notes: Age relationship between eastern and western Sevilleta Terrains (rr vs. as-aq) uncertain. Age relationship between western Sais-Blue Springs and Sevilleta uncertain.

SYMBOLS

Contact - may be a tectonic (transpositional) contact in places; dashed where inferred

Fault - U, upthrown side; D, downthrown side dashed where inferred

Probable fault

F_1 minor antiform; showing direction of plunge

F_1 minor synform; showing direction of plunge

F_2 minor antiform; showing direction of plunge

F_2 minor synform; showing direction of plunge

F_2 antiform - showing direction of plunge.; dashed where approximate; with value of plunge

F_2 synform - showing direction of plunge; dashed where approximate; with value of plunge

F_2 overturned antiform; showing direction of plunge; dashed where approximate; with value of plunge

F_2 overturned synform; showing direction of plunge; dashed where approximate; with value of plunge

Uncertain F_2 fold; showing direction of plunge

Area of many F_2 minor folds; generally "M" type; showing direction of plunge

F_3 kink folds; showing direction of plunge

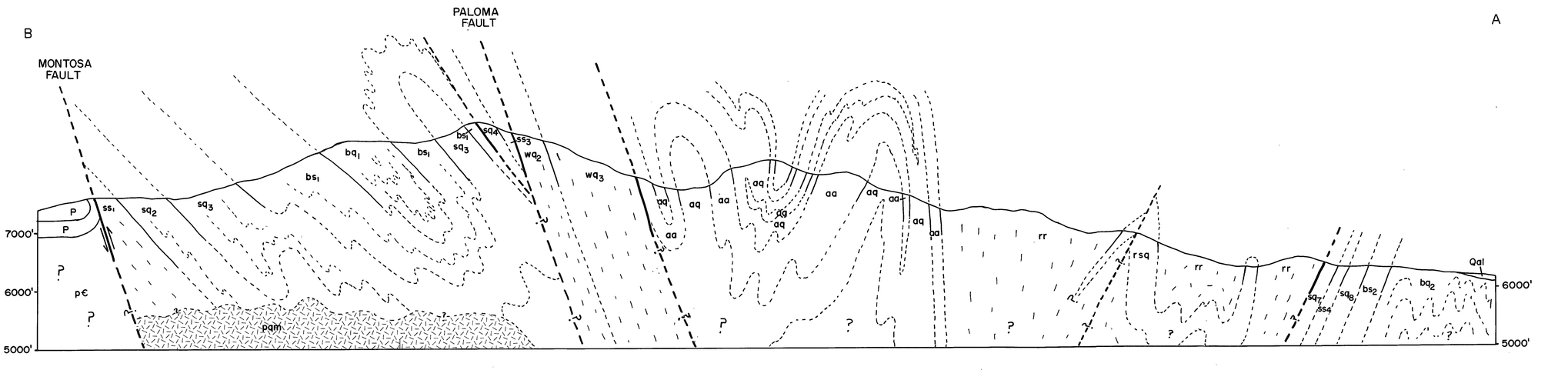

SCALE 1:12,000 NO VERTICAL EXAGGERATION
VIEW SOUTHWEST

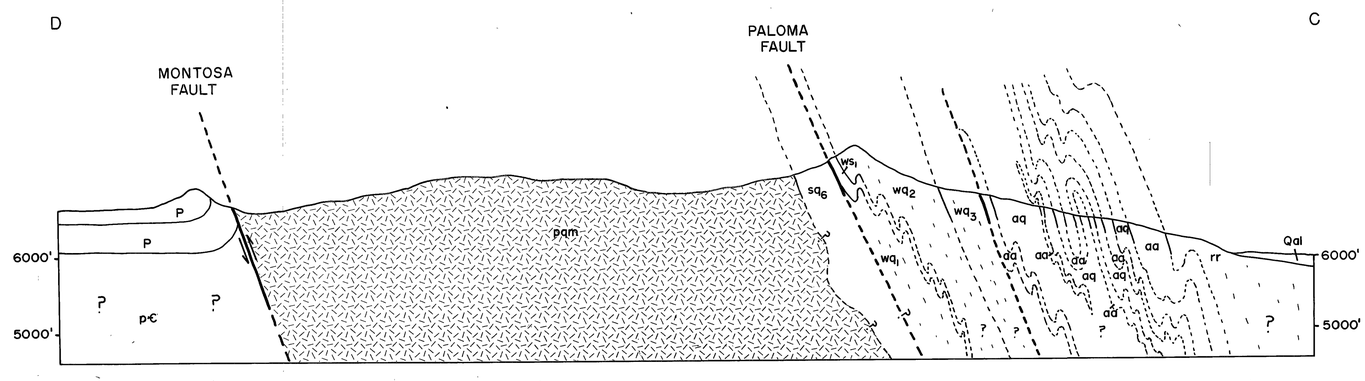

PLATE 2

STRUCTURAL DATA MAP TO ACCOMPANY GEOLOGIC MAP OF THE SOUTHERN MANZANO MOUNTAINS, NEW MEXICO

by
Paul W. Bauer
1982

SYMBOLS

- 80 / 15 — Strike and dip of compositional layering, with bearing and plunge of intersection lineation (L_{01}, L_{02}, or L_{12}); may be parallel to S_0 in some areas and S_1 in others
- 85 / 70 — Strike and dip of dominant axial plane foliation (generally S_2, but may be S_1 locally), with bearing and plunge of intersection lineation (L_{10}, L_{20}, or L_{21})
- 40 / 15 — Strike and dip of S_3 foliation, with bearing and plunge of L_{31} or L_{32} intersection lineation
- 60 — **Strike and dip of compositional layering (S_0) with direction of younging from sedimentary crossbed structure**
- 55 — **Strike and dip of overturned compositional layering (S_0) with direction of younging from sedimentary crossbed structure**

Notes: Dot on symbol indicates station location. For explanation of general lithologic symbols, see geologic map.

SCALE 1:12,000